Fakultät für Mathematik und Naturwissenschaften | RWTH AACHEN UNIVERSITY

‘’Optimisation of electrical stimulation in the retina of retinitis pigmentosa mouse model *rd10*’’

Von der Fakultät für Mathematik und Naturwissenschaften der RWTH Aachen University zur Erlangung des akademischen Grades einer Doktorin der Naturwissenschaften genehmigte Dissertation

vorgelegt von

Nruthyathi, MSc

aus

Kerala, India

Berichter: Prof. Dr. Frank Müller

Prof. Dr. Björn Kampa

Tag der mündlichen Prüfung: 09 September 2025

Erklärung

Hiermit erkläre ich, dass ich die hier vorliegende Doktorarbeit selbstständig verfasst habe. Es wurden keine anderen als die in der Arbeit angegebenen Quellen und Hilfsmittel benutzt. Die wörtlichen oder sinngemäß übernommenen Zitate habe ich als solche kenntlich gemacht.

I hereby declare that I have written this doctoral thesis independently. I have used no sources or resources other than those indicated in the thesis. I have identified any quotations, either verbatim or paraphrased, as such.

Nruthyathi

17 February, 2026

Abstract

The loss of photoreceptors during retinal degeneration diseases like retinitis pigmentosa (RP) leads to blindness. One of the therapeutic strategies to treat this disease is to electrically stimulate the remaining cells in the retina using a retinal implant. However, the effectiveness of retinal implants in the treatment of blindness falls behind expectations. In this study, I show different methods to optimise the electrical stimulation produced by an implant to improve its performance.

In vitro recordings from the retina of a retinal degeneration mouse model, *rd10,* that mimics human RP, were used in this study. In the degenerated retina, an intrinsic oscillatory activity with rhythmic bursts in the action potential firing has been observed. The oscillations were shown to reduce the efficiency of electrical stimulation. Therefore, one way to improve the stimulation efficiency will be to abolish the oscillations. In this regard, I have tested several pharmacological drugs and found a $GABA_A$ receptor agonist, THIP, that can abolish oscillations and improve stimulation efficiency. This shows that an electro-pharmacological therapy is one of the solutions to improve the electrical stimulation of an implant. Another way to optimise electrical stimulation is to stimulate at certain phases in the oscillation. In the *rd10* recordings, we observed cells that have spikes phase-locked to the minima of the oscillation and cells with spikes that are not phase-locked. On stimulation at the maxima, a better response is elicited from the non-phase-locked spiking cells. Therefore, applying electrical stimulation in a temporarily restricted manner to stimulate the non-phase-locked spiking cells would produce a better response from a degenerated retina. The current retinal prostheses do not differentiate between the different retinal ganglion cells (RGCs), like the ON RGCs, which are active with light, and OFF RGCs, which are active in the dark. Equal activation would affect the resolution of the image and cause a mixed response. Here, I had identified certain shapes, amplitudes and durations of the electrical pulse that would selectively excite ON RGCs over OFF RGCs, mimicking a light response. The selective stimulation of ON RGCs and OFF RGCs was achievable in the degenerated retina, *rd10*. This shows that these stimulation pulses can be used to selectively target different RGCs with an implant on the RP retina.

In this study, I have identified ways to generate electrical responses with greater efficiency and enhanced resolution in a degenerated retina. The implementation of these findings in a functional implant would therefore improve the visual percepts elicited by an implant and thereby improve the quality of life for individuals with visual impairments.

Zusammenfassung

Der Verlust von Photorezeptoren bei Netzhautdegenerationskrankheiten wie Retinitis pigmentosa (RP) führt zur Erblindung. Eine der therapeutischen Strategien zur Behandlung dieser Krankheit besteht darin, die verbleibenden Zellen in der Netzhaut mithilfe eines Netzhautimplantats elektrisch zu stimulieren. Allerdings bleibt die Wirksamkeit von Netzhautimplantaten bei der Behandlung von Blindheit hinter den Erwartungen zurück. In dieser Studie zeige ich verschiedene Methoden zur Optimierung der elektrischen Stimulation, um die Leistung eines Implantats zu verbessern.

Für diese Studie wurden in-vitro-Ableitungen von der Retina eines Mausmodells mit Netzhautdegeneration, *rd10*, verwendet, das die menschliche RP nachahmt. In der degenerierten Netzhaut wurde eine intrinsische oszillatorische Aktivität mit rhythmischen Salven von Aktionspotenzialen beobachtet. Es hat sich gezeigt, dass diese Oszillationen die Effizienz der elektrischen Stimulation verringern. Eine Möglichkeit zur Verbesserung der Stimulationseffizienz besteht daher darin, die Oszillationen zu beseitigen. In diesem Zusammenhang habe ich mehrere pharmakologische Medikamente getestet und einen $GABA_A$-Rezeptor-Agonisten, THIP, gefunden, der die Oszillationen aufheben und die Stimulationseffizienz verbessern kann. Dies zeigt, dass eine elektropharmakologische Therapie eine Möglichkeit ist, um die elektrische Stimulation eines Implantats zu verbessern. Eine weitere Möglichkeit, die elektrische Stimulation zu optimieren, besteht darin, in bestimmten Phasen der Oszillation zu stimulieren. Bei den *rd10*-Aufzeichnungen beobachteten wir Zellen mit Spikes, die mit den Minima der Oszillation phasengekoppelt sind, und Zellen mit Spikes, die nicht phasengekoppelt sind. Bei Stimulation an den Maxima wird eine bessere Reaktion der Zellen mit nicht phasengekoppelten Spikes hervorgerufen. Daher würde eine zeitlich begrenzte elektrische Stimulation eine bessere Reaktion der degenerierten Netzhaut hervorrufen. Die derzeitige Netzhautprothese unterscheidet die verschiedenen retinalen Ganglienzellen (RGCs), wie die ON-RGCs, die bei Licht aktiv sind, und die OFF-RGCs, die im Dunkeln aktiv sind, nicht. Eine gleich starke Erregung könnte die Auflösung des Bildes beeinträchtigen und eine gemischte Reaktion hervorrufen. Hier habe ich bestimmte Formen, Amplituden und Dauern des elektrischen Impulses identifiziert, die selektiv die ON-RGCs gegenüber den OFF-RGCs anregen und eine Lichtreaktion imitieren würden. Die selektive Stimulierung von ON-RGCs und OFF-RGCs konnte in der degenerierten Netzhaut *rd10* erreicht werden. Dies zeigt, dass diese Stimulationsimpulse verwendet werden können, um verschiedene RGCs mit einem Implantat auf der RP-Netzhaut selektiv anzusprechen.

In dieser Studie habe ich Wege gefunden, um elektrische Antworten mit größerer Effizienz und verbesserter Auflösung in einer degenerierten Netzhaut zu erzeugen. Die Umsetzung dieser Erkenntnisse in ein funktionelles Implantat würde daher die durch ein Implantat hervorgerufenen visuellen Wahrnehmungen verbessern und damit die Lebensqualität von Menschen mit Sehbehinderungen erhöhen.

Contents

1. Introduction

The eye is a fascinating sensory organ that is essential for seeing. Throughout human evolution, it has played a huge role in our survival by helping us escape from predators, find food, communicate and transfer knowledge. The fact that you can read this sentence is because of the eye. The eye is a ball-shaped organ in front of the face and consists of different parts. Light from the environment enters the eye through the cornea and pupil and is focused by the crystalline lens onto the retina as an image. The image is then processed in the retina and transferred to the brain in form of neuronal activity.

1.1. Retina

The retina is a complex neuronal network present in the back of the eye that converts the image to neuronal signals, processes the image information, and sends it to the brain. The retinal network is composed of different cell classes, namely, photoreceptors, bipolar cells, retinal ganglion cells, horizontal cells and amacrine cells. These cells are arranged in different layers in the retina, where three layers are formed by the somata of the cells and two by the synapses (Figure 1.1). The layers formed by the somata are: 1) the outer nuclear layer (ONL) from the photoreceptor cell bodies, 2) the inner nuclear layer (INL) containing the cell bodies of bipolar cells, horizontal cells, amacrine cells and Müller cells, and 3) the ganglion cell layer (GCL) comprising the cell bodies of retinal ganglion cells. The two layers with the synapses are the outer plexiform layer (OPL) from the synapses of the photoreceptors to horizontal cells and bipolar cells and the inner plexiform layer (IPL) with synapses between bipolar cells, amacrine cells and retinal ganglion cells (Veleri et al., 2015; Wässle, 2004).

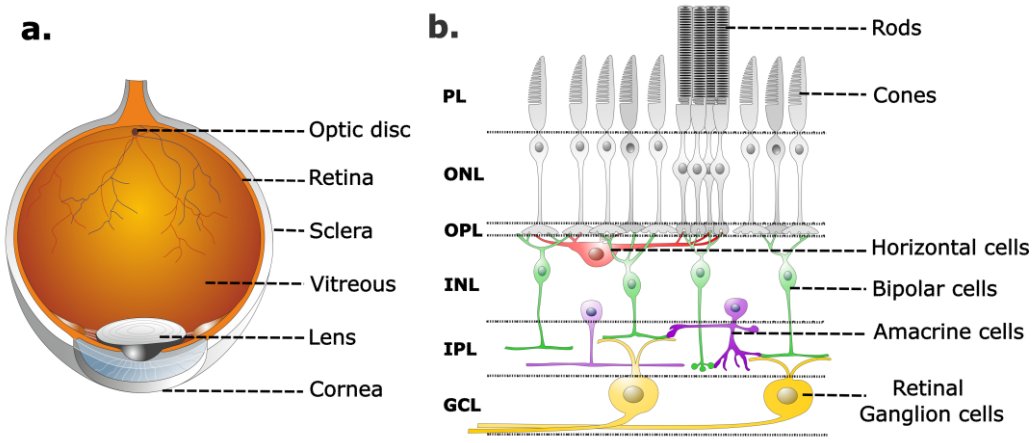

Figure 1.1. Eye and retina: (a) The light enters the eye through the cornea, lens and reaches the retina. The image is processed and sent to the brain via the optic nerve. The outer layer of the eye is the sclera, followed by choroid and the RPE. The inside of the eye is filled with a gel-like substance called the vitreous body. (b) Different cells in the retina. Photoreceptor layer (PL): outer and inner segments of the photoreceptors, outer nuclear layer (ONL): photoreceptor cell bodies, outer plexiform layer (OPL): synapses from the photoreceptors to horizontal cells and bipolar cells, inner nuclear layer (INL): bipolar, amacrine and Müller cell bodies, inner plexiform layer (IPL): synapses from the bipolar to amacrine cells and retinal ganglion cells, ganglion cell layer (GCL): retinal ganglion cells (The eye and retina schematic drawings made by Dr. Anja Ehlers).

The light is detected by the group of cells called the photoreceptors, which are located adjacent to the retinal pigment epithelium (RPE) and choroid. RPE helps in the photoreceptor function by providing nutrients and recycling retinoids (Veleri et al., 2015). To reach the photoreceptors, light has to travel through the different layers of the retina. The photoreceptors consist of outer segments, inner segments, cell body and axon. The outer segment has disc-shaped membrane structures containing visual pigments called opsin. Photoreceptors can be classified into two types: rods and cones. Rods contain rhodopsin and are highly light sensitive, making them essential for low-light vision. In the human retina, cones are responsible for bright-light vision and contain opsins that respond to different spectral wavelengths. The L-opsin is for long (absorption maximum 564 nm), M-opsin for medium (absorption maximum 533 nm) and S-opsin for short (absorption maximum 437 nm) wavelengths (Veleri et al., 2015).

Opsins are G-protein coupled receptors (GPCR) covalently bonded with the chromophore 11-cis retinal (vitamin A isomer) and with transducin as the G-protein. Absorption of a photon isomerises the 11-cis retinal to all-trans-retinal, causing a conformational change in the opsin. This triggers a series of events, in which the GDP is replaced by GTP, α-subunit and βγ–subunit of transducin dissociate and the α-subunit activates the cGMP phosphodiesterase (PDE). PDE hydrolyses cGMP to GMP, causing a reduction in the cGMP levels, leading to the closing of the cGMP-gated channels (cyclic nucleotide-gated (CNG) channels). This hyperpolarises the cell and stops the release of the neurotransmitter, glutamate, from the terminals of the photoreceptor. In the dark, everything goes back to the depolarised state. cGMP is synthesised by guanylate cyclase by converting GTP to cGMP, reopening the CNG channels. To end the transduction cascade, RGS-9 speeds up the hydrolysis of GTP by the α-subunit of transducin. The α-subunit dissociates from the PDE and α-subunit and βγ–subunit reunite. Rhodopsin is inactivated by its phosphorylation by rhodopsin kinase and by the binding of arrestin, which blocks its interaction with transducin (Veleri et al., 2015). The photoreceptors are depolarised and release glutamate in the dark. With light, these cells are hyperpolarised and do not release glutamate. Glutamate released from the photoreceptors binds to the glutamate receptors present on the bipolar cells and horizontal cells.

In most retinae, there are 14 to 16 types of cone bipolar cells and one type of rod bipolar cell (Famiglietti, 2025; Masland, 2001; Wässle et al., 2009). Every cone is connected to multiple kinds of bipolar cells. Bipolar cells form the origin of the two opposing light responses: ON response (with excitation at light ON) and OFF response (with excitation at light OFF and inhibition at light ON). The rod bipolar cell is an ON bipolar cell and receives inputs from rods. In the cone system, both ON bipolar cells and OFF bipolar cells are found. The rod synapse has a single release site at the axon terminals with only one synaptic ribbon flanked by synaptic vesicles. The cone synapse consists of multiple release sites to maintain a continuous and high rate of neurotransmitter release. The cone synapse invaginates and the processes of the horizontal cells and ON bipolar cells are found in this invagination. Dendrites of OFF bipolar cells are seen at the base of the cone synapse. At the invagination of the rod synapse, horizontal cells and rod bipolar cells processes are present. Horizontal cells and OFF bipolar cells express ionotropic glutamate receptors (iGluRs) like AMPA (α-amino-3-hydroxy-5-methyl-4-

isoxazole propionic acid) and kainate receptors, whereas ON bipolar cells and rod bipolar cells express the metabotropic glutamate receptor mGluR6 (Hoon et al., 2014; Wässle, 2004).

In the dark, glutamate released from the photoreceptors binds to AMPA and kainate receptors (cation channels) on OFF-bipolar cells and horizontal cells and depolarises them. In ON-bipolar cells and rod bipolar cells, the glutamate binds mGluR6 receptors and inhibits the cation channel TRPM1, hyperpolarising these cells. With light, the photoreceptors hyperpolarise and, depending on the light intensity, reduce or even stop the release of glutamate. This hyperpolarises the horizontal cells and OFF bipolar cells (sign-conservative response via AMPA and kainate receptors). But ON bipolar cells and rod bipolar cells are depolarised with light by relieving inhibition of the cation channel TRPM1 (sign-inverting response) (Hoon et al., 2014).

The horizontal cells provide feedback inhibition to rods and cones and feedforward inhibition to the dendrites of bipolar cells. These cells are laterally spread and are coupled to their neighbours through gap junction connections. Horizontal cells help to keep the signals within an operating range by measuring the average level of illumination and subtracting a proportionate value from the output of photoreceptors. The inhibition by these cells is achieved by: 1) releasing GABA that acts on GABA receptors on photoreceptor terminals and bipolar cell dendrites, 2) non-synaptic ephaptic action through hemichannels, 3) pH change in the synaptic cleft surrounding photoreceptor terminals or 4) autaptic action of GABA on horizontal cell GABA receptors (Hoon et al., 2014; Wässle, 2004).

The bipolar cell releases glutamate upon depolarisation and its axon also forms ribbon synapses. The ON bipolar cell axons and OFF bipolar cell axons stratify at different depths, with the OFF bipolar cell axons seen at the outer half and the ON bipolar cell axons at the inner half of the IPL. In its postsynapse, the sign-conserving iGluRs, AMPA, kainate and NMDA receptors, are found on amacrine cells and retinal ganglion cells. Sustained and transient responses of bipolar cells are, at least in part, caused by the different expression ratios of kainate and AMPA receptors, respectively (Hoon et al., 2014; Wässle, 2004).

Amacrine cells influence the bipolar cells and the output of bipolar cells onto retinal ganglion cells. They provide feed-forward inhibition to retinal ganglion cells or feed-back inhibition to bipolar cells. They can be either GABAergic (in most cases) or glycinergic (Hoon et al., 2014). $GABA_C$ inhibition shapes the responses of ON cone bipolar cells and rod bipolar cells and glycinergic inhibition for OFF bipolar cells (Hoon et al., 2014). Amacrine cells are necessary for centre-surround antagonism and vertical integration by carrying ON cell information into OFF strata and vice versa, which is called crossover inhibition (Demb & Singer, 2012; Hoon et al., 2014; Masland, 2012; McGuire et al., 1984; Wässle, 2004; Wässle et al., 1986).

There may be up to 60 types of amacrine cells (Yan et al., 2020), which can be divided into two main classes: narrow field amacrine cells and medium or wide field amacrine cells. The narrow field amacrine cells have small dendritic arbours and are glycinergic. They mediate local interactions, some of them between ON and OFF sublamina. The medium field or wide field amacrine cells have large dendritic arbours. They are mostly GABAergic and mediate

lateral interactions as well as feedback inhibition (Masland, 2012; Wässle, 2004). Interestingly, many amacrine cell types have additional neurotransmitters or neuropeptides. Some wide field amacrine cells release dopamine or adrenaline. Dopaminergic amacrine cells are presynaptic to other amacrine cells. They express different GABA receptor subunits within them. Adrenergic amacrine cells have $GABA_A$ and glycine receptors. Blocking input to these cells causes oscillatory activity (Hoon et al., 2014; Knop et al., 2011).

Rod bipolar cells make excitatory iGluRs synapses to A17 and AII amacrine cells. AII amacrine cells produce glycinergic inputs and A17 amacrine cells produce GABAergic inputs. The A17 amacrine cells produce feedback inhibition to rod bipolar cells. AII amacrine cells are not presynaptic to other amacrine cells. The AII amacrine cells produce crossover inhibition between the ON and OFF strata (Demb & Singer, 2012; Hoon et al., 2014; Masland, 2012; McGuire et al., 1984; Wässle, 2004; Wässle et al., 1986).

1.1.1. Retinal ganglion cells (RGCs)

The retinal ganglion cells are the cells present in the inner part of the retina towards the crystalline lens. They receive excitatory glutamatergic inputs from bipolar cells and GABAergic or glycinergic inhibitory inputs from amacrine cells. The axons of the RGCs project to different areas in the brain, like the suprachiasmatic nucleus, lateral geniculate complex, pretectum, superior colliculus and accessory optic nuclei (Wässle, 2004).

RGCs can be classified based on the morphology, synaptic connections and dendritic structure as well as their response to light. Recent studies suggest that there are more than 30 types of RGCs (Baden et al., 2016). Two of the major types are the alpha cells and beta cells. Alpha cells have a large cell body, wide dendritic tree with sparsely branched dendrites and a thick axon. They project their axons onto various subcortical visual areas. Alpha cells are identified in several mammalian retina. In the cat retina, they comprise almost 3% of the total RGCs. The parasol cells or M cells are the homologues of alpha cells in the primate retina. Beta cells have small dendritic fields and occur at high density. They comprise 50% of RGCs in the cat retina. Beta cells are also identified in other mammalian retina and the midget cells in primates are considered to be homologues to them. In the primate retina, 70-80% of all RGCs are midget cells, comprising the most frequently occurring RGC type (Wässle, 2004).

From electrophysiological recordings of the RGCs, two main classes can be identified based on the light responses: ON retinal ganglion cells (ON RGCs) and OFF retinal ganglion cells (OFF RGCs). ON RGCs receive inputs from ON bipolar cells and produce an increase in spiking activity in response to light, whereas OFF RGCs receive inputs from OFF bipolar cells and are inhibited by light but become activated when the light intensity decreases. This is because with light, the photoreceptors are hyperpolarised, which hyperpolarises the OFF bipolar cells and depolarises the ON bipolar cells. ON RGCs and OFF RGCs stratify in different depths in the IPL and connect with bipolar cells and amacrine cells in the IPL (Wässle, 2004).

1.1.2. AII amacrine cell- bipolar cell network

The AII amacrine cells receive inputs from rod bipolar cells. They make sign-conserving gap junctions with other AII amacrine cells and with ON bipolar cells that transmit these signals to ON RGCs. They also make glycinergic synapses onto axons of OFF bipolar cells that send output to OFF RGCs (Demb & Singer, 2012; Famiglietti & Kolb, 1975; Kolb & Nelson, 1983). Therefore, depolarisation of AII amacrine cells causes depolarisation in ON bipolar cells and, in turn, in ON RGCs. On the contrary, depolarisation of AII amacrine cells inhibits OFF bipolar cells and OFF RGCs. Fig. 1.2 shows a simple representation of this connection.

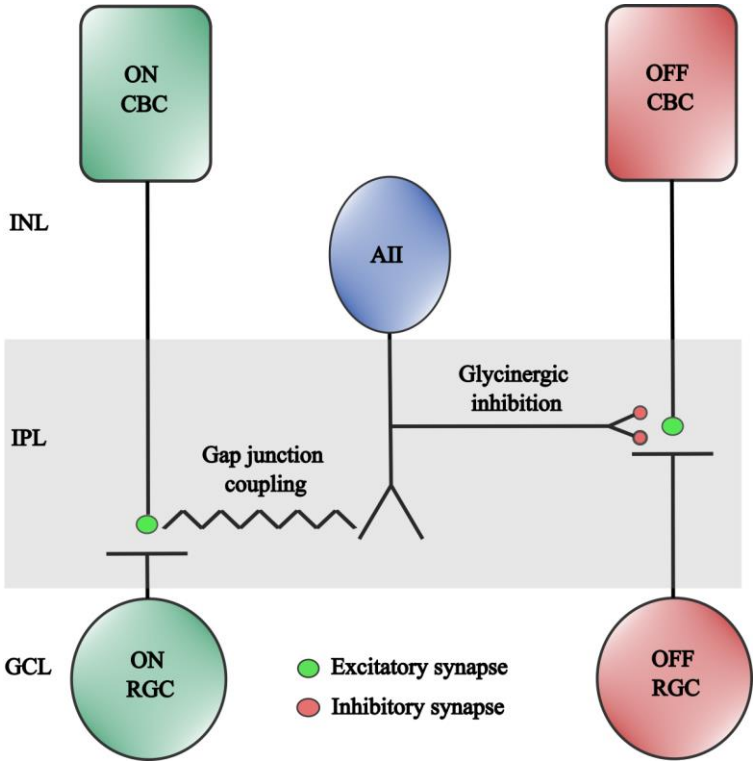

Figure 1.2. AII amacrine cell- bipolar cell network: AII amacrine cell (AII) is electrically coupled with ON cone bipolar cells (ON CBC) through gap junction connections and connected with OFF cone bipolar cells (OFF CBC) through glycinergic connections (Inspired from Borowska et al., 2011; Müller et al., 1988).

This network is shown to play a role in producing pathological oscillations in retinal degeneration animal models like *rd1* and *rd10*. The involvement of this network in oscillations is explained in detail in section 3.1. Once the oscillations are generated in AII amacrine cells, the oscillatory signals are conveyed back to the ON bipolar cells and ON RGCs through the same gap junction connection and to OFF bipolar cells and OFF RGCs through the glycinergic connection. In this manner, the ON and OFF RGCs show oscillations but with opposite polarities (Margolis et al., 2014; Menzler et al., 2014; Zeck, 2016).

With electrical stimulation, the ON bipolar- AII amacrine cell network influences the responses of the RGCs. These responses produced by the presynaptic cells are called the indirect response. With electrical stimulation, the AII amacrine cells get activated either directly or indirectly from the ON bipolar cells or rod bipolar cells and this activates the ON RGCs and

inhibits OFF RGCs differentially (Carleton & Oesch, 2024). Similar effects were observed in this thesis using certain stimulation pulses as described in chapter 5.

1.2. Retinal degeneration

The degeneration of retina causes diseases where the patient undergoes partial to complete blindness. The common retinal degeneration diseases are retinitis pigmentosa and age-related macular degeneration.

Retinitis Pigmentosa (RP) is a genetic disorder that leads to the loss of vision in one in 3000-7000 individuals (Hartong et al., 2006; Veleri et al., 2015). RP is characterised by the deposition of retinal pigments in the peripheral retina. Vision loss starts in the periphery and gradually spread towards the central retina (Hamel, 2006). There are different variations of this disease caused by different gene mutations. Depending on the gene mutation, the disease onset, progression and severity vary from person to person. Nearly 45 gene mutations have been identified and a common one is the mutation of the rhodopsin. This causes the rods to degenerate with the progression of the disease. In the initial stage, the rods in the peripheral retina degenerate. As the disease progresses, this leads to tunnel vision. The loss of rods causes night blindness. Cone degeneration is secondary to rod degeneration. At the final stages of the disease, the entire layer of photoreceptors is degenerated leading to complete blindness (Hamel, 2006).

Age-related macular degeneration (AMD) is the most common retinal degeneration disease that is observed in older individuals (Veleri et al., 2015). It is characterised by the accumulation of retinal pigments called drusen (Thomas et al., 2021). This causes the degeneration of the macula and the fovea. The fovea is a reddish blood vessel-free spot present in the centre of a region called the macula. The macula is slightly thicker than the rest of the retina because of a higher number of photoreceptors, especially cones and associated bipolar and RGCs (Hoon et al., 2014). The damage to the fovea causes loss of central vision in patients. There are two types of AMD: nonneovascular AMD or dry AMD and neovascular or wet AMD. 80-85% of AMD cases are dry AMD and the remaining 15-20% are wet AMD, of which the majority of wet AMD leads to severe loss of vision. The early stage of dry AMD shows the presence of drusen and in the advanced stages, atrophy of the outer retina and surrounding tissues. The wet AMD is caused by the ingrowth of new blood vessels that leak fluids into the subretinal space causing fibrosis of the macula and thereby permanent vision loss if left untreated (Gheorghe et al., 2015; Thomas et al., 2021).

1.3. Treatments

As these diseases cause partial to complete vision loss, it is necessary to find therapies to treat them. The genes responsible for diseases like RP have been identified, and replacing or modifying the responsible genes, called gene therapy, is an area of research to treat these conditions. Another method is the addition of growth factors, neuroprotective agents or pharmacological agents to reduce the progression of the disease or the complete loss of photoreceptors (Hamel, 2006). Vascular endothelial growth factor (VEGF) is necessary for

neovascularisation and fluid leakage in AMD. Treatment by intravitreal injection of anti-VEGF is shown to reduce the progression of AMD and is effective for the treatment of the disease (Thomas et al., 2021; Veleri et al., 2015). Treatment with pharmacological drugs that would abolish the pathological oscillations observed in the degenerated retina is explored in this thesis (chapter 3). The transplantation of retinal cells, such as photoreceptors, is also explored to restore vision in the diseased retina (Bovi Dos Santos et al., 2024; Du & Shen, 2025). Another similar approach is tagging optogenetically inducible opsins into remaining retinal cells, like bipolar cells or RGCs (Hamel, 2006; Hoon et al., 2014; Poboży et al., 2025) making the tagged cells responsive to light.

Another therapeutic strategy will be to stimulate the remaining retinal cells using a retinal implant. The possibility of using retinal prostheses came into being in the 1990s when blind patients were implanted and tested with a temporary stimulation device in their visual cortex. Upon stimulating the cortex, a bright spot could be perceived in the visual field contralateral to the stimulated cortex (Weiland & Humayun, 2014). Currently, this is further advanced to a multielectrode array implant with 2-dimensional or 3-dimensional electrodes to be implanted into the eye or visual cortex. In this thesis, we tested ways to improve the electrical stimulation of the implant that stimulates the retina of the eye.

Based on the position of the implant relative to the eye, there are three types of retinal implants: suprachoroidal implant, subretinal implant and epiretinal implant.

1.3.1. Suprachoroidal implant

The electrodes are implanted on the choroid by cutting a flap in the sclera and placing them on the flap. A return electrode is placed in the vitreous body. With electrical stimulation, the current passes through the choroid to the retina and stimulates the retina. A suprachoroidal implant with 9 electrodes was tested in patients where patients showed light perception and were able to reach and grasp objects (Weiland & Humayun, 2014).

1.3.2. Subretinal implant

The implant is placed in the remaining photoreceptor or bipolar cell side of the retina in the gap created by the degenerated photoreceptors. The electrodes used in this device are photodiodes that are sensitive to light. As the light enters the eye and reaches the electrodes, the electrodes respond to light and stimulate the retina. The benefit of this approach is that the retinal signaling pathway can be recreated artificially as the stimulation is given at the photoreceptor side. The Alpha IMS Wireless implant is a subretinal implant tested in 9 blind subjects. The subjects were able to identify objects and read large letters. One limitation of this approach is that placing the implant in the subretinal space requires mechanically detaching the retina and inserting the device between its layers, a procedure that carries a risk of retinal detachment. In Alpha IMS, this is rectified by injecting silicon oil into the eye to prevent retinal detachment (Weiland & Humayun, 2014).

1.3.3. Epiretinal implant

The epiretinal implants have the electrodes placed on the ganglion cell layer. These implants would therefore stimulate the RGCs directly. However, using an epiretinal stimulation, an indirect activation of RGCs by electrical stimulation of the presynaptic network is also shown to occur (Jensen et al., 2005; Roh et al., 2022; Weitz et al., 2015). There are several epiretinal implants developed and tested in patients: IMI device, Epi-Ret, Argus I and Argus II. Argus II has been tested in 200 patients and showed good performance in tasks like object localisation, motion detection and letter reading. It has 60 electrodes placed on the ganglion layer in the eye and the remaining electronics placed outside the eye. The camera sends inputs to the implant about the image in front of the subject. These implants are inserted by making an incision on the eyewall and inserting them through this gap, but according to this procedure, the size of the epiretinal implants has to be limited. A novel idea to overcome this is by using a foldable implant that unfolds itself once inside the eye (Palanker, 2023; Weiland & Humayun, 2014).

In this thesis, the retinal recording is achieved by placing the retina with the ganglion cell layer side down on the multielectrode array and therefore, the recording and electrical stimulation mimic the situation in an epiretinal implant.

1.4. Retinal degeneration animal model

To study retinal degeneration, several mouse models with naturally occurring retinal degeneration have been identified. Among them are the mouse models *rd1*, *Rd2*, *rd7*, *rd8*, *rd9*, *rd10* and *rd16,* each carrying a mutation in different genes that causes photoreceptor cell death and retinal degeneration (Chang et al., 2002; Veleri et al., 2015). The rat models are the P23H rat strain carrying a mutation in rhodopsin and the *RCS* rat that carries a mutation which causes a deficit in the phagocytosis of photoreceptor outer segments by the RPE and photoreceptor death (Hamel, 2006; Sekirnjak et al., 2009; Veleri et al., 2015).

Two of the well-studied mouse models are the *rd1* and *rd10* mice. Both strains show a mutation in the gene *Pde6b* encoding the beta-subunit of the rod cGMP phosphodiesterase (β-PDE), causing the loss of photoreceptors (Chang et al., 2007). In *rd1* retina, the photoreceptors start to degenerate before eye opening by P14 and by P17, only 2% of rods remain in the central retina. By P36, all the rods are gone. On the contrary, cones degenerate at a slower pace, with 75% cones remaining at P17 and 5% by 18 months (Carter-Dawson et al., 1978). The degeneration starts at P16 in *rd10* retina, reaching peak at P25. By P63, no rod-driven light responses are observed, confirming the complete loss of rods (Chang et al., 2007; Gargini et al., 2007; M. J. Phillips et al., 2010). The rate of cone degeneration is slower than rod degeneration with cones persisting even at 9 months of age. The photoreceptor loss causes a reduction in the thickness of the retina by the degradation of the ONL, whereas the thickness of the inner retinal layers seems to be much less affected (Gargini et al., 2007; M. J. Phillips et al., 2010; Rösch et al., 2014). Since the onset of degeneration is later and the disease progression is slower in the *rd10* retina compared to the *rd1* retina, the *rd10* mouse model is more suitable to study RP as it mimics human RP more closely.

An oscillatory activity has been observed in the local field potentials (LFPs) and action potential firing of RGCs in both *rd1* and *rd10* retina (Fig 1.3). Oscillations occur at a frequency of 10 Hz in *rd1* retina and at 3-6 Hz in *rd10* retina (Biswas et al., 2014; Goo, Ahn, et al., 2011; Haselier et al., 2017). It has been observed that the oscillations may not be present throughout the entire recording and cells could switch from an oscillatory state to a non-oscillatory state within a recording (Biswas et al., 2014; Gehlen et al., 2020). The oscillations are often accompanied by action potentials spiking in rhythmic bursts with a frequency of 4- 15Hz, similar to the frequency of oscillation (J. Ahn et al., 2022; Biswas et al., 2014; Haselier et al., 2017; Margolis et al., 2008; Menzler et al., 2014; Menzler & Zeck, 2011; Poria & Dhingra, 2015; Zeck, 2016).

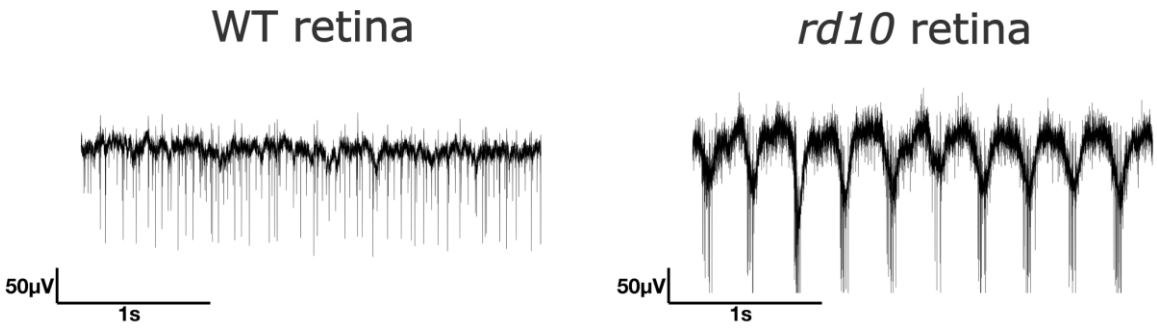

Figure 1.3. Recording of wt and *rd10* retina: Oscillatory activity with phase-locked spiking is observed in *rd10* retina and not in wt retina.

Several studies showed that rhythmic activity can be observed in wt mouse when photoreceptor degeneration was induced artificially. On pharmacologically inducing photoreceptor damage by injecting MNU (N-Methyl-N-Nitrosourea), a 7 Hz oscillation has been observed (Haselier et al., 2017). Damaging photoreceptors with UV irradiation produced a 5.2 Hz oscillation (Meer et al., 2020). Pharmacologically blocking the input from photoreceptors to bipolar cells also induced oscillations (Trenholm et al., 2012). And bleaching photoreceptors with a longer illumination with full-field white light also produced rhythmic RGC spiking (Menzler et al., 2014). Similar abnormal rhythmic activity has also been observed in other animal models, like in an *RCS* rat and pharmacologically induced photoreceptor degenerated macaque monkey retina (J. Ahn et al., 2022; Nruthyathi et al., 2025). But there is no clear evidence of oscillatory activity in human RP patients. Some RP patients have reported phosphenes, which could probably be caused by the spontaneous hyperactivity associated with the oscillation (Bittner et al., 2009; Brown et al., 2015; Heckenlively et al., 1988).

The efficiency of electrical stimulation is lower in the degenerated retina compared to wildtype (Gehlen et al., 2020; Goo, Ahn, et al., 2011; Haselier et al., 2017; Menzler & Zeck, 2011; Rincón Montes et al., 2019). When stimulated during the non-oscillatory phase or after pharmacological abolishing oscillations, stimulation efficiency improved and is similar to wildtype levels (Gehlen et al., 2020; Haselier et al., 2017). This shows that these oscillations are interfering with the electrical stimulation.

1.5. Objective of the study

Retinal prostheses were successful in few patients where they were able to read large letters and recognise simple shapes (Humayun et al., 2003; Weiland & Humayun, 2014; Zrenner et al., 2011). But in majority of patients, implants had little to no success. Therefore, it is important to identify ways to improve the performance of a retinal implant.

My project aims at optimising the electrical stimulation given by the implant. To test this, we used the *rd10* mouse model that shows retinal degeneration similar to human RP. The retina from the mouse was isolated and placed on a multielectrode array epiretinally. The activity of the RGCs was recorded and different kinds of electrical stimulations were tested. The three different approaches that we tested to optimise stimulation efficiency are:

i. Pharmacologically abolishing oscillations

An intrinsic oscillatory activity is observed in retinal degenerated animal models like *rd1* and *rd10* (Biswas et al., 2014; Borowska et al., 2011; Gehlen et al., 2020; Goo, Ahn, et al., 2011; Haselier et al., 2017; Menzler & Zeck, 2011; Trenholm et al., 2012). The oscillations were shown to reduce the efficiency of electrical stimulation (Gehlen et al., 2020; Haselier et al., 2017) and abolishing them using pharmacological drugs improved stimulation efficiency (Gehlen et al., 2020). In this regard, we tested possible pharmacological drugs that can abolish oscillations and improve stimulation efficiency.

ii. Phase specific stimulation

The oscillations are often accompanied by a rhythmic spontaneous activity (J. Ahn et al., 2022; Biswas et al., 2014; Haselier et al., 2017; Margolis et al., 2008, 2014; Menzler et al., 2014; Menzler & Zeck, 2011; Poria & Dhingra, 2015; Zeck, 2016) with more spikes phase-locked to the minima of the oscillation than at the maxima (Biswas et al., 2014; Gehlen et al., 2020; Goo, Ahn, et al., 2011). Here, we selectively stimulated the *rd10* retina at these phases in the oscillation and identified the phase that produced a better response. In this way, we can improve stimulation efficiency without abolishing oscillations.

iii. Identifying the optimal electrical stimulation pulse

Stimulating with an optimal stimulation pulse is shown to produce better RGC responses (K. N. Ahn et al., 2015; Hadjinicolaou et al., 2015; Im & Fried, 2016; Jensen et al., 2003; Jensen & Rizzo, 2009; Ryu, Ye, Lee, Goo, & Kim, 2009; Ryu, Ye, Lee, Goo, Kim, et al., 2009) and selectively stimulate different types of RGCs (Cai et al., 2011; Guo et al., 2018; Im et al., 2018; Im & Fried, 2016; Roh et al., 2022; Twyford et al., 2014). The two main types of RGCs are the ON RGCs which are active with light and the OFF RGCs which are active in the dark. Here, we tested different pulse parameters like the shape, amplitude and duration and identified the combination of parameters that would selectively stimulate ON and OFF RGCs.

Background information and rationale for each approach will be provided in the individual chapters.

2. Materials and Methods

2.1. Animals

C57Bl/6J (referred to as wild type, wt) mice and C57Bl/6J-Pde6b^{rd10}/J mutants (referred to as *rd10*) mice were used for the experiments. The breeding pairs for the *rd10* strain were obtained from Jackson Laboratory (strain name: B6.CXB1-Pde6brd10/J) and bred locally at the animal house of Forschungszentrum Jülich. In this strain, the *rd10* mutation had been backcrossed onto the C57Bl/6J background for five generations prior to intercrossing to achieve homozygosity. To test the different pharmacological drugs to abolish oscillations (chapter 3) and for phase specific stimulation (chapter 4), *rd10* mice of age 4-7 months were used. At this age, oscillations were seen at a frequency of 3-6Hz in the retina of *rd10* mouse. For testing different pulse parameters (chapter 5), 5-6 months old wt and 1 month old *rd10* mice were used. 1 month old *rd10* mice showed light responses needed for RGC classification as well as showed low amplitude and inconsistent oscillations. All animals were kept in the animal house of Forschungszentrum Jülich in a 12-hour dark/light cycle with water and food provided in the cage. Experiments were performed as per the German law for the Protection of Animals and after approval obtained by the regulatory authorities, the Forschungszentrum Jülich and the Landesamt für Natur, Umwelt und Verbraucherschutz of North Rhine-Westphalia.

2.2. Multielectrode array

In-vitro recordings were acquired using a device developed by Multi Channel Systems (MCS) GmbH, Reutlingen Germany. This device consists of a multielectrode array (MEA) chip on which we placed the retina and a headstage with an amplifier.

Table 2.1: Devices and software used for the experiments

MEA system:	MEA60-Up System
MEA amplifier with blanking circuit for upright microscopes :	MEA1060-Up-BC
Headstage:	MEA2100-HS60
Amplifier:	FA60S-BC
Stimulus Generator:	STG 4002-1.6 mA
LED Stimulator:	MEA2100-opto-stim
MEA chips:	60 MEA 200/30iR-ITO-gr
Software for recording:	MC_Rack
Software for light and electrical stimulation:	MC_Stimulus II
Software for selecting stimulation electrodes:	MEA_Select
MCS software for analysis of data	Neuroexplorer
Other software for data analysis	Matlab, JupyterLab

The MEA chip has 60 electrodes arranged in an 8x8 grid with each electrode having a diameter of 30µm and a pitch of 200µm. This chip was placed inside the MCS headstage (MEA2100-HS60) and tightly closed. This causes the contact pins on the head stage to press onto the chip enabling the recording of the signal from the MEA chip. The recording headstage and most of the additional equipment connected to this device were placed inside a Faraday cage to prevent outside noise in the recordings. The recorded signal was first transferred to an amplifier (FA60S-BC) and then to the data acquisition computer through 68-pin MCS standard cable. The amplified data was digitised by MC_Card on the computer.

The recordings were made at a sampling frequency of 25kHz and can be visualised using the software, MC_Rack. Using the software MEA_Select, 8 electrodes were selected: one in each row and column to stimulate and 1 electrode as the ground: electrode 15. The parameters for stimulation like the amplitude, duration and shape of the pulse were written in MC_Stimulus II software. Recordings using MC_Rack are in .mcd format, this was converted to a .txt file using MC_DataTool software or to a .h5 file using Multi Channel DataManager software.

2.3. Pretreatment of MEA chip

Before each experiment, the MEA chips must be treated to obtain better attachment of the retina to the electrodes. The chips were first treated in a plasma cleaner (Diener Electronics, Germany) for 2min at 50% power in 0.4atm of O_2 gas. Chips were then incubated in 0.5mg/ml of poly-D lysine overnight at 4°C. The next day, poly-D lysine was removed and chips were washed with double distilled water and dried with air.

2.4. Retinal Preparation

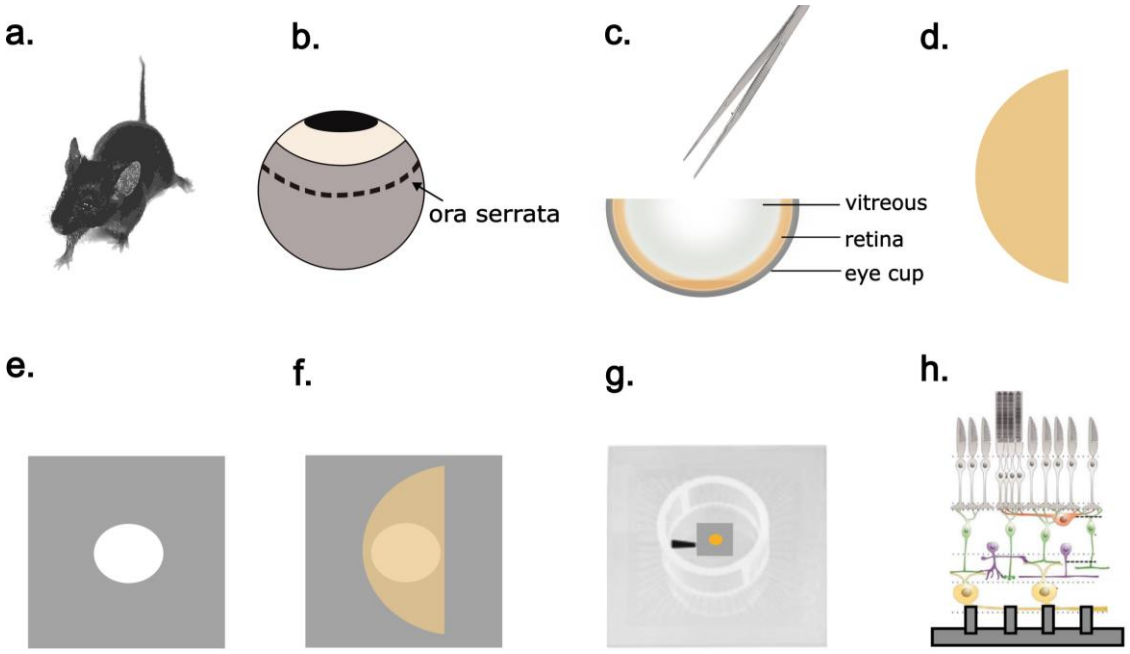

Fig 2.1. *In-vitro* preparation of retina: (a) Mouse anesthetised with isoflurane, decapitated and eyes enucleated. (b) Eye cut along ora serrata (dashed line) and both cornea and crystalline lens separated from the eyecup. (c) Vitreous body above retina carefully removed. (d) Retina cut in half along blind spot and

isolated from eye cup. (e) Filter paper with a hole of diameter 2mm is cut in the center to enable light stimulation. (f) Retina placed on the filter paper with photoreceptor side facing filter paper. (g) Retina with filter paper placed on the array of electrodes on MEA chip. (h) Electrodes are recording and stimulating from the RGC layer.

The retina was kept in freshly prepared AMES medium (Sigma-Aldrich, A1420) during preparation and recording. This media comes in powder form from Sigma-Aldrich (A1420) and has to be dissolved in double distilled water, then adjusted to pH 7.4 using sodium bicarbonate while bubbling with carbogen (gas mixture of 95% O_2 and 5% CO_2).

For the preparation of the retina, mice were deeply anesthetized with isoflurane (Piramal Healthcare Ltd., UK) using an anaesthesia unit (Eickemeyer Narkovet), decapitated and the eyes were enucleated into AMES medium. The eyes were punctured with a needle and cut along the ora serrata using micro scissors. The cornea, iris, crystalline lens and vitreous body were removed and the remaining retina along with the eye cup was cut in two pieces through the blind spot. Both pieces were stored in continuously oxygenated AMES medium and were taken for recording separately. The retina was separated from the eye cup and the remaining vitreous body was removed, then the retina was transferred onto a filter paper (pore size 0.8 µm, MF-MilliporeTM Membrane Filters, Millipore, Germany) with the photoreceptor side facing the filter paper. This was then placed on the electrodes of the MEA chip with the RGC layer facing the electrodes. The retina was left to dry for a minute to foster better adhesion onto the electrodes and then some AMES media was added to the MEA chamber. The MEA chip was connected to the recording device and the signals from the retina were recorded at room temperature.

During the recording, the retina was superfused with continuously oxygenated AMES medium using a homemade perfusion system. The reserve for AMES medium was placed higher than the recording device in the Faraday cage so that the medium flows in due to gravity with a flow rate of 3-4 mL/min. A rolling pump was attached to draw out this medium back to the reserve for recycling it. This perfusion system was also grounded to the Faraday cage.

2.5. Pharmacologically abolishing oscillations

2.5.1. Experimental procedure

In this experiment, we tested different pharmacological drugs to abolish oscillations and improve stimulation efficiency in *rd10* retina. The effect of drugs was determined in a standardized paradigm where upon observing oscillations, the drug was applied for 15-30 minutes and activity compared to the control condition (before application of the drug). To determine the reversibility of the drug, we washed it out with AMES for 20-40 minutes.

2.5.2. Stimulus

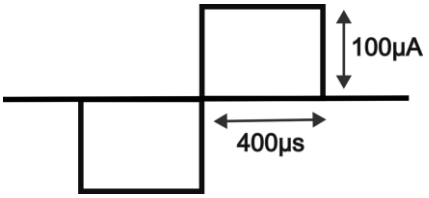

Fig 2.2. Electrical stimulus for pharmacological experiments: Biphasic square pulse of amplitude 100µA and duration 400µs used to electrically stimulate the *rd10* retina.

To estimate the effect of electrical stimulation in the *rd10* retina, a cathodic first biphasic current pulse of duration 400µs and amplitude 100µA was used. Five single electrical pulses with a gap of 20s were applied for each condition: pre-drug, during-drug and post-drug.

2.5.3. Pharmacological drugs

Table 2.2: List of pharmacological drugs tested

Drugs	**Purpose**	**Distributor**
Bicuculline methbromide	$GABA_A$ receptor antagonist	Sigma- B7561
GABA	$GABA_A$, $GABA_B$, $GABA_C$ receptor agonist	Sigma- A2129
THIP hydrochloride	$GABA_A$ receptor agonist	Tocris- 0807
CGS 9895	$GABA_A$ receptor agonist	Sigma-SML0376
Baclofen	$GABA_B$ receptor agonist	Sigma- B5399
CGP 54626 hydrochloride	$GABA_B$ receptor antagonist	Tocris- 1088
TPMPA	$GABA_C$ receptor antagonist	Tocris- 1040/ Sigma- T200
Memantine hydrochloride	NMDA receptor antagonist	Sigma- M9292
D-AP5	NMDA receptor antagonist	Tocris- 0106
R-CPP	NMDA receptor antagonist	Tocris- 0247
Strychnine hydrochloride	Glycine receptor antagonist	Sigma- S8753
Vigabatrin	GABA degradation blocker	Tocris- 0808
Nipecotic acid	GABA reuptake blocker	Sigma- 211672
Carvedilol	Adrenergic antagonist	Sigma- C3993
voriconazole	Antifungal drug: affects TRPM1	Sigma- PZ0005
Psora 4	Kv1.3 potassium channel blocker	Tocris- 4367
Quinine hydrochloride dihydrate	Cx36-Cx45 gap junction blocker	Sigma- Q1125
Carbenoxolone disodium	Non-selective gap junction blocker	Tocris- 3096

GABA: Gamma-Aminobutyric Acid, NMDA: N-Methyl-D-Aspartate, TRPM1: Transient Receptor Potential Melastatin 1

2.5.4. Analysis

The effect of electrical stimulation was determined by examining the change in spike rates with stimulation. For this, we need to first identify the spikes from the signal. This was done by first high pass filtering the data at a frequency of 200Hz- 3000Hz and marking a threshold below the baseline so that all the deflections that cross this threshold, which are the spikes, were separated from the recording. Threshold marking was done manually for each electrode and using the SpikeSorting plugin in MC_Rack software. On rerecording using SpikeSorting plugin, the time and voltage series of each spike waveform was saved. From this, the timing of the occurrence of each spike was determined using Neuroexplorer software and saved into an excel sheet.

To determine the change in spike rate with electrical stimulation, we calculated a parameter called stimulation efficiency. The equation used for the calculation is shown below:

$$\textbf{Stimulation efficiency} = \frac{\textbf{Post stimulus action potential rate}}{\textbf{Prestimulus action potential rate}}$$

Here, the prestimulus action potential rate was calculated from a window of 8s before the electrical stimulus and the post stimulus action potential rate was calculated from 0.4s after the stimulus.

Stimulation efficiency were compared between three conditions: pre-drug, during-drug and post-drug. The calculation for all electrodes and conditions was automated in MATLAB. To find the frequency of the oscillation, the raw data was converted into a text file using MC_Datatool, Fourier transformed using a MATLAB script written by Dr. Janis Brusis and plotted in MATLAB. Images of unfiltered raw data were also made in MATLAB. The statistical analysis (Mann-Whitney student t-test) was performed in GraphPad Prism.

2.6. Phase specific stimulation

2.6.1. Experimental procedure

The *rd10* retina was electrically stimulated at different phases in the oscillations. The phase dependent triggers were achieved by developing a setup in collaboration with project B2 of RTG2610 (Philipp Löhler, Karsten Seidl's group, University of Duisburg).

2.6.2. Stimulation setup

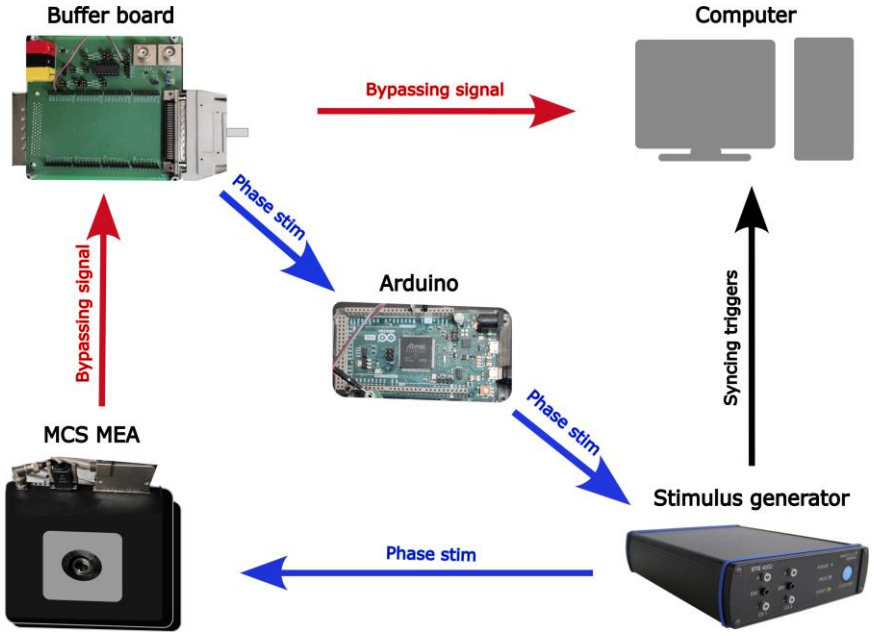

Fig 2.3. Phase dependent stimulation setup: Data recorded by MCS MEA transferred to buffer board that sends the data to both Arduino and computer. Arduino determines the phases in oscillation and sends trigger to the stimulus generator to electrically stimulate the retina on the MEA. The stimulus generator also sends input to the computer for syncing the stimulus with the recording.

During a regular MCS recording, the data recorded by MCS MEA was transferred directly to the computer for visualisation. To stimulate phase specifically, the data from MCS MEA was first sent to a buffer board before sending to the computer. From the buffer board, the signal from one chosen electrode was transferred to the Arduino which ran a script to determine the phase of the oscillation. Arduino was also connected to the stimulus generator. Once the desired phase was detected, Arduino triggered the stimulus generator to immediately send electrical stimulation to MCS MEA. The stimulations were also synced to the computer through a connection established between the computer and the stimulus generator.

2.6.3. Stimulus

A biphasic cathodic first single current pulse with an amplitude of 100µA and duration of 400µs was used (Fig 2.2). A minimum gap of 10s was given between each pulse.

Different recordings were obtained during which the Arduino was asked to stimulate either at the maxima, which is the baseline region of the oscillation or at the minima, which is at the dip of the oscillation.

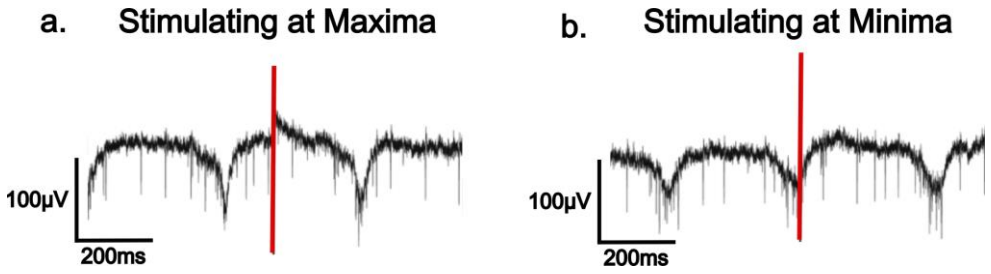

Fig 2.4: Stimulating at maxima and minima in *rd10* retina: (a) Arduino stimulating retina at maxima of oscillation. (b) Arduino stimulating at minima of oscillation. Red line shows stimulation trigger.

Two discrepancies emerged during this experiment. 1) In most cases even without a stimulation, a higher spike rate can be recorded at the minima than at the maxima. This increase will skew the comparison of the stimulation effect between maxima and minima. 2) The electrical stimulation was sent at different points in the minima (decreasing phase, dip or increasing phase) for each stimulation and this would also influence the spike rate evaluated for each stimulation as more spikes are observed at the dip than at the decreasing or increasing phase of the oscillation minima. To resolve these issues, we decided to record an additional condition called sham, where the connection between the stimulus generator and MCS MEA was detached. This produces trigger events in the recording without the retina receiving any stimulation. Taking the ratio of the spike rate of stim with sham would balance out these discrepancies.

2.6.4. Analysis

To compare the effect of electrically stimulating at maxima and minima, we calculated the spike rate (estimated using MC_Rack SpikeSorting plugin, Neuroexplorer and MATLAB, explained in section 2.5.4) for a window of 130ms around the stimulation trigger which is 65ms prestimulus (prestim) and 65ms post stimulus (poststim). This was taken for: stim minima, stim maxima, sham minima and sham maxima. The ratio of stim and sham was compared between maxima and minima. The analysis protocol used in section 2.5.4, using the stimulation efficiency, was not suitable here because at an oscillation of 4 Hz, the phases are very short. Therefore, the spike rate has to be estimated at a smaller window of 130ms and the stimulation-elicited spike rate normalised with sham rather than prestim.

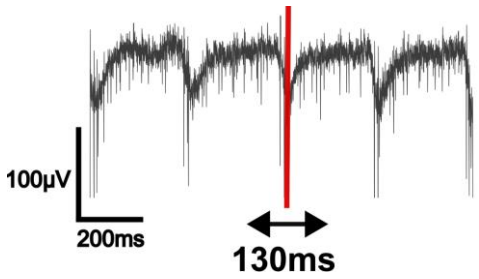

Fig 2.5: Analysing phase dependent stimulation. Recording from a *rd10* retina, the red line is the stimulation trigger. Spike rate calculated for a window of 130ms around stimulation trigger: 65ms prestimulus + 65ms post stimulus.

The device allowed the phase detection in only one of the 60 channels. As oscillations observed on the other electrodes may be slightly phase-shifted (Biswas et al., 2014), the other channels may receive the stimulation at different points in the oscillation. The phases of these channels were visually identified and separated using MATLAB.

The spike rate for prestim, poststim, stim, sham and stim/sham for each sample were calculated for maxima and minima stimulation using MATLAB and the figures and Wilcoxon signed-rank test were made using GraphPad Prism.

2.7. Identifying the optimal electrical stimulation pulse

2.7.1. Experimental procedure

The effect of different stimulation parameters like the amplitude, duration and shape of pulse on the spike rate of wt and *rd10* retina was tested in this experiment.

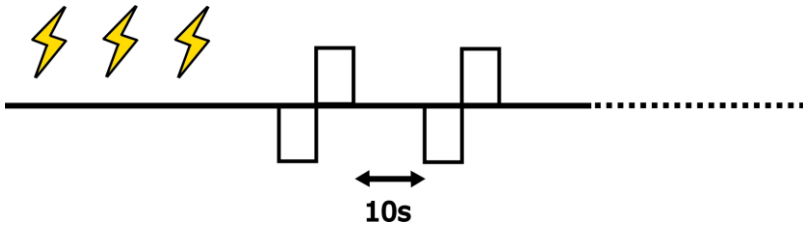

Fig 2.6: Protocol: Each recording has 6 light triggers (1200mV, 100ms for 3 times and 1200mV, 500ms for 3 times) followed by electrical pulses of one shape at different amplitudes and durations. A gap of 10s was given between the electrical pulses. Different shapes are recorded as different recordings.

Here, we tested 6 different shapes, 6 durations and 5 amplitudes of electrical pulses. Each recording had stimulations of one shape and all different amplitudes and durations. In this manner, 6 recordings were obtained for each shape and the order in which each shape tested was randomised.

The mice were dark-adapted overnight. The preparation of the retina was done under dim red light conditions and the retinal activity was recorded in complete darkness. This was to reduce the bleaching of the visual pigments in the photoreceptors. The light stimulations were produced by a white LED placed below the MEA headstage, controlled by the stimulus generator and MC_Stimulus software. Each recording started with three light stimulations with an intensity of 1200mV and a duration of 100ms (corresponding to 281 rhodopsin isomerisations per rod and stimulus calculated in the doctoral thesis of Stefan Esser (Esser et al., 2019)) applied with an interval of 5s, followed by another three light stimulations of the same intensity but 500ms duration (corresponding to 1405 rhodopsin isomerisations per rod and stimulus) applied with 5s gap. This was done to distinguish different RGCs based on their spiking response to light. The light stimuli were followed by a set of electrical pulses of different amplitudes and durations applied with a gap of 10s and generated by the stimulus generator controlled by MC_Stimulus.

2.7.2. Stimulus

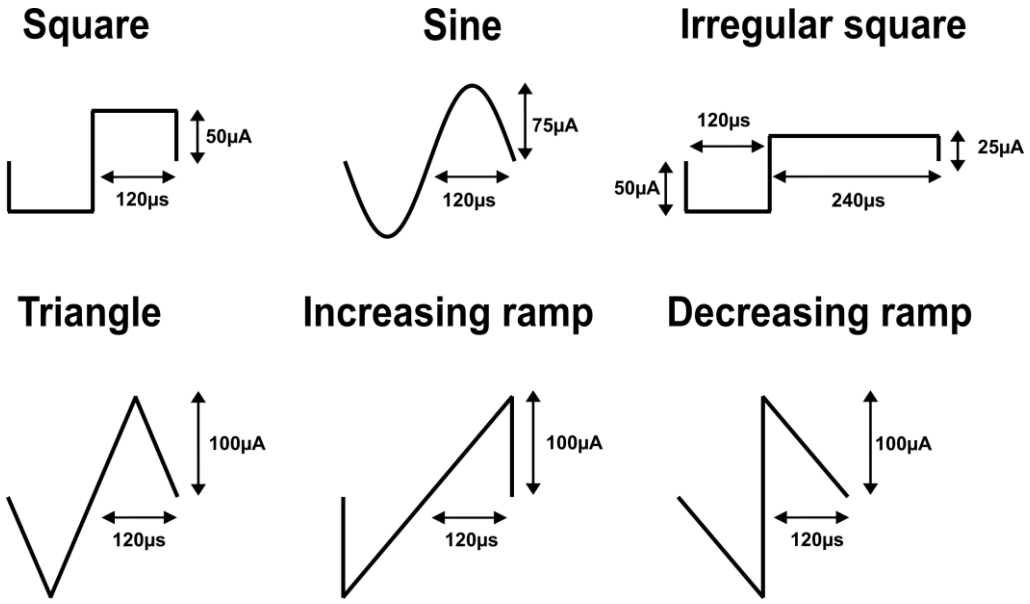

Fig 2.7: Shapes of pulse: An example of one parameter for each of the six shapes of electrical pulses: square, sine, irregular square, triangle, increasing ramp and decreasing ramp.

There were six different shapes of pulse tested: square, sine, irregular square, triangle, increasing ramp and decreasing ramp. All these shapes were given as a single biphasic cathodic first current pulse. To keep the net charge (area under a single phase of a shape) similar between shapes, the amplitudes were adjusted accordingly and the durations were kept constant. An example of stimulus duration and amplitude of different shapes for 6nC stimulation is shown in Fig 2.7. Apart from the pulse shape, different amplitudes and durations of the pulse were tested. The following table shows the amplitude and duration of the square pulse. These parameters were different for the other shapes and were calculated by keeping the net charge constant between shapes. The grey area in Table 2.3 depicts the values that are beyond the limit of these MEA electrodes (based on the manual of 60 MEA 200/30iR chips) and would possibly cause saturation. Therefore, those parameters were not tested.

Table 2.3: Amplitudes and durations of the square pulse

	120µs	**200µs**	**320µs**	**400µs**	**640µs**	**800µs**
50µA	6nC	10nC	15nC	20nC	32.5nC	40nC
100µA	12nC	20nC	30nC	40nC	65nC	80nC
200µA	24nC	40nC	60nC	80nC	**Beyond charge injection limit of electrodes**	
300µA	36nC	60nC	90nC			
400µA	48nC					

2.7.3. Analysis

The analysis of this experiment was performed in the coding platform, Jupyter Lab. The procedure and code for analysis were developed with the help from data analyst, Nikhil Mohan. The recordings from MCS MEA were converted from .mcd format to HDF5 format using the software Multi Channel DataManager. This data was then processed using the McsPyDataTools which is a package developed by Multichannel Systems and has several Python tools to access the HDF5 files. From the data, the required information can be found in two subfolders named AnalogStream and EventStream. AnalogStream gives the signal information as ChannelData and time information as ChannelDataTimestamps. EventStream gives trigger information as EventEntity.

2.7.3.1. Detection of spikes

To separate spikes from the signal, the data was first bandpass filtered with a frequency of 200Hz- 3000Hz and a threshold was marked above the baseline. Fluctuations in the data that crossed this threshold were taken as the spikes. We calculated the threshold as a multiple (4 times) of the noise level of the channel. This was because every channel had variable noise levels and taking 4 times of this noise was found to conservatively select only spikes from the channel.

To find the noise levels, we can calculate the standard deviation of the data, but this has a drawback as the spikes have a strong influence on the standard deviation and therefore result in a very high threshold. Instead, we calculated MAD (median absolute deviation), which is a method that is more resilient to the outliers. MAD is calculated for individual data points in the dataset, $\mathbf{Y_i}$.

$$\mathbf{MAD} = \mathbf{median}(|\mathbf{Y_i} - \mathbf{median}(\mathbf{Y_i})|)$$

$$\boldsymbol{\sigma} = \mathbf{K} \times \mathbf{MAD}$$

$$\mathbf{Threshold} = \mathbf{4} \times \boldsymbol{\sigma}$$

To use MAD as an estimator of standard deviation, we multiplied it with a constant factor K. K depends on the types of probability distribution. Here we use the K as 1.4826 (= 1/0.6745) which is derived from the properties of the normal distribution.

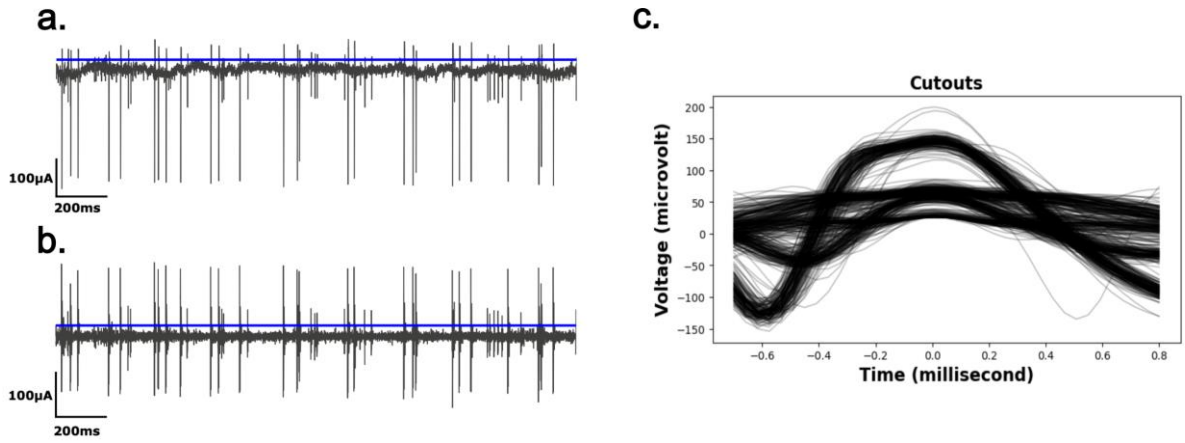

Fig 2.8: Detection of spikes: (a) Unfiltered recording of wt mouse retina, blue line shows the threshold. (b) Band pass filtered at 200Hz- 3000Hz for the same data in a. and blue line is the threshold. The filtered data in b. seems to separate spikes better using the threshold than unfiltered data in a. (c) Overlay of spikes for the data in a. The maxima of each spike placed at 0ms and a window of 0.7ms before and 0.8ms after the maxima is displayed here. Spikes from 2-3 different cells can be observed in this overlay.

After labeling the threshold and identifying the spikes, the spike timestamps and spike waveforms were saved. These waveforms were overlayed on top of each other with the maxima placed at 0ms. Around 0.7ms before and 0.8ms after the peak were also displayed. An example showing the overlay of spikes was shown in Fig 2.8c. During this process, waveforms with values above 300µA were removed as this would most likely be the stimulation artefact.

2.7.3.2. Clustering of spikes

Each electrode can, at the same time, record spikes from different cells that may differ in amplitude and spike waveform. The only retinal cell class that fires action potentials regularly are the RGCs. They are a heterogeneous group and can be classified into different cell types, with the most basic classification into ON and OFF RGCs. ON RGCs are the RGCs that show activity in the presence of light and OFF RGCs are the cells that are active without light. For the analysis, the spiking responses of these two major classes of cells need to be sorted.

We can achieve this by identifying the similarity in the shape of the waveform and applying a feature extraction method. Here, we used Principle Component Analysis (PCA) where the data was transformed into a principle component space with each component representing the variance in the data. Since we identified that the first five principle components represent majority of the signal variance, we looked at only these components. Among these, principle component 1 and principle component 2 were seen as the best components to represent different RGCs.

From the PCA-transformed data, the outliers were removed using z-score. These PC-separated data were then clustered using an algorithm called DBSCAN (Density-Based Spatial Clustering of Applications with Noise). This is a density-based clustering algorithm that separates high-density regions from low-density regions. It is particularly effective for tasks where you need to separate spatial clusters of arbitrary shape.

For the clustering with DBSCAN, we need to provide two variables, eps and min_sample. The variable eps refers to the maximum distance between two points and min_sample refers to the number of points needed for it to be considered as a cluster.

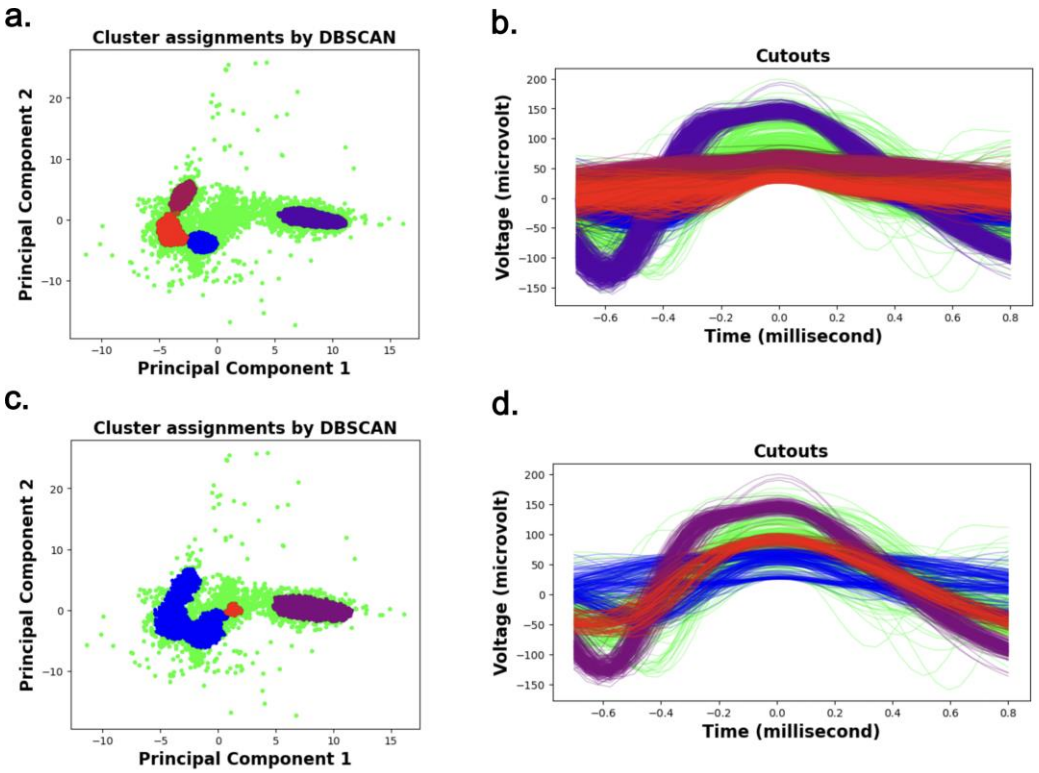

Fig 2.9: Clustering of OFF and ON RGCs: (a) PC 1 and PC 2 for clustering of OFF RGC. The diameter of the clusters can be seen to be smaller than in c. (b) The overlay plot for the clusters in a. (c) PC 1 and PC 2 for clustering of ON RGC. We take the outliers as ON RGCs and the diameter of the clusters is larger than in a. (d) The overlay plot for the clusters in c.

Fig 2.9 shows an example of clustering for ON and OFF RGCs. The clustering was always cross-checked with the light stimuli response to confirm the process. If needed, the eps and min_sample values were tweaked to improve the clustering of ON and OFF RGCs.

We have noticed that for OFF RGCs, taking the clusters with a smaller diameter was more beneficial whereas for ON RGCs, taking the outliers with wider diameters of clusters was better. This can be considered as a conservative approach as we only take the signals that we find to be an ON or OFF RGC with the highest confidence.

2.7.3.3. Classification of ON RGCs and OFF RGCs

To classify the clusters into ON and OFF RGCs, we calculated the elicited spike rate (ESR) after the light stimulation.

Elicited spike rate = Post stimulus action potential rate − Prestimulus action potential rate

The prestimulus action potential rate is calculated for a window of 2s before the light trigger for both ON and OFF RGCs. The post stimulus action potential rate is calculated for different

windows because ON RGCs showed an increase in spikes immediately after the light trigger whereas OFF RGCs showed a decrease in spikes after the light trigger and activity returned after a delay longer than the light stimulus.

The windows were determined from previous recordings of light stimulation and the post stimulus window suitable for ON RGCs is 80ms-430ms after the light trigger and for OFF RGCs is 130ms- 530ms after the trigger. To automate the process of classifying the cluster, we have confirmed that the elicited spike rate values above 10 can be taken as ON RGCs and values below -4 can be taken as OFF RGCs.

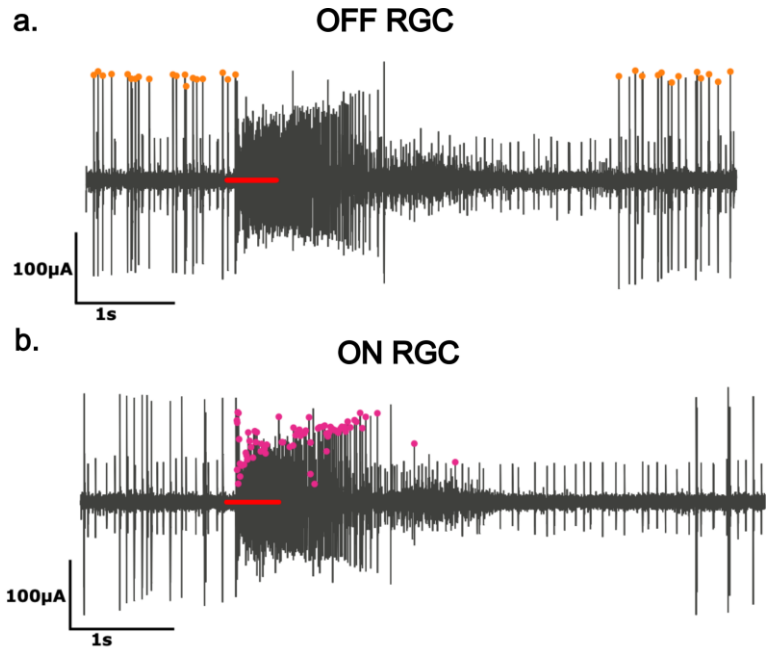

Fig 2.10: Classification of RGCs: (a) Light response after clustering and classification of OFF RGC. The orange dotted spikes are OFF RGC as their elicited spike rate value is below -4. Note the long absence of spikes during and after the light stimulus before activity recovers. (b) Light response after clustering and classification of ON RGC. Pink doted spikes as ON RGC as the elicited spike rate is above 10. The red line represents the 500ms light stimulation.

2.7.3.4. Effect of electrical stimulation

Finally, we need to compare the effect of different electrical stimulation parameters on ON RGCs and OFF RGCs. With the previous steps, spikes from the entire recording that included the electrical stimulations were now clustered, classified and separated into two different sets for ON and OFF RGCs. From each of these, we computed the elicited spike rate after electrical stimulation for every parameter. The prestimulus action potential rate window was 5s before the stimulus and the post stimulus action potential rate window was 0.4s after the stimulus.

The results were displayed in the form of line plots and bar graphs. All the figures were made in JupyterLab and GraphPad Prism. The significance was tested using one-way ANOVA in GraphPad Prism.

2.7.3.5. Selectivity heatmap

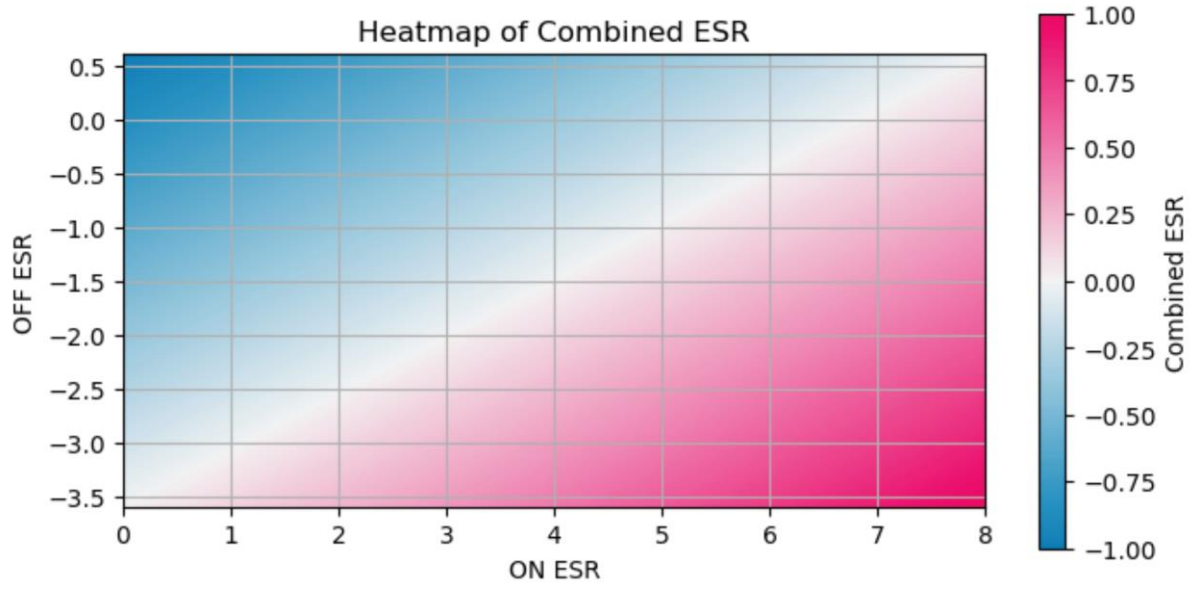

Fig 2.11: Combined ESR: Heatmap of combined ESR plotted with a weight = 1.

Selectivity heatmap shows the preferred parameter to selectively excite ON RGCs and at the same time inhibit OFF RGCs. This was calculated by first normalising the ON and OFF elicited spike rate (ESR) and bringing them onto a similar scale. We used min-max normalisation to achieve this. The normalised x can be calculated using the following formula:

$$\textbf{Normalised x} = \frac{\textbf{x} - \textbf{min}(\textbf{ESR values})}{\textbf{max}(\textbf{ESR values}) - \textbf{min}(\textbf{ESR values})}$$

After normalising the ON and OFF ESR values, we computed the selectivity metric using the following formula:

$$\textbf{Selectivity metric or Combined ESR} = \textbf{Normalised ON ESR} - \textbf{w} \times \textbf{Normalised OFF ESR}$$

where w is the weighting parameter that can be adjusted based on the relative influence of the OFF ESR on the selectivity metric. In this experiment, weight is kept at 1.

This gives a selectivity metric in the range of -1 to 1, where values closer to 1 represent the parameters that excite ON RGCs and inhibit OFF RGCs and values closer to -1 represent the parameters that inhibit ON RGCs and excite OFF RGCs (Fig 2.11). This metric was plotted for each shape and for different combinations of amplitude and duration to identify the best suited combination of parameters to selectively activate ON RGCs and OFF RGCs, respectively.

2.7.3.6. Removing saturated channels

Sometimes, larger amplitude and duration of electrical pulses cause the signal on some electrodes to saturate. The process of saturation occurs when you apply stimulation parameters that are beyond the charge injection limit of the electrodes. This limit can get lower with age of the chip.

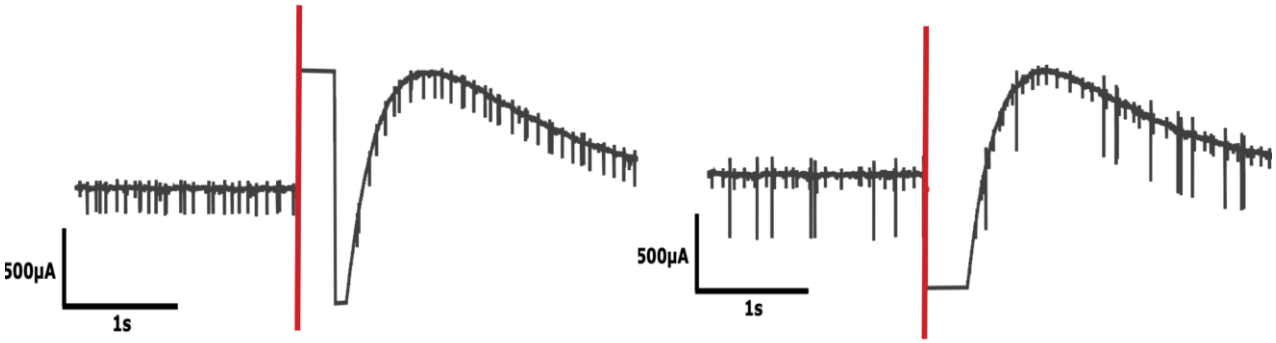

Fig 2.12: Saturation at an electrode: Examples of two different electrodes showing saturation. Saturation is reflected by curtailed curves remaining at one particular value in the positive or negative region after the trigger (red line).

To identify the saturated regions in the data, we took a 10ms interval after electrical stimulation and looked for repeated values that repeat for any 5ms in this interval. This works well because we have noticed that during saturation, the signal tends to remain constant for a while either at the positive values or at the negative values or in some cases both. This method of identifying saturation was also computationally efficient. Fig 2.12 shows examples of saturated regions. The stimulation triggers showing saturation were noted and removed from the final analysis.

3. Pharmacologically abolishing oscillations

3.1. Introduction

With the loss of photoreceptors, an intrinsic oscillatory activity has been observed in the local field potentials and action potential firing of RGCs. The oscillations are at a frequency of 10Hz in the *rd1* retina (Borowska et al., 2011; Goo, Ahn, et al., 2011; Menzler & Zeck, 2011; Trenholm et al., 2012) and 3-6Hz in the *rd10* retina (Biswas et al., 2014; Gehlen et al., 2020; Goo, Ahn, et al., 2011; Haselier et al., 2017) with the spikes often phase-locked to the oscillation (Biswas et al., 2014; Gehlen et al., 2020; Goo, Ahn, et al., 2011).

In the *rd1* retina, the degeneration of photoreceptors starts before eye opening by P14; by P21, most of the rods are lost and by P36, the rods are completely gone. The degeneration of cones occurs at a slower rate with 75% of cones remaining by P17 (Carter-Dawson et al., 1978). Here, the oscillations and rhythmic spiking are first observed at P12 (Poria & Dhingra, 2015). The degeneration in the *rd10* retina starts at P16, peaks at P25 and by P45, the rod photoreceptors are completely lost. The rate of degeneration is slower in cones than in rods with cones persisting even at 9 months of age (Chang et al., 2007; Gargini et al., 2007). The photoreceptor loss causes a reduction in the thickness of ONL, with only a single layer of cells present after P45. Using immunofluorescent staining, the outer segments of rod cells were detected only until P70, and the outer segments of cone cells until P140 (Cha et al., 2022). The onset of oscillation and rhythmicity in the *rd10* retina was at P30, when the rods were mostly lost (J. Ahn et al., 2022). These oscillations were also detected in the visual cortex V1 and superior colliculus of the *rd10* mouse and were shown to prevent cross-modal plasticity of the visual areas in the retina degenerated mice (Rüland et al., 2025). The oscillations occurred at a frequency of 10 Hz at all postnatal ages in the *rd1* retina. In *rd10* retina, the oscillations occurred at the highest frequency with no phase-locked spiking at postnatal week 4. However, from postnatal week 8 onwards, they showed stable oscillations at 4-5 Hz and phase-locked spiking activity (Goo, Ahn, et al., 2011; Goo et al., 2016).

These oscillations were identified in many different cells in the retinal network, namely ON bipolar cells, OFF bipolar cells, AII amacrine cells, other displaced amacrine cells, ON RGCs and OFF RGCs (Borowska et al., 2011; Margolis & Detwiler, 2011; Trenholm et al., 2012). The ON and OFF RGCs were found to receive the oscillatory inputs from the presynaptic cells as blocking the glutamate receptors on RGCs abolished oscillations (Biswas et al., 2014; Margolis & Detwiler, 2011; Menzler et al., 2014; Menzler & Zeck, 2011; Ye & Goo, 2007). Among the presynaptic cells, the role of photoreceptors, rod bipolar cells and amacrine cells were tested by blocking the inputs from these cells and observing the oscillations persisting in bipolar cells and AII amacrine cells (Borowska et al., 2011). From these results, it was hypothesised that the oscillations are formed by the electrical coupling between ON bipolar cells and AII amacrine cells. This was confirmed by testing the gap junction blocker, MFA which abolished oscillations (Biswas et al., 2014; Borowska et al., 2011; Menzler et al., 2014; Menzler & Zeck, 2011; Toychiev et al., 2013; Trenholm et al., 2012). Further to elucidate the role of ON bipolar cells and AII amacrine cells, both these cells were measured after the

application of Cs^+, which blocks the hyperpolarisation-activated current in ON bipolar cells, and TTX, which blocks the Na^+ current in AII amacrine cells. There was a reduction in oscillatory frequency with Cs^+ but with TTX, the oscillations disappeared completely in both cells (Biswas et al., 2014; Cembrowski et al., 2012; Trenholm et al., 2012). This showed that ON bipolar cells have a modulatory effect on oscillations, whereas AII amacrine cells are the ones that produce the oscillations. From computational models, it was identified that the oscillations are only produced when the membrane potential of AII amacrine cells stays at a certain potential range that opens the voltage-gated Na^+ channel (Trenholm et al., 2012). Therefore, during retinal degeneration, the lack of glutamate inputs from photoreceptors causes a change in the potential in ON bipolar cells, thereby shifting the membrane potential in AII amacrine cells through electrical coupling to produce oscillations.

Another study states that the oscillations were produced solely by the amacrine cells, mainly AII amacrine cells (Choi et al., 2014; Yee et al., 2012). They stated that the MFA abolished oscillations not from uncoupling but by hyperpolarising the AII amacrine cells as this effect was reversible on injecting a depolarising current (Choi et al., 2014). Along with the voltage-gated Na^+ channels, the M-type K channels were also shown to be involved in producing the oscillations in AII amacrine cells (Cembrowski et al., 2012; Choi et al., 2014). These inhibitory oscillatory inputs were then sent to the bipolar cells, RGCs and other amacrine cells. In the absence of this inhibitory input, the bipolar cells showed a low frequency oscillation found to be produced by L-type Ca^{2+} channels (Biswas et al., 2014; Borowska et al., 2011; Margolis & Detwiler, 2011; Menzler et al., 2014; Ye & Goo, 2007; Yee et al., 2012).

Another kind of oscillation was also observed in the degenerated eye at a frequency of 1-3Hz in cones, rod bipolar cells and horizontal cells of the *rd1* retina (Euler & Schubert, 2015; Haq et al., 2014). They were produced due to the morphological changes in cones from retinal degeneration and the lack of inhibition from the horizontal cells (Euler & Schubert, 2015). The oscillatory inputs were transferred from cones to rod bipolar cells using glutamate transporter, EAAT5 which is a sign-conserving synaptic transmission (Haq et al., 2014).

The oscillations were shown to affect the electrical stimulation in the *rd10* retina and MNU-induced retinal degenerated primate retina (Gehlen et al., 2020; Haselier et al., 2017; Yoo et al., 2024). With electrical stimulation, multiple temporally and spatially spread spiking responses were observed in these retinas (J. Ahn et al., 2022). There was also variability seen in the electrically evoked responses with age with postnatal week 4.5- 6.5 showing the highest response in the *rd10* retina (Goo et al., 2016; D. J. Park et al., 2015). In *rd10* retina, the oscillations were not present throughout the entire recording and cells sometimes switch from an oscillatory state to a non-oscillatory state (Biswas et al., 2014; Gehlen et al., 2020). A series of electrical pulses were applied during these phases with and without oscillations and the change in spiking rate was calculated as stimulation efficiency (ratio of poststimulus action potential rate to the prestimulus action potential rate). There was a significant decrease in stimulation efficiency during oscillations compared to the case without (Gehlen et al., 2020; Haselier et al., 2017). This confirms that oscillations reduce stimulation efficiency and abolishing them could be a way to achieve better retinal stimulation.

Based on the proposed mechanisms, we have found the following different targets to abolish oscillations:

1. Targeting ON bipolar cells
2. Blocking the coupling between ON bipolar cells and AII amacrine cells
3. Hyperpolarising ON bipolar cells or AII amacrine cells
4. Blocking NMDA receptors
5. Blocking adrenergic amacrine cells

3.2. Results

3.2.1. Targeting ON bipolar cells

ON bipolar cells are hyperpolarised in the dark because the glutamate released by the photoreceptors binds to mGluR6 receptors and inhibits the cation channel TRPM1. With light, the photoreceptors hyperpolarise and stop the release of glutamate. This depolarises ON bipolar cells by activating the cation channel TRPM1 (Hoon et al., 2014). In the absence of glutamate release by the photoreceptors during retinal degeneration, the mGluR6 receptors are no longer inhibiting TRPM1 receptors. Therefore, one would expect a depolarisation of ON bipolar cells similar to the light response. However, on measuring the membrane potential of ON bipolar cells and AII amacrine cells, they were more hyperpolarised in the *rd1* retina compared to the wt (Borowska et al., 2011; Choi et al., 2014; Trenholm et al., 2012). The change in membrane potential in ON bipolar cells also changes the potential of AII amacrine cells through electrical coupling, thereby producing oscillations. In this section, we propose to abolish the oscillations by targeting the ON bipolar cells and changing their membrane potential by either depolarising or further hyperpolarising them.

The hyperpolarisation in ON bipolar cells as described above could be due to the increased expression of potassium channels, specifically Kv1.3, in the degenerated retina. Antagonists of Kv1.3, psora-4, were shown to improve the optogenetically induced light responsiveness of ON bipolar cells (Schilardi et al., 2023). Therefore, in the following experiment, we tested if inhibiting these potassium channels using psora-4 would abolish oscillations.

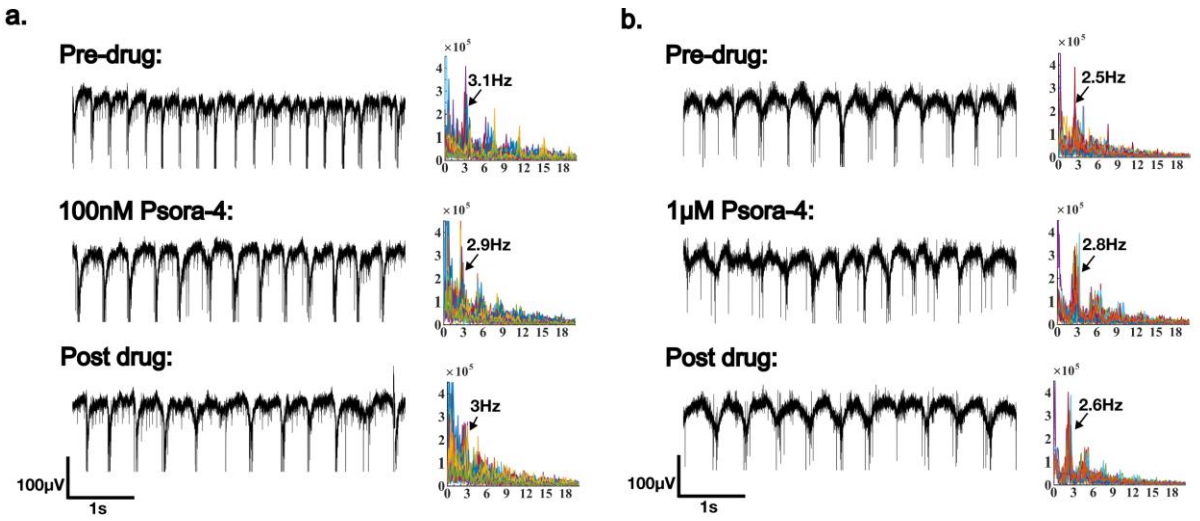

Fig 3.2.1: Effect of psora-4 in *rd10* retina: Unfiltered recording (left) and FFT spectra of multiple active channels (right) during pre-drug, with psora-4, 100nM in (a) and 1µM in (b) and after washing out drug. Psora-4 in both concentrations did not abolish oscillations (drug applied for 15-20 mins and washout for 20-25mins; a total of 3 retinal pieces from 2 *rd10* mice and 2 pieces from 2 *rd10* mice were analysed for 100nM and 1µM, respectively; the x-axis of FFT represents frequencies (Hz), y-axis represents FFT amplitudes (µV) and the different colours in FFT represent different channel recordings).

Psora-4 did not abolish oscillations, the frequency of the oscillations seems to be unchanged with the application of the drug. This shows that blocking the potassium channels, Kv1.3 does not abolish oscillations.

Further hyperpolarising the AII amacrine cells using MFA was shown to abolish oscillations (Choi et al., 2014). This hyperpolarisation in AII amacrine cells can also be achieved by hyperpolarising ON bipolar cells as they are electrically coupled. This can be done by blocking TRPM1 receptors on ON bipolar cells. Voriconazole is a clinically approved antifungal drug that has been shown to block the TRPM1 receptors specifically (Xiong et al., 2015). The following experiment shows the effect of voriconazole on oscillations.

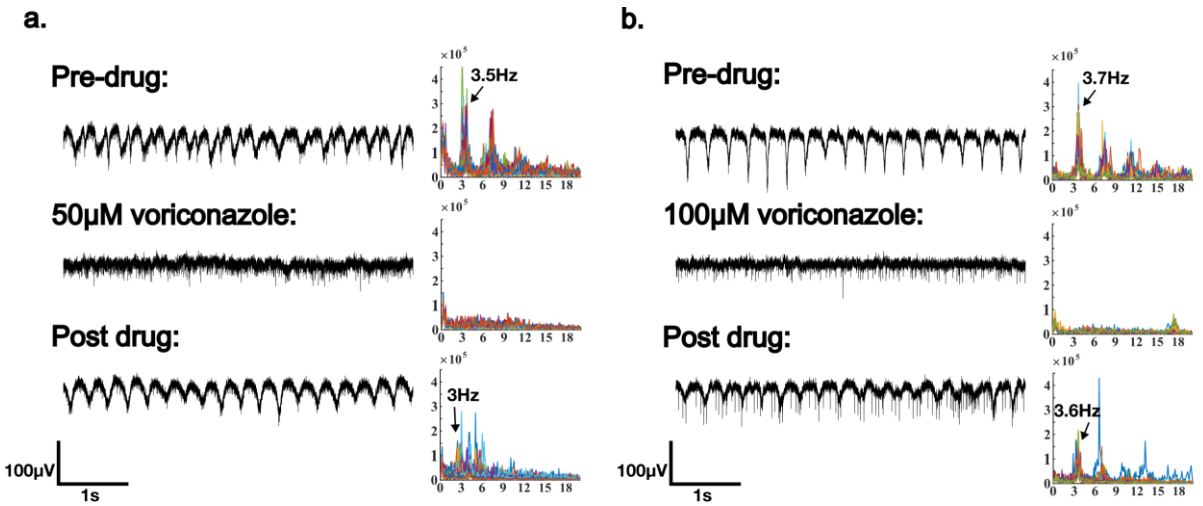

Fig 3.2.2: Effect of voriconazole in *rd10* retina: Unfiltered recording (left) and FFT spectra of multiple active channels (right) during pre-drug, with voriconazole, 50µM in (a) and 100µM in (b) and after washing

out drug. Voriconazole in both concentrations abolished oscillations and the effect was reversible with washout (drug applied for 5-10 mins and washout for 25-30min; a total of 7 retinal pieces from 3 *rd10* mice and 2 pieces from 2 *rd10* mice were analysed for 50µM and 100µM, respectively; the x-axis of FFT represents frequencies (Hz), y-axis represents FFT amplitudes (µV) and the different colours in FFT represent different channel recordings).

The oscillations were reversibly abolished by voriconazole in all channels and for all mice retinae, the peak in FFT at 3.5-3.7Hz disappeared with the application of the drug and reappeared with washout. This confirms the finding that further hyperpolarising ON bipolar cells shifts the membrane potential of AII amacrine cells outside the range where the voltage-gated Na^+ channels open and abolish oscillations. The effect of electrical stimulation in the presence of voriconazole is shown in section 3.2.7.

3.2.2. Blocking the coupling between ON bipolar cells and AII amacrine cells

The electrical coupling through gap junctions between ON bipolar cells and AII amacrine cells is causing the change in potential in AII amacrine cells to open voltage-gated Na^+ channels. This has been confirmed by the application of the non-selective gap junction blocker, MFA which abolished oscillations (Biswas et al., 2014; Borowska et al., 2011; Menzler et al., 2014; Menzler & Zeck, 2011; Toychiev et al., 2013; Trenholm et al., 2012). However, MFA at various concentrations showed a variable effect on oscillations (doctoral thesis of Christine Haselier (Haselier et al., 2017)). Therefore, we tested another non-selective gap junction blocker, carbenoxolone (Azarashvili et al., 2011).

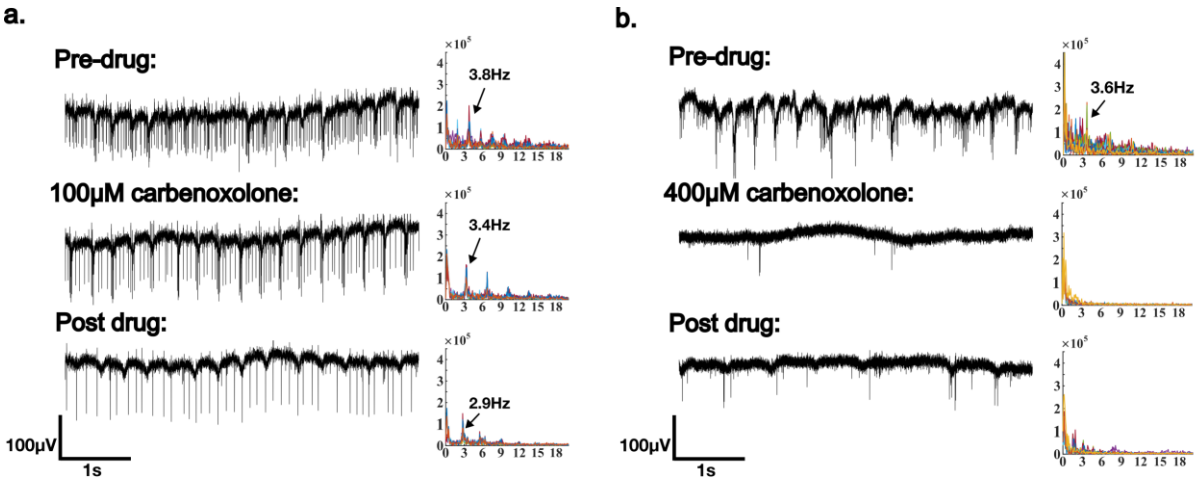

Fig 3.2.3: Effect of carbenoxolone in *rd10* retina: Unfiltered recording (left) and FFT spectra of multiple active channels (right) during pre-drug, with carbenoxolone, 100µM in (a) and 400µM in (b) and after washing out drug. High concentration of carbenoxolone abolished oscillations but the effect was not reversible with washout (drug applied for 15-20 mins and washout for 20- 40mins; a total of 3 retinal pieces from 2 *rd10* mice and 2 pieces from 2 *rd10* mice were analysed for 100µM and 400µM, respectively; the x-axis of FFT represents frequencies (Hz), y-axis represents FFT amplitudes (µV) and the different colours in FFT represent different channel recordings).

With 100µM carbenoxolone, the amplitude and frequency of the oscillation were reduced but oscillations were not completely abolished. 400µM carbenoxolone abolished oscillations, but

this effect was not fully reversible even with an extended time of washout (40 mins). This shows that a high concentration of carbenoxolone can abolish oscillation, but the drug seems to have a long-term effect on the retina. Contrary to this finding, Menzler & Zeck, 2011 showed that carbenoxolone reversibly abolished oscillation. The effect of this drug on stimulation efficiency is shown in section 3.2.7.

Both carbenoxolone and MFA are non-selective gap junction blockers and block gap junctions which are present between almost all cell types in the retina (Trenholm & Awatramani, 1995). The gap junction between ON bipolar cells and AII amacrine cells is made by the connexin Cx45 in ON bipolar cells and Cx36 in AII amacrine cells (Bloomfield & Völgyi, 2009; Han & Massey, 2005; Lin et al., 2005). Quinine is a gap junction blocker that specifically blocks gap junctions formed by connexin Cx36 and Cx45 (Srinivas et al., 2001).

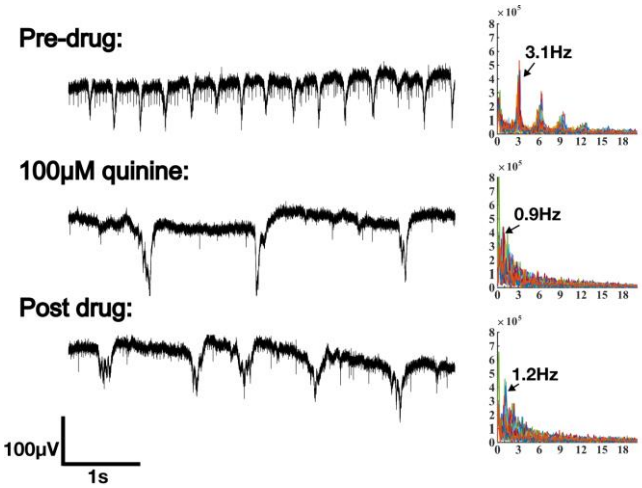

Fig 3.2.4: Effect of quinine in *rd10* retina: Unfiltered recording (left) and FFT spectra of multiple active channels (right) during pre-drug, with 100µM quinine and after washing out drug. With quinine, a low frequency oscillation is observed (drug applied for 20-25 mins and washout for 30- 35 mins; a total of 3 retinal pieces from 2 *rd10* mice were analysed; the x-axis of FFT represents frequencies (Hz), y-axis represents FFT amplitudes (µV) and the different colours in FFT represent different channel recordings).

Quinine did not abolish oscillations; it reduced the frequency of the oscillation from 3-6Hz to 0.9-1Hz. This effect was partially reversible with washout. As Cx36 and Cx45 are also present in cones, rods and OFF bipolar cells (Feigenspan et al., 2004; Trenholm & Awatramani, 1995), the effect of quinine may not be limited to ON bipolar cells and AII amacrine cells.

The low frequency oscillations could originate from two sources: 1) outer retinal oscillations have been described in the network of photoreceptors, rod bipolar cells and horizontal cells (Euler & Schubert, 2015; Haq et al., 2014). These occur at a lower frequency (<3Hz in *rd1* retina) and are thought to be masked by the higher frequency inner retinal oscillations. 2) ON bipolar cells were shown produce a low frequency oscillation (~1Hz in *rd10* retina, 0.2–2.0 Hz in *rd1* retina) mediated by Ca^{2+} channels, unveiled by abolishing amacrine cell oscillations with inhibitory receptor antagonists, APB or LP (Biswas et al., 2014; Borowska et al., 2011; Cembrowski et al., 2012; Choi et al., 2014; Yee et al., 2012). In any case, we did not see a complete inhibition of oscillatory activity with quinine.

3.2.3. Hyperpolarising ON bipolar cells or AII amacrine cells

Here, we have tested different methods to hyperpolarise ON bipolar cells or AII amacrine cells and shift the membrane potential of AII amacrine cells outside the range that produced oscillations. We can hyperpolarise the cells by targeting GABA or glycine receptors (Suzuki et al., 1990). This has been tested before, where GABA, glycine and $GABA_A$ receptor modulators like benzodiazepines (clinically approved drugs) abolished oscillations and also improved stimulation efficiency (Gehlen et al., 2020). However, the drugs tested, benzodiazepines are not ideal for chronic use as they can lead to addiction and a comatose-like state (Fraser, 1998). Therefore, here we have tested several ways to mimic the effect of GABA by: 1) targeting different GABA receptors- $GABA_A$, $GABA_B$ and $GABA_C$; 2) inhibiting the reuptake of GABA from the synapses; and 3) blocking the degradation of GABA.

3.2.3.1. Targeting $GABA_A$ receptors

The $GABA_A$ receptor is an ionotropic receptor and is expressed throughout the entire retina both presynaptically and postsynaptically (Lukasiewicz & Shields, 1998). It consists of pentameric combinations of different subunits: α, β, γ, ρ, δ, ε, π and θ. GABA binds to the $\alpha^-\beta^+$ interface and opens the chloride channels leading to the hyperpolarisation of the cells (Ghit et al., 2021).

The $GABA_A$ modulatory drug benzodiazepines, which have been shown to abolish oscillations (Gehlen et al., 2020), bind to the $\alpha^+\gamma^-$ interface and cause a change in receptor conformation, thereby increasing Cl^- conductance (Ghit et al., 2021). Since these drugs do not directly activate the $GABA_A$ receptors, they tend to have low toxicity (Sieghart et al., 2012). However, due to the side effects of benzodiazepines from chronic use, we have looked for other alternatives.

In this section, we tested two other GABA modulatory drugs: THIP (gaboxadol) and CGS9895. THIP is a muscimol analog that targets mainly the δ subunit of the $GABA_A$ receptor (Hoehn-Saric, 1983; Peng et al., 2002). It has comparatively fewer tolerance and addiction side effects (Drasbek & Jensen, 2006). CGS9895 produces benzodiazepine-like modulatory effects by targeting the $\alpha^+\beta^-$ interface and is also more suitable for long-term use (Ramerstorfer et al., 2011; Sieghart et al., 2012).

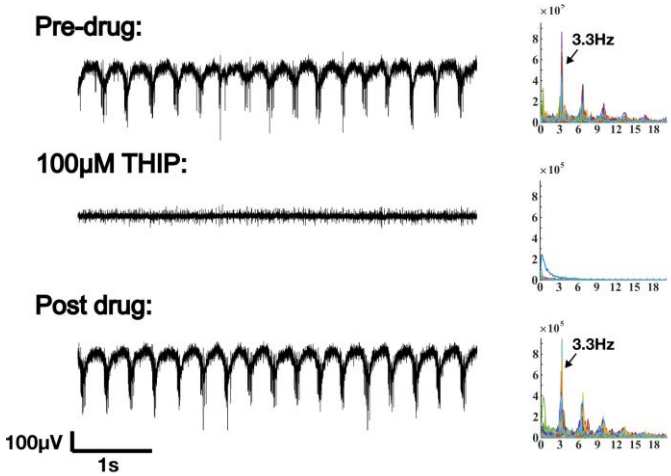

Fig 3.2.5: Effect of THIP in *rd10* retina: Unfiltered recording (left) and FFT spectra of multiple active channels (right) during pre-drug, with 100µM THIP and after washing out drug. THIP abolished oscillations and the effect was reversible upon washout (drug applied for 10-15 mins and washout for 15- 20 mins; a total of 4 retinal pieces from 2 *rd10* mice were analysed; the x-axis of FFT represents frequencies (Hz), y-axis represents FFT amplitudes (µV) and the different colours in FFT represent different channel recordings).

With the application of THIP, the oscillations were completely abolished. This effect was reversible with washout. This can also be observed in the FFT, the peak at 3.3Hz and its subsequent harmonics disappeared with THIP and reappeared with washout.

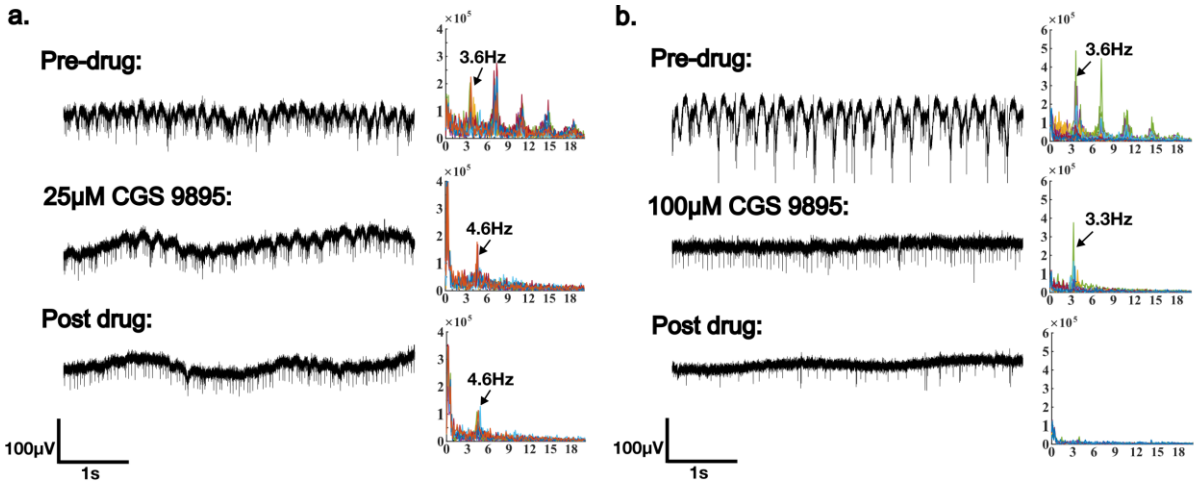

Fig 3.2.6: Effect of CGS9895 in *rd10* retina: Unfiltered recording (left) and FFT spectra of multiple active channels (right) during pre-drug, with CGS 9895, 25µM in (a) and 100µM in (b) and after washing out drug. In a, oscillations were not affected (25µM), in b, oscillations disappeared (100µM). In the FFTs at both concentrations, the first peak between 3-6Hz is maintained, while the higher harmonics vanish during CGS 9895. The effect was not reversible with washout, there is a permanent loss of oscillations especially for 100µM (drug applied for 15-25 mins and washout for 20-30mins; a total of 3 retinal pieces from 2 *rd10* mice and 5 pieces from 3 *rd10* mice were analysed for 25µM and 100µM, respectively; the x-axis of FFT represents frequencies (Hz), y-axis represents FFT amplitudes (µV) and the different colours in FFT represent different channel recordings).

CGS 9895 produced a variable effect on the oscillations. Both concentrations reduced oscillations in very few cases but most of the time, it did not abolish oscillations. The effect of the drug was not reversible with washing out the drug. As effects were variable, they were quantified (Table 3.1).

Table 3.1

Number of channels showing oscillations in pre-drug, during CGS9895 and post drug (Mann-Whitney student t-test is used to compute the p-value**).**

	Number of channels showing oscillations			P- value	
	Pre-drug	**CGS9895**	**Post drug**	**Pre-drug : CGS9895**	**CGS9895 : post drug**
25µM	39.4% ± 12.3	42.8% ± 8.9	43.9% ± 8.2	>0.9999	>0.9999
100µM	34.3% ± 6.7	41.3% ± 11.1	16% ± 7.4	0.6905	0.1508

There was no significant change in the number of channels showing oscillations between pre-drug and with drug (both 25µM and 100µM). For 100µM CGS9895, the channels showing oscillations increased with drug and then reduced drastically with the washout (not significant). This difference in washout could be due to the drug permanently damaging the cells in the retina, making the effect irreversible. The effect of electrical stimulation in the presence of these drugs is shown in 3.2.7.

In conclusion, we observed that pharmacological drugs targeting $\alpha^{+}\gamma^{-}$ interface (benzodiazepines) and δ-subunit (THIP) abolished oscillations effectively. Currently, neither of these drugs is approved for chronic use, but recently a new $GABA_A$ receptor agonist, ganaxolone has been approved by the FDA and EU. Ganaxolone is a $GABA_A$ modulatory agonist that acts on the receptor synaptically and extrasynaptically, but the exact mechanism of action is still under investigation. This drug is given to patients with seizures and has fewer side effects, making it suitable for chronic use (Knight et al., 2022; Monaghan et al., 1999). Therefore, the effect of this drug on oscillations should be determined and it would be a possible alternative that can be given to patients.

3.2.3.2. Targeting $GABA_B$ receptors

Since drugs targeting $GABA_A$ receptors have many side effects, we decided to target another GABA receptor, the $GABA_B$ receptor. $GABA_B$ receptor is a metabotropic receptor that is mostly found postsynaptically in amacrine cells and RGCs and, in some animals, presynaptically in bipolar cells (Lukasiewicz & Shields, 1998). Baclofen is a clinically approved $GABA_B$ agonist and has fewer side effects compared to $GABA_A$ drugs (Bowery et al., 1980; Evenseth et al., 2020).

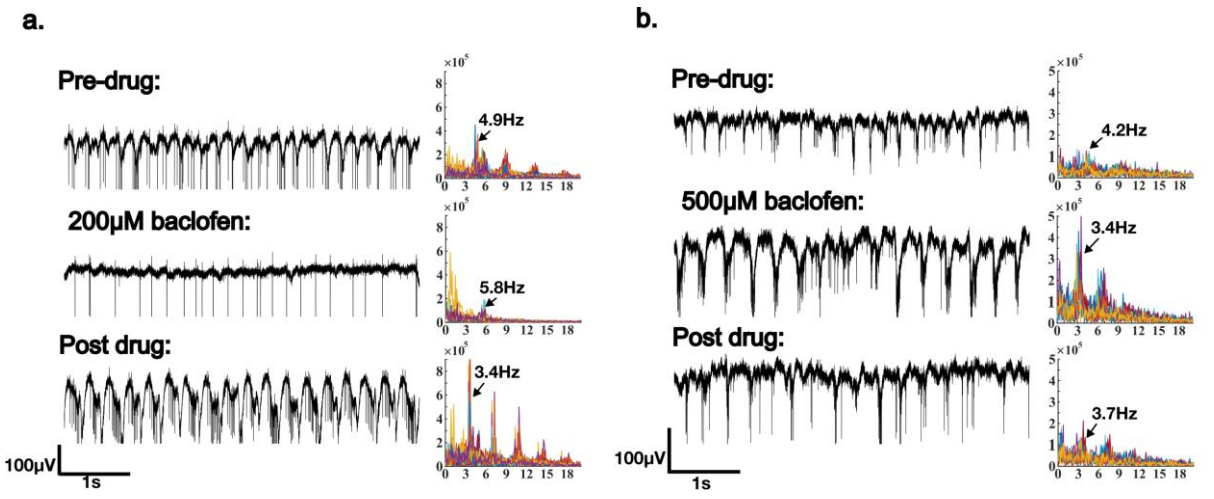

Fig 3.2.7: Effect of baclofen in *rd10* retina: Unfiltered recording (left) and FFT spectra of multiple active channels (right) during pre-drug, with baclofen, 200µM in (a) and 500µM in (b) and after washing out drug. Baclofen at both concentrations showed an inconsistent and variable effect on oscillations (drug applied for 30-35 mins and washout for 30- 40mins; a total of 5 retinal pieces from 3 *rd10* mice and 5 pieces from 3 *rd10* mice were analysed for 200µM and 500µM respectively; the x-axis of FFT represents frequencies (Hz), y-axis represents FFT amplitudes (µV) and the different colours in FFT represent different channel recordings).

Baclofen had a variable effect on oscillations. The frequency and amplitude of the oscillation was reduced in some cases, as shown in the representative figure (Fig 3.2.7a) for 200µM baclofen, but in many other times, there was no change in oscillations, even at higher concentrations. This was quantified in Table 3.2.

Table 3.2

Number of channels showing oscillations in pre-drug, during baclofen and post drug (Mann-Whitney student t-test is used to compute the p-value**).**

	Number of channels showing oscillations			P- value	
	Pre-drug	**Baclofen**	**Post drug**	**Pre-drug: Baclofen**	**Baclofen: post drug**
200µM	48.7% ± 9.7	37.7% ± 7.9	49.3% ± 10.3	0.4206	0.4603
500µM	34.3% ± 9.2	29.7% ± 10.9	34.3% ± 8.5	0.6905	0.5952

The number of channels showing oscillations reduced slightly with both concentrations of baclofen. But this change was not significant. With washout, oscillations returned like before. This shows that targeting $GABA_B$ receptors had an insignificant effect on oscillations. The effect of electrical stimulation with baclofen is shown in section 3.2.7.

3.2.3.3. Targeting $GABA_C$ receptors

$GABA_C$ receptor is an ionotropic receptor found in bipolar cells, primarily at their axon terminals and in some species also in horizontal cells (Lukasiewicz & Shields, 1998). The contribution of $GABA_C$ receptors to the oscillation is unknown. To find this, we need a specific agonist for $GABA_C$ receptors, however, there is no known specific agonist for $GABA_C$ receptors, therefore, it is not possible to directly determine the role of $GABA_C$ receptors in oscillations.

An alternative idea to identify the role of $GABA_C$ receptors will be to block $GABA_A$ and $GABA_B$ receptors using their antagonists and apply GABA on top of it. Now, only $GABA_C$ receptor sites should be available for GABA. If the oscillations are abolished with GABA, then it could be mediated through $GABA_C$ receptors.

First as a control, we tested the $GABA_A$ receptor antagonist bicuculline, the $GABA_B$ receptor antagonist CGP 54626 and the $GABA_C$ receptor antagonist TPMPA individually (Fig. 3.2.8a - c). In a further experiment, all three antagonists were applied together and GABA was applied on top. In this case, GABA should not have any effect on oscillations, as all GABA receptors were blocked.

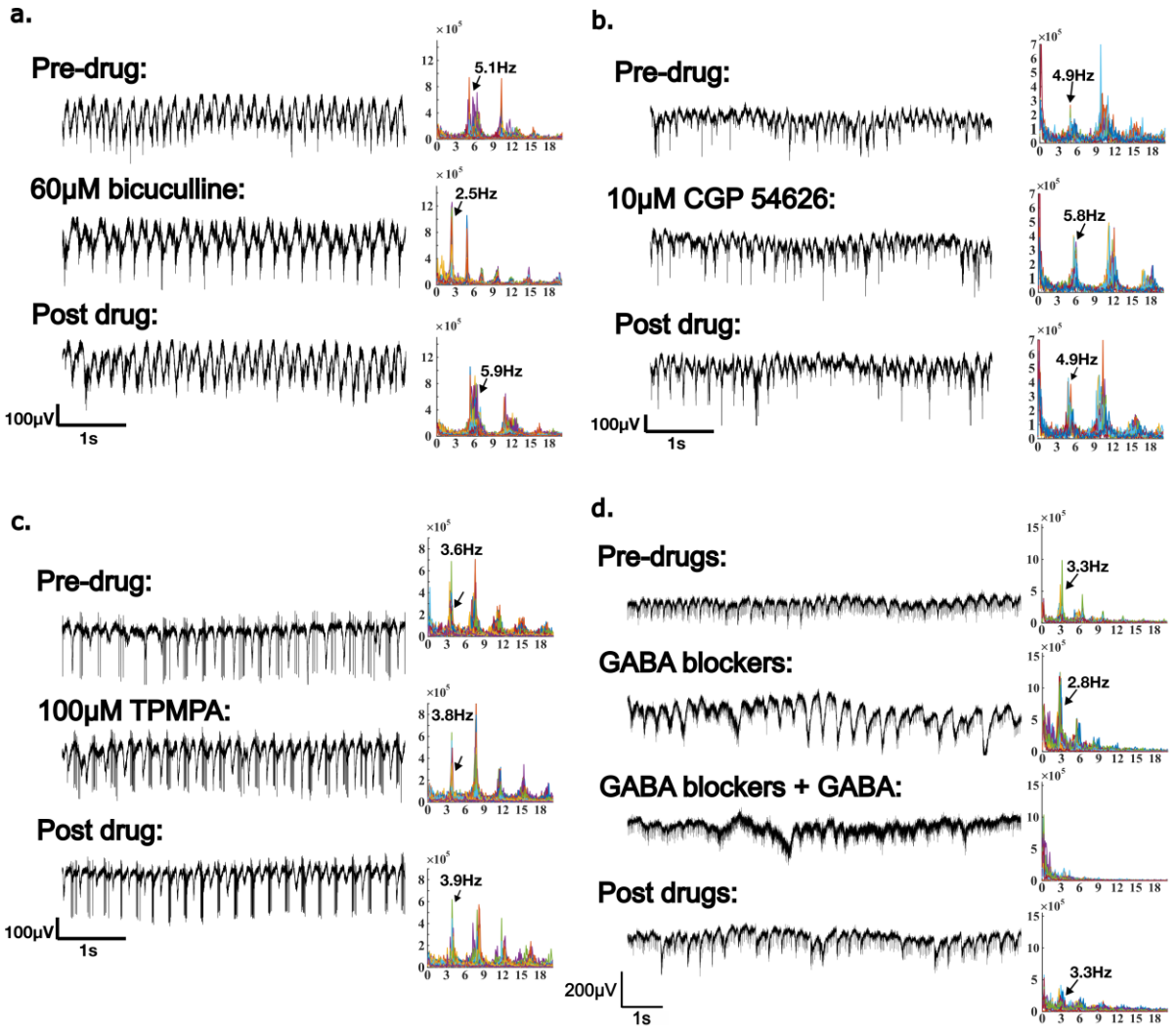

Fig 3.2.8: Blocking all GABA receptors: Unfiltered recording (left) and FFT spectra of multiple active channels (right) during pre-drug, with 60µM bicuculline in (a), 10µM CGP54626 in (b), 100µM TPMPA in (c) and after washing out drug. Bicuculline produced a low frequency oscillation while CGP54626 and TPMPA did not affect the oscillations. (d) Unfiltered recording and FFT showing pre-drug, with GABA receptor blockers: 60µM bicuculline ($GABA_A$ antagonist), 10µM CGP54626 ($GABA_B$ antagonist) and 100µM TPMPA ($GABA_C$ antagonist), with GABA receptor blockers + 500µM GABA and after washing out of all drugs. With GABA blockers, the amplitude of the oscillations increased and frequency decreased but with the co-application of GABA, the oscillations disappeared for a while, returned back and kept fluctuating throughout the entire recording. This shows that GABA still influences oscillations irrespective of blocking all GABA receptors. This effect was reversible with washout (individual drugs applied for 10-20 mins, GABA blockers and GABA blockers+GABA applied for 20-25 minutes and washout for 15-35mins; 2 retinal pieces from 1 *rd10* mouse, 8 retinal pieces from 2 *rd10* mice, 2 retinal pieces from 1 *rd10* mouse and 8 retinal pieces from 3 rd10 mice were analysed for (a), (b), (c) and (d) respectively; the x-axis of FFT represents frequencies (Hz), y-axis represents FFT amplitudes (µV) and the different colours in FFT represent different channel recordings).

The frequency of the oscillations decreased while the amplitude increased with the $GABA_A$ antagonist, but there was no change in the oscillations with $GABA_B$ and $GABA_C$ receptor antagonists alone.

In the experiment on applying GABA with GABA blocker cocktail, we observed that GABA was able to temporarily abolish oscillations. This showed that GABA is still able to influence oscillations, irrespective of blocking all three receptors to which GABA could possibly bind. All antagonists were employed in concentrations several folds above the concentrations typically used to block the corresponding receptors.

Upon further consideration, the two other likely receptors through which GABA could influence the oscillations were the glycine receptors and GABA transporters (Ito, 2016; Scimemi, 2014). Therefore, in the following experiment, we blocked all three GABA receptor types as above, glycine receptors using strychnine, and GABA transporters using nipecotic acid and tested GABA over them.

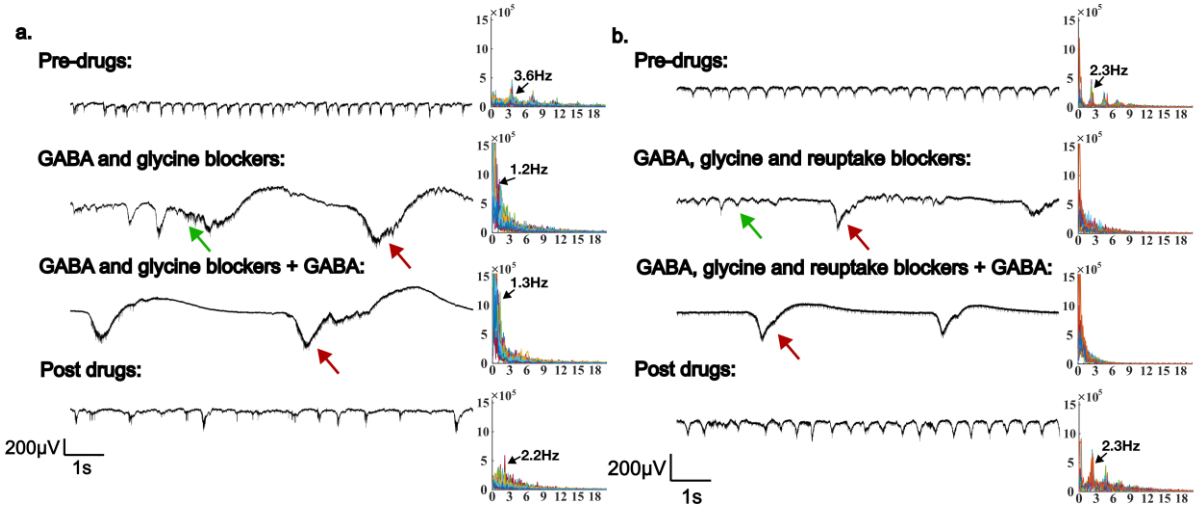

Fig 3.2.9: Blocking all GABA receptors, glycine receptor and GABA transporters: Unfiltered recording (left) and FFT spectra of multiple active channels (right) during pre-drug, with blockers: in (a) 80µM bicuculline ($GABA_A$ antagonist), 20µM CGP54626 ($GABA_B$ antagonist), 200µM TPMPA ($GABA_C$ antagonist) and 50µM strychnine (glycine receptor antagonist) and in (b) all drugs as in (a) + 600µM nipecotic acid (GABA transporter blockers), with blockers + 500µM GABA and after washing out of all drugs. In both cases, the application of blockers produced high amplitude and low frequency oscillations (red arrow) with high frequency oscillations appearing on top of them (green arrow); with the co-application of GABA, the high amplitude low frequency oscillations remained (red arrow), but the high frequency oscillations disappeared. This confirms that GABA has an effect even after blocking all the receptors to which GABA binds. These effects were reversible with washout (blockers and blockers+GABA applied for 20-25mins and washout for 20-30 mins; 6 retinal pieces from 2 *rd10* mice and 7 retinal pieces from 3 *rd10* mice were analysed for (a) and (b) respectively; the x-axis of FFT represents frequencies (Hz), y-axis represents FFT amplitudes (µV) and the different colours in FFT represent different channel recordings).

In both cases, the amplitude of oscillations increased, and the frequency decreased with the blockers. There is a low frequency large amplitude oscillation (red arrow in Fig 3.2.9) seen with a high frequency low amplitude fluctuation (green arrow in Fig 3.2.9) on top of it, reminiscent of oscillations found typically in *rd10* retina. The high frequency fluctuations were abolished with GABA and only the low frequency large amplitude oscillations (red arrow in Fig 3.2.9) remained. This shows that GABA was still able to influence the oscillations even

after blocking all the possible receptors through which this effect could have occurred. Thus, further experiments must be performed to determine the cause of this effect.

Since these control experiments showed that GABA influences oscillations through an unknown mechanism, the experiment to determine the role of the $GABA_C$ receptor in blocking oscillations cannot be performed.

3.2.3.4. Blocking the reuptake of GABA

The GABA released into the synaptic cleft is taken up by GABAergic neurons to utilise again or by the glial cells to degrade into glutamine (Ghit et al., 2021; Rowley et al., 2012). This is achieved by GABA transporters that belong to the solute carrier 6 (SLC6) family, consisting of neurotransmitter: sodium symporters (Scimemi, 2014). The blocking of GABA reuptake would increase the concentration of GABA in the synaptic cleft and hence would possibly abolish oscillations. Here, we tested nipecotic acid, which blocks the reuptake of GABA into both GABAergic neurons and glial cells (Johnston et al., 1976; Krogsgaard-Larsen, 1980).

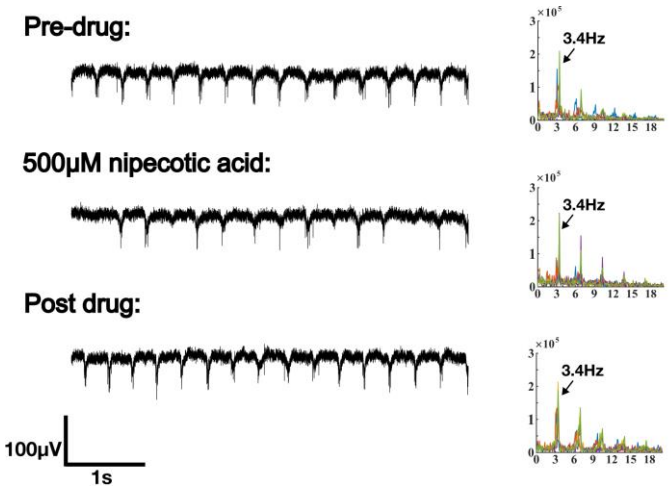

Fig 3.2.10: Effect of nipecotic acid in *rd10* retina: Unfiltered recording (left) and FFT spectra of multiple active channels (right) during pre-drug, with 500µM nipecotic acid and after washing out drug. Nipecotic acid did not affect oscillations (drug applied for 10-20mins and washout for 20-30mins; a total of 3 retinal pieces from 2 *rd10* mice were analysed; the x-axis of FFT represents frequencies (Hz), y-axis represents FFT amplitudes (µV) and the different colours in FFT represent different channel recordings).

Nipecotic acid had a variable effect on the oscillations. In the example shown here, oscillations were unaffected with nipecotic acid as seen in most cases. However, in a few recordings, we observed that oscillations were abolished in some channels with nipecotic acid. An estimate for the overall effect on oscillations by this drug is shown in Table 3.3.

Table 3.3

Number of channels showing oscillations in pre-drug, during nipecotic acid and post drug (Mann-Whitney student t-test is used to compute the p-value**).**

	Number of channels showing oscillations			P- value	
	Pre-drug	Nip acid	Post drug	Pre-drug: Nip acid	Nip acid: post drug
500µM	19.4% ± 2.8	20.6% ± 4.7	23.3% ± 4.2	>0.9999	0.4

We observe no significant change in the number of channels showing oscillations confirming that nipecotic acid does not abolish oscillations.

3.2.3.5. Blocking the catabolism of GABA

GABA that is not reuptaken by the neurons or glial cells is taken up and degraded by an enzyme called GABA transaminase (GABA-T) (Juvenal et al., 2025). GABA-T converts GABA into succinate semialdehyde, which is further degraded through the citric acid cycle (Ghit et al., 2021). Vigabatrin replaces GABA as a substrate for GABA-T and thereby prevents GABA catabolism (Grant & Heel, 1991). Therefore, this drug might increase the concentration of GABA in the synaptic cleft and could abolish oscillations.

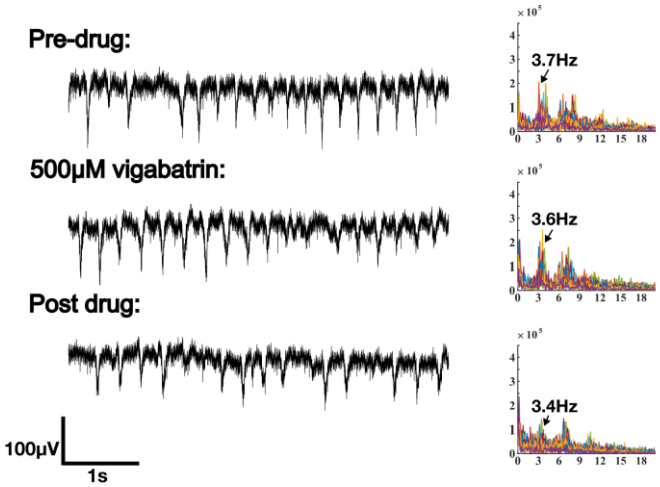

Fig 3.2.11: Effect of vigabatrin in *rd10* retina: Unfiltered recording (left) and FFT spectra of multiple active channels (right) during pre-drug, with 500µM vigabatrin and after washing out drug. Vigabatrin did not affect oscillations (drug applied for 20-30mins and washout for 20-30mins; a total of 8 retinal pieces from 3 *rd10* mice were analysed; the x-axis of FFT represents frequencies (Hz), y-axis represents FFT amplitudes (µV) and the different colours in FFT represent different channel recordings).

Application of 500µM vigabatrin did not abolish oscillations. Both the frequency and amplitude of the oscillation seem to be unaffected by the drug.

3.2.4. Blocking NMDA receptors

The oscillations produced in the ON bipolar cells and AII amacrine cells are transferred to RGCs through glutamate receptors (Biswas et al., 2014; Margolis & Detwiler, 2011; Menzler

et al., 2014; Menzler & Zeck, 2011; Ye & Goo, 2007). There are three glutamate receptor types: AMPA, kainate and NMDA receptors. Blocking all glutamate receptors abolished oscillations (Biswas et al., 2014) but may also affect the excitability of the retina. Hence, we are investigating if blocking specifically the NMDA receptors would abolish oscillations as NMDA receptors get activated when there is excess glutamate in the synapses (Matsui et al., 1998; Sagdullaev et al., 2006).

In the *rd10* retina, the presence of oscillatory activity could release more glutamate from bipolar cells and thus activate NMDA receptors. This was confirmed by observing a reduced RGCs spiking after blocking the NMDA receptors using 50µM D-AP5 (Yee et al., 2018). But it was not stated if D-AP5 abolishes oscillations. Therefore, we have tested the effect on oscillations of D-AP5 and another NMDA antagonist, CPP.

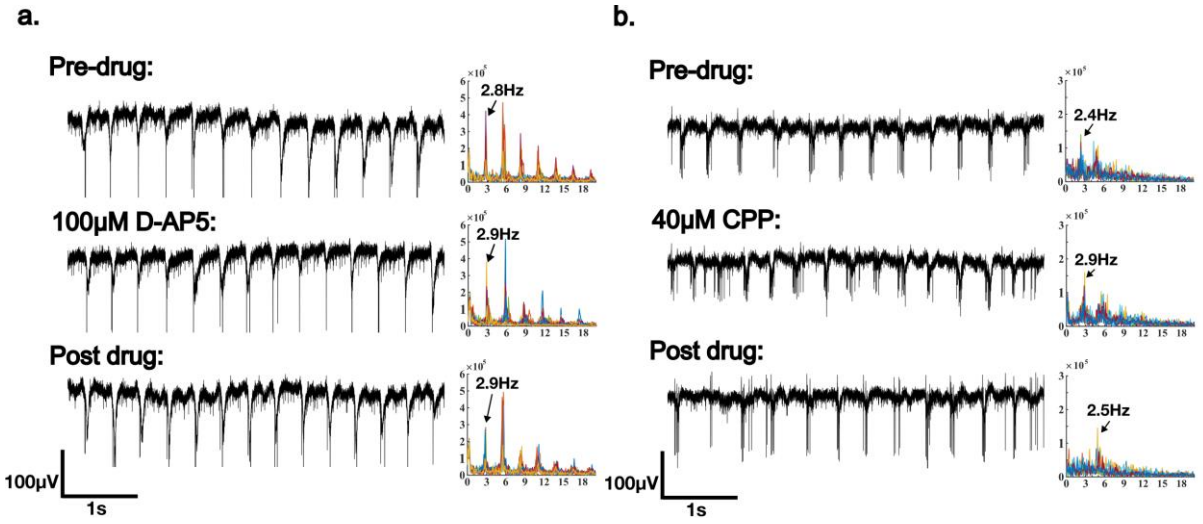

Fig 3.2.12: Effect of D-AP5 and CPP in *rd10* retina: Unfiltered recording (left) and FFT spectra of multiple active channels (right) during pre-drug, with 100µM D-AP5 in (a) and 40µM CPP in (b) and after washing out drug. D-AP5 and CPP did not affect oscillations (drug applied for 10-25mins and washout for 15-40mins; a total of 12 retinal pieces from 6 *rd10* mice and 4 retinal pieces from 2 *rd10* mice were analysed for D-AP5 and CPP respectively; the x-axis of FFT represents frequencies (Hz), y-axis represents FFT amplitudes (µV) and the different colours in FFT represent different channel recordings).

D-AP5 and CPP did not abolish oscillations. No change was observed in the peaks in FFT and in the number of channels showing oscillations (Table 3.4) after the application of the drug.

Table 3.4

Number of channels showing oscillations in pre-drug, during D-AP5, CPP and post drug (Mann-Whitney student t-test is used to compute the p-value**).**

	Number of channels showing oscillations			P- value	
	Pre-drug	**D-AP5**	**Post drug**	**Pre-drug: D AP5**	**D AP5: post drug**
100µM	37.2% ± 4.9	35.1% ± 6	39% ± 4.9	0.8759	0.6178
	Pre-drug	**CPP**	**Post drug**	**Pre-drug: CPP**	**CPP: post drug**
40µM	22.9% ± 9.1	28.8% ± 10.5	23.75% ± 11.1	0.5429	0.8571

Both D-AP5 and CPP block all NMDA receptor subunits. However, the GluN2A subunits of NMDA receptors were found to be highly expressed in the *rd10* retina (Yee et al., 2018) and could be involved in the oscillations. Therefore, we tested a clinically approved drug that targets the GluN2A subunit specifically, memantine (M. B. Phillips et al., 2024).

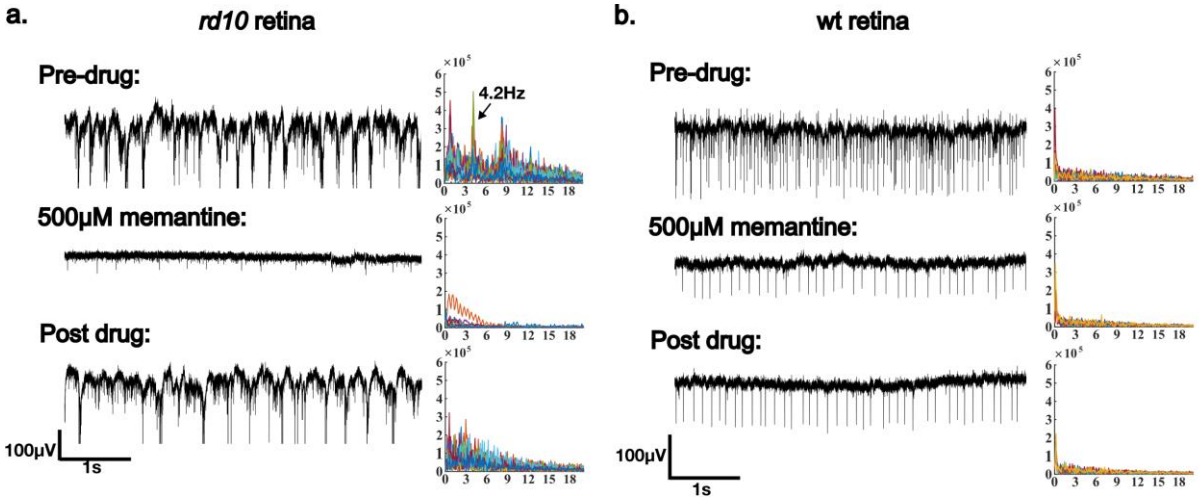

Fig 3.2.13: Effect of memantine in *rd10* and wt retina: Unfiltered recording (left) and FFT spectra of multiple active channels (right) during pre-drug, with 500µM memantine and after washing out memantine. In the *rd10* retina (a), 500µM of memantine abolished oscillations but also reduced the frequency and amplitude of spikes. 500µM memantine also reduced the frequency and amplitude of spikes in wt retina (b) (drug applied for 20-30mins and washout for 20-30 mins; a total of 7 retinal pieces from 2 *rd10* mice and 2 retinal pieces from 1 *wt* mouse were analysed; the x-axis of FFT represents frequencies (Hz), y-axis represents FFT amplitudes (µV) and the different colours in FFT represent different channel recordings).

The higher concentration of memantine abolished oscillations and reduced spike frequency. However, it also reduced the spike amplitude which is not in agreement with an action specific to NMDA receptors. I, therefore, tested the effect of memantine in wt retina. Similar effects on spike frequency and spike amplitude were seen in wt. While the effect on spike frequency might be attributed to the blockade of NMDA receptors, and hence excitatory input, the effect on the spike amplitude argues for an action of memantine at sites different from NMDA receptors. Hence, the specificity of this drug must be questioned. We did not observe the spike

amplitude reducing with D-AP5 and CPP confirming that the effect in spike amplitude is an effect specific to the drug memantine that may be unrelated to NMDA receptor blockade.

In conclusion, memantine could abolish oscillations at high concentrations, but it seems to have unspecific side effects on other receptors thereby affecting the spiking amplitude. This non-specificity of the drug makes it not suitable to be given chronically to patients with retinal implants.

3.2.5. Blocking adrenergic amacrine cells

The last method is to target a wide field amacrine that is hypothesised to play a role in the oscillation. These cells are adrenergic (Versaux-Botteri et al., 1986) and therefore could be inhibited by using a pharmacological drug that acts as an adrenergic antagonist like carvedilol (Ruffolo et al., 1990).

There are two types of wide field amacrine cells that release catecholamines: dopaminergic type 1 cells and adrenergic type 2 cells. The type 2 cells in wt mice showed oscillatory activity at a frequency of 7-11 Hz when GABA receptors were blocked and at a frequency of 3 Hz when glycine receptors were blocked (Knop et al., 2011). Since these cells showed oscillations after blocking the inhibitory neurotransmitters at frequencies similar to that observed in *rd10* (oscillations are at 3- 4Hz) and *rd1* (10Hz) mouse retina, we would like to see if wide field cells might be involved in the generation of oscillations in *rd10*. Type 2 cells are shown to release GABA and adrenaline. Therefore, we blocked the adrenergic output from these cells using carvedilol (Ruffolo et al., 1990) and tested its effect on oscillations.

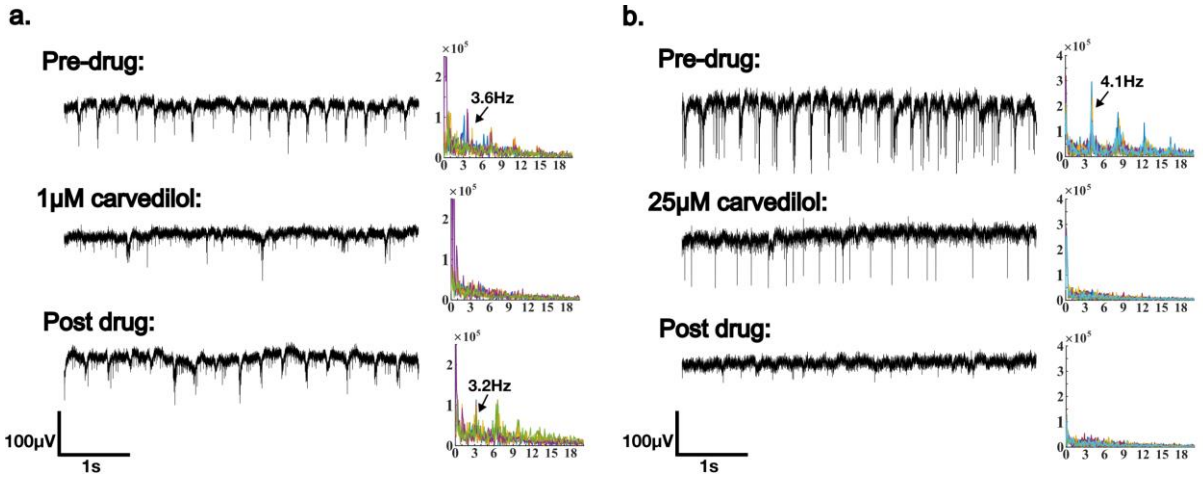

Fig 3.2.14: Effect of carvedilol in *rd10* retina: Unfiltered recording (left) and FFT spectra of multiple active channels (right) during pre-drug, with carvedilol, 1μM in (a), 25μM in (b) and after washing out drug. High concentration of carvedilol abolished oscillations but the effect was not reversible with washout (drug applied for 10-20mins and washout for 15-30mins; a total of 3 retinal pieces from 2 *rd10* mice and 5 retinal pieces from 2 *rd10* mice were analysed for 1μM and 25μM respectively; the x-axis of FFT represents frequencies (Hz), y-axis represents FFT amplitudes (μV) and the different colours in FFT represent different channel recordings).

1µM carvedilol reduced the frequency of the oscillation and this effect was reversible with washout. On testing a higher concentration, 25µM carvedilol, the oscillations disappeared. This shows that carvedilol at a higher concentration completely abolished oscillation. But we observed that the oscillations have not reappeared after washing out the drug. The spiking rate was also reduced during washing. Therefore, a high concentration of carvedilol can abolish oscillations but also cause a permanent effect on the cells in the retina making it irreversible.

Therefore, in conclusion, carvedilol seems to have a permanent effect on the retina and is not suitable to be given to patients to treat RP with retinal implants.

3.2.6. Summary of the effect of different pharmacological drugs

The following table shows a summary of the effects of different pharmacological drugs tested.

Table 3.5

Effect of all pharmacological drugs on oscillations. The drugs that caused an effect on the oscillations in the *rd10* retina are highlighted in green.

	Drugs	Concentration	Target	Effect
1.	Voriconazole	50µM, 100µM	Antifungal drug: affects TRPM1	Both concentrations reversibly abolished oscillations.
2.	Psora-4	100nM, 1µM	Kv1.3 potassium channel blocker	No effect on oscillations.
3.	Carbenoxolone	100µM, 400µM	Non-selective gap junction blocker	Only higer concentration abolished oscillations. Oscillations did not reappear with washout.
4.	Quinine	100µM	Cx36-Cx45 gap junction blocker	Low frequency oscillation observed.
5.	THIP	100µM	$GABA_A$ receptor agonist	Reversibly abolished oscillations.
6.	CGS 9895	25µM, 100µM	$GABA_A$ receptor agonist	Only higher concentration abolished oscillations. Oscillations did not reappear with washout.
7.	Baclofen	200µM, 500µM	$GABA_B$ receptor agonist	Very variable and inconsistent effect on oscillations.
8.	Bicuculline	60µM	$GABA_A$ receptor antagonist	Low frequency oscillation observed.
9.	CGP 54626	10µM	$GABA_B$ receptor antagonist	No effect on oscillations.
10.	TPMPA	100µM	$GABA_C$ receptor antagonist	No effect on oscillations.

11.	Nipecotic acid	500µM	GABA reuptake blocker	No effect on oscillations.
12.	Vigabatrin	500µM	GABA degradation blocker	No effect on oscillations.
13.	Memantine	500µM	NMDA receptor antagonist	Reversibly abolished oscillations but also has an effect on spikes.
14.	D-AP5	100µM	NMDA receptor antagonist	No effect on oscillations.
15.	CPP	40µM	NMDA receptor antagonist	No effect on oscillations.
16.	Carvedilol	1µM, 25µM	Adrenergic antagonist	Only higer concentration abolished oscillations. Oscillations did not reappear with washout.

Voriconazole which blocks TRPM1 receptors in ON bipolar cells, carbenoxolone which blocks gap junctions, THIP and CGS9895 which are $GABA_A$ receptor agonists, memantine which blocks NMDA receptors and carvedilol which blocks adrenergic amacrine cells have abolished oscillations. Among these, the effect of voriconazole, THIP and memantine can be reversed by washing out the drug. Since the rest of the drugs showed a permanent effect/damage on the retina, they are not ideal to be given to patients for chronic use. Memantine also seemed to have non-specific binding on another receptor other than NMDA receptors, thereby causing an effect on the spiking amplitude and making it unsuitable for chronic use.

Targeting $GABA_B$ receptors using baclofen had a variable and inconsistent effect on oscillations. The oscillations were abolished in some channels but this reduction was found to be not significant.

On the other hand, quinine which targets gap junctions Cx36 and Cx45 that are present in AII amacrine cells and ON bipolar cells produced a low frequency oscillation. In the same manner, the $GABA_A$ antagonist, bicuculline also produced a low frequency oscillation.

The pharmacological drugs psora-4 (blocker of a specific potassium channel in ON bipolar cells), CGP54626 ($GABA_B$ antagonist), TPMPA ($GABA_C$ antagonist), nipecotic acid (GABA reuptake blocker), vigabatrin (GABA degradation blocker), D-AP5 (non-specific NMDA antagonist) and CPP (non-specific NMDA antagonist) did not affect oscillations.

The effect of electrical stimulation with the drugs that affected oscillations (highlighted as green in Table 3.5) is shown in the next section.

3.2.7. Stimulation efficiency

Abolishing oscillations were shown to increase stimulation efficiency, the ratio of poststimulus action potential rate to prestimulus action potential rate. Inhibitory neurotransmitters like GABA and glycine, and the $GABA_A$ modulatory drugs, benzodiazepines, were able to abolish oscillations and thereby improve stimulation efficiency (Gehlen et al., 2020). In this study, we

have found several drugs that can abolish oscillations, the change in stimulation efficiency with these drugs is quantified here.

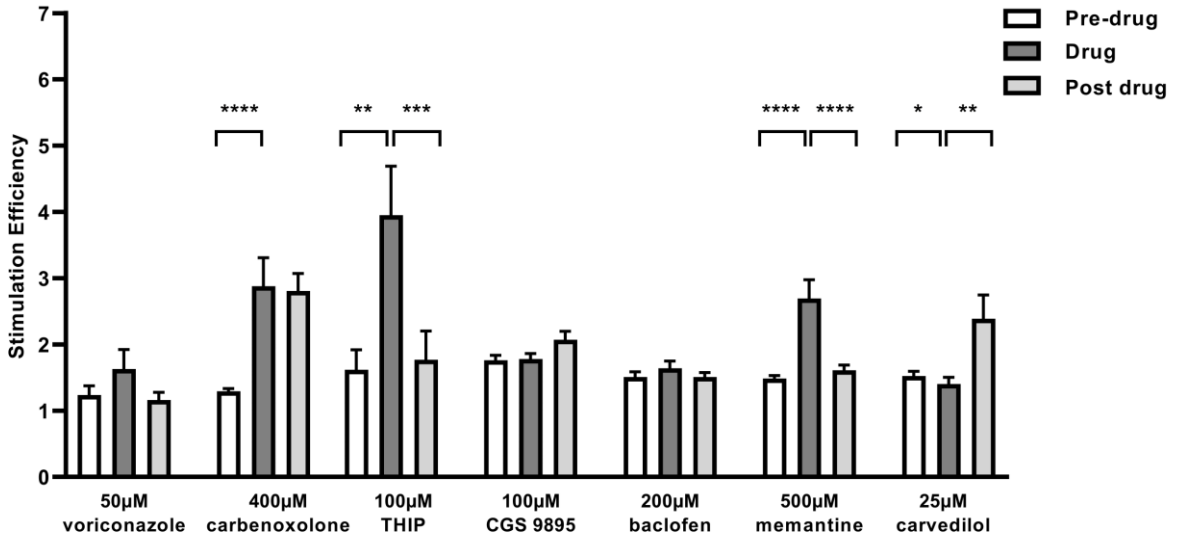

Fig 3.2.15: Stimulation efficiency: Comparison between pre-drug, during drug and after washing out the drug (post drug). Mann-Whitney student t-test was used to compare the stimulation efficiency between each group (****: $p<0.0001$; ***: $p\leq0.001$; **: $p\leq0.01$; *: $p\leq0.05$).

Voriconazole, a blocker of TRPM1 channels in ON bipolar cells (Xiong et al., 2015), had reversibly abolished oscillations but it did not increase stimulation efficiency. With the drug, we see a small increase in stimulation efficiency but this was not significant. Therefore, this drug may not be suitable for patients with retinal implants as it cannot improve the electrical stimulation produced by the implant.

Carbenoxolone, a non-specific gap junction blocker (Azarashvili et al., 2011), had abolished oscillations but the oscillations did not reappear with washout. A similar effect can be seen with electrical stimulation. The stimulation efficiency has increased significantly with carbenoxolone and remained at a higher value with washout. The irreversibility of the drug makes it not suitable to be used in RP patients.

THIP (gaboxadol), which targets the δ subunit of $GABA_A$ receptors (Hoehn-Saric, 1983; Peng et al., 2002), had reversibly abolished oscillations. Here, we see that it also increased stimulation efficiency significantly. This effect was also reversible with washout, making this an ideal drug to be given to patients to improve the electrical stimulation of an implant. Currently, THIP is not approved for chronic use, but recently a new $GABA_A$ receptor agonist, ganaxolone, which has fewer side effects has been approved by the FDA and EU (Knight et al., 2022; Monaghan et al., 1999). Therefore, this drug would be a possible alternative that can be given to patients once its effect on oscillations is determined.

On the other hand, CGS9895, which targets $\alpha^+\beta^-$ interface of $GABA_A$ receptors (Ramerstorfer et al., 2011; Sieghart et al., 2012), abolished oscillations but this effect was not reversible. With electrical stimulation, there was no change in stimulation efficiency with the application of the

drug. This shows that targeting only certain subunits in $GABA_A$ can abolish oscillations and improve stimulation efficiency.

Baclofen, a $GABA_B$ agonist (Bowery et al., 1980; Evenseth et al., 2020) had an inconsistent effect on the oscillations. The oscillations were only abolished in some channels and not in others. In the same way, we observed no significant change in stimulation efficiency with the drug. Therefore, it can be confirmed that baclofen does not have any influence on the oscillations or the stimulation efficiency.

GluN2A subunit-specific antagonist, memantine (M. B. Phillips et al., 2024) had reversibly abolished oscillations. We also observed an increase in stimulation efficiency with the drug which was also reversible upon washout. However, we observed an unspecific effect of memantine on the spike amplitude (3.2.4).

Carvedilol, which is an adrenergic blocker (Ruffolo et al., 1990), had irreversibly abolished oscillations. However, the stimulation efficiency did not improve with the drug. We observe an increase in stimulation efficiency with washout, which could likely be because of the calculation artefact from having low spiking activity during washout which means lower prestimulus action potential rate and therefore higher stimulation efficiency.

In conclusion, we can see that the pharmacological drug, THIP which targets the δ-subunit of $GABA_A$ receptors can abolish oscillations effectively and improve stimulation efficiency. This result is in concordance with the previous finding that benzodiazepines that target the $\alpha^+\gamma^-$ interface of the $GABA_A$ receptor are most suitable to abolish oscillations and improve electrical stimulation by an implant.

3.3. Discussion

The therapeutic effect of retinal implants in the treatment of blindness falls behind expectations. The intrinsic oscillatory activity in the degenerated retina is shown to be a contributing factor for the reduced stimulation efficiency (Gehlen et al., 2020; Haselier et al., 2017). In this study, we tested five methods to abolish oscillations and improve the electrical stimulation of RGCs, from our understanding of the origin of oscillation: 1) Targeting ON bipolar cells, 2) Blocking the coupling between ON bipolar cells and AII amacrine cells, 3) Hyperpolarising ON bipolar cells or AII amacrine cells, 4) Blocking adrenergic amacrine cells and 5) Blocking NMDA receptors.

With the degeneration of photoreceptors, the ON bipolar cells and AII amacrine cells were found to be hyperpolarised and this change in potential in AII amacrine cells shifted the potential to a range that produced oscillations (Borowska et al., 2011; Choi et al., 2014; Trenholm et al., 2012). Therefore, one of the strategies to abolish oscillations is by depolarising or further hyperpolarising ON bipolar cells, so that the potential of AII amacrine cells shifts out of this range. Depolarising these cells by blocking the potassium channel, Kv1.3 did not abolish oscillations. Hyperpolarising it further using voriconazole, a clinically approved drug which blocks TRPM1 receptors (Xiong et al., 2015), abolished oscillations. This further proves

that oscillations are seen when the membrane potential of AII is within a certain potential range that opens voltage-gated Na^+ channels. Voriconazole would have hyperpolarised it further and shifted it outside this range, abolishing oscillations. However, the reason for the hyperpolarised resting potential of ON bipolar cells after photoreceptor degeneration remains unclear and may involve downregulation of the mGluR6 signaling cascade (Borowska et al., 2011). Hyperpolarising the ON bipolar cells with metabotropic glutamate agonist, 2-amino-4-phosphonobutric acid (APB or L-AP4) was shown to have an inconsistent effect on the oscillations with some cells showing low frequency oscillations.

Our findings are in alignment with the hypothesis that the oscillations are formed by the electrically coupled network of ON bipolar cells and AII amacrine cells (Borowska et al., 2011; Trenholm et al., 2012; Trenholm & Awatramani, 2015). The blocking of TRPM1 receptors with voriconazole and the resultant hyperpolarisation of ON bipolar cells changed the membrane potential of AII amacrine cells by electrical coupling. This abolished the oscillations. However, the second hypothesis that the oscillations are solely formed by the rhythmic spiking of the hyperpolarised AII amacrine cells (Choi et al., 2014; Yee et al., 2012) cannot be discredited from our results either. Voriconazole would have further hyperpolarised the AII amacrine cell and shifted it outside the range that produced rhythmic bursts in them.

Even though voriconazole reversibly abolished oscillations, the stimulation efficiency did not increase with the drug. This could be because voriconazole also blocks TRPM3 receptors (Xiong et al., 2015), which are found in RGCs (Webster et al., 2020), thereby reducing the excitability of the RGCs.

The next strategy is to block the gap junction electrical coupling between ON bipolar cells and AII amacrine cells. The influence of gap junction coupling on oscillations has been a topic of debate. The studies that support the hypothesis that oscillations originate from an electrically coupled network of ON bipolar cells and AII amacrine cells claim that gap junctions are necessary, as blocking them using MFA abolished oscillations (Biswas et al., 2014; Borowska et al., 2011; Menzler et al., 2014; Menzler & Zeck, 2011; Toychiev et al., 2013; Trenholm et al., 2012). The other hypothesis states that amacrine cells are solely responsible for oscillation and that gap junctions do not play a role (Choi et al., 2014; Yee et al., 2012). In this work, we have tested carbenoxolone, a non-selective gap junction blocker like MFA. It was able to abolish oscillations and improve stimulation efficiency, but the effect was not completely reversible. This finding suggests that the electrical coupling between ON bipolar cells and AII amacrine cells may be necessary for the generation of the oscillations.

On testing a gap junction blocker quinine, that targeted gap junctions with connexins Cx45 and Cx36 (Srinivas et al., 2001) that are present in ON bipolar cells and AII amacrine cells (Bloomfield & Völgyi, 2009; Han & Massey, 2005; Lin et al., 2005), a low frequency oscillation was observed. This can be explained by the fact that quinine also acts on the M-type K channel and blocks it (Imai et al., 1999). Also, the low frequency oscillation observed here with quinine looked very similar to the low frequency oscillation produced by linopiridine hydrochloride (LP), an M-type K channel antagonist (Choi et al., 2014). Therefore, this would propose that this oscillation could be the result of the binding of quinine to these channels.

In the same manner, MFA also acts as an M type K channel enhancer (Peretz et al., 2005). M type K channel agonist, flupirtine, was shown to abolish oscillation (Choi et al., 2014). Therefore, MFA abolishing oscillations could be due to the non-specific binding of MFA onto M type K channels. However, MFA showed an inconsistent effect on oscillations and stimulation efficiency (doctoral thesis of Christine Haselier (Haselier et al., 2016)). Another drug that would enhance the M-type K channel and could abolish oscillations is retigabine. Retigabine is a commonly used M-type K channel enhancer (Cooper & Jan, 2003) which was FDA-approved until 2013, but due to side effects from long-term use, the approval was withdrawn (Clark et al., 2015). Similar drugs with fewer side effects are currently being developed.

Hyperpolarising ON bipolar cells or AII amacrine cells should shift the membrane potential of AII amacrine cells outside of the potential range that would open oscillation-producing voltage-gated Na^+ channels. This can be achieved by activating glycine, GABA or $GABA_A$ receptors and was shown to abolish oscillations (Gehlen et al., 2020). In this study, we showed that THIP, which targets the δ subunit of $GABA_A$ receptors, reversibly abolished oscillations and improved stimulation efficiency. Therefore, targeting $GABA_A$ receptors containing the δ-subunit using THIP (present study) and $GABA_A$ receptors containing $\alpha^+\gamma^-$ subunit using benzodiazepines (Gehlen et al., 2020) both abolished oscillations, indicating that different types of $GABA_A$ receptors are employed on cells involved in the generation of oscillations. $GABA_B$ agonist, baclofen, or $GABA_B$ antagonist, CGP54626, did not have any effect on oscillations. This shows that $GABA_B$ receptors are not involved in the generation or transmission of oscillations.

Another possibility on how GABA-modulating drugs influence oscillations is through the generation of sporadic postsynaptic potentials (sPSPs). These are small events that occur at low frequency in bipolar cells. They were only found in bipolar cells that do not have oscillations and, therefore, were thought to be the reason for non-oscillatory activity in some RGCs (Borowska et al., 2011). sPSPs were found to be mediated by Cl^- channels (Borowska et al., 2011), mostly gated by GABA or glycine receptors, which are upregulated at bipolar cell terminals (Varela et al., 2003). Therefore, GABA-modulating drugs could be binding to the bipolar cell terminals, hyperpolarising the cells and producing more sPSPs, thereby abolishing oscillations in RGCs.

Amacrine cells provide inhibitory input to bipolar cells through GABA and glycine. Blocking the inhibitory inputs produced low frequency oscillations in bipolar cells (Biswas et al., 2014; Borowska et al., 2011; Margolis & Detwiler, 2011; Menzler et al., 2014; Ye & Goo, 2007), which are mediated by L-type Ca^{2+} channels (Choi et al., 2014; Yee et al., 2012). Ligands for cholinergic receptors targeted by one of the few exciting amacrine cell types, the cholinergic amacrine cell, have never been tested and could be a possible strategy to abolish oscillations, as this would mimic the GABAergic inhibition.

Amacrine cells receive inputs from both bipolar cells and other amacrine cells. Bipolar cells give glutamatergic inputs, whereas amacrine cells provide GABAergic, glycinergic, dopaminergic and cholinergic inputs (Gleason, 2012). To enhance the activity of amacrine

cells, we can either increase the glutamatergic input or block the inhibitory inputs. However, increasing the glutamate input would lead to overall excitation in the retina and not only in the amacrine cells. This might trigger a high tonic activity in RGCs and might lead to excitotoxicity.

In this thesis, we have tested blocking the effect of adrenergic type 2 wide field amacrine cells using carvedilol (Ruffolo et al., 1990). This abolished oscillations but the effect was not reversible showing a long-term effect on the retina. The stimulation efficiency did not change with the application of the drug. Blocking GABAergic or glycinergic input had been shown to produce a low frequency oscillation and is not suitable either (Biswas et al., 2014; Borowska et al., 2011; Menzler & Zeck, 2011; Yee et al., 2012). Therefore, identifying a drug that would specifically activate the amacrine cells would be a possible way to abolish oscillation.

Another method to abolish oscillations is to block glutamatergic inputs to the RGCs. There are three glutamatergic receptor types, AMPA, kainate and NMDA and blocking all three was shown to abolish oscillations (Biswas et al., 2014; Margolis & Detwiler, 2011; Menzler et al., 2014; Menzler & Zeck, 2011; Ye & Goo, 2007) but could affect the excitability of the cells. On testing two non-selective NMDA antagonists, D-AP5 and CPP and a GluN2A-specific NMDA antagonist, memantine, we observed that only memantine reversibly abolished oscillations and improved stimulation efficiency. In a previous study, the spontaneous activity associated with oscillations was abolished with D-AP5, however, its effect on oscillations was not determined (Yee et al., 2018). Here, on testing D-AP5 and CPP, we observed no change in the oscillation. Memantine, which targeted a specific subunit of NMDA receptors, GluN2A, that was upregulated in the degenerated retina (Yee et al., 2018), abolished oscillations and improved stimulation efficiency. However, memantine showed a non-specific effect on the amplitude of the spikes and may not be an ideal drug to improve retinal stimulation.

4. Phase specific stimulation

4.1. Introduction

An intrinsic oscillatory activity is observed with the loss of photoreceptors during retinal degeneration. These oscillations are accompanied by action potentials spiking in rhythmic bursts as observed in the *rd1* mouse retina, *rd10* mouse retina and MNU-induced degenerated macaque retina (J. Ahn et al., 2022; Biswas et al., 2014; Haselier et al., 2017; Margolis et al., 2008, 2014; Menzler et al., 2014; Menzler & Zeck, 2011; Poria & Dhingra, 2015; Zeck, 2016). The frequency of the rhythmic spiking bursts is in the range of 4-15Hz in these mouse models (Zeck, 2016), which is equivalent to the frequency of oscillation.

In the *rd1* retina, rhythmic firing was observed in 85% of RGCs at P35- P70 and 75% in P160-P200 mice (Menzler & Zeck, 2011). Here, the earliest age at which oscillations and spiking rhythmicity were observed is at P12, which is at the onset of rod degeneration, and the spikes were bursting as doublets with two spikes per burst (Poria & Dhingra, 2015). In the *rd10* retina, the onset of oscillation and rhythmic firing is at P30, during which rods are mostly lost (J. Ahn et al., 2022; Haselier et al., 2017). As oscillation and rhythmic firing initially occur when cones remain intact, it could mean that it is produced through the rod pathway, probably in the cells that are postsynaptic to rods like AII amacrine cells. By P90- P100, 50% of RGCs showed rhythmic firing in the *rd10* retina (Menzler et al., 2014). The spiking in the rest of the RGCs was continuous without rhythmicity.

The ON bipolar cell and AII amacrine cell network that is involved in producing oscillation is also involved in rhythmic spiking. With degeneration, the change in membrane potential of ON bipolar cells causes a change in potential in AII amacrine cells through electrical coupling between these cells, which shifts the potential to a range that opens voltage-gated Na^+ channels in AII amacrine cells, producing oscillation (Borowska et al., 2011; Trenholm et al., 2012). Through the same electrical coupling, the oscillatory signals are sent back to ON bipolar cells. But AII amacrine cells have inhibitory glycinergic synapses to OFF bipolar cells. Therefore, inhibitory oscillatory signals are sent to OFF bipolar cells. Through glutamatergic synapses, the activity of ON and OFF bipolar cells is transferred to ON and OFF RGCs, respectively. It is hypothesised that the glutamatergic input from ON and OFF bipolar cells is also transferred to an unidentified GABAergic or glycinergic amacrine cell. These cells have inhibitory connections to the respective RGCs, thereby causing rhythmicity in the spiking activity in these RGCs (Margolis et al., 2014; Zeck, 2016).

The involvement of ON bipolar cell and AII amacrine cell network was formulated from several findings. The inhibition of AMPA and kainate glutamatergic input abolished both oscillations and rhythmic spiking (Biswas et al., 2014; Menzler et al., 2014; Menzler & Zeck, 2011). This shows that the origin of oscillations and rhythmic spiking is presynaptic to RGCs. Gap junction blockers abolished oscillations and rhythmic spiking, in agreement with the involvement of ON bipolar and AII amacrine cell networks (Biswas et al., 2014; Menzler et al., 2014; Menzler & Zeck, 2011). Blocking the glycinergic input using strychnine abolished

oscillations and reduced rhythmic spiking in OFF RGCs but had no effect on ON RGCs (Poria & Dhingra, 2015). This shows that the oscillatory and rhythmic spiking information is transferred from AII amacrine cells to OFF RGCs via the glycinergic synapse. Therefore, the oscillatory and rhythmic spiking inputs are likely transferred from the AII amacrine cells to ON RGCs through electrical coupling with ON bipolar cells and to OFF RGCs through the glycinergic synapse onto OFF bipolar cells.

Using patch-clamp recording, rhythmic spiking was observed in ON RGCs, OFF sustained RGCs and OFF transient RGCs. ON cells showed monophasic inward-shaped oscillatory synaptic current, whereas OFF sustained and OFF transient cells showed biphasic oscillatory synaptic currents (Margolis et al., 2008). There is a phase shift between the rhythmic spiking of ON and OFF RGCs. As AII amacrine cells transferred excitatory inputs to ON RGCs and inhibitory inputs to OFF RGCs, these cells received in and out of phase oscillatory inputs respectively (Margolis et al., 2014; Menzler et al., 2014; Zeck, 2016).

Rhythmic spiking is correlated with the oscillation minima, with 2-10 spikes per burst in the *rd1* retina (Margolis et al., 2014; Menzler & Zeck, 2011; Zeck, 2016). This was mostly observed in alpha RGCs. In non-alpha RGCs, spikes were rarely rhythmic, and the few rhythmic bursts consisted of one or two spikes (Margolis et al., 2014). Another proposed reason for rhythmic spiking in some RGCs is the strong gap junction electrical coupling of RGCs or presynaptic cells in some regions of the degenerated retina (Zeck, 2016).

Degenerated retina showed a reduced response to electrical stimulation (Gehlen et al., 2020; Haselier et al., 2017; Yoo et al., 2024). Multiple oscillatory peaks and spatially spread responses were seen in these retina with electrical stimulation (J. Ahn et al., 2022). The electrically evoked responses were mostly mediated by presynaptic cells rather than by the direct activation of RGCs. This was shown by glutamate receptor blockers producing no electrically evoked responses in the *rd1* retina (J. Ahn et al., 2022). On the other hand, with the application of gap junction blockers, a single peak in electrically evoked response is observed, similar to that in wt. This shows that gap junction-mediated electrical coupling is involved in spreading the electrically evoked response temporally, producing multiple peaks. Therefore, in conclusion, the bipolar cells get activated with electrical stimulation and thereby activate the downstream RGCs. ON bipolar cells also activate AII amacrine cells via electrical coupling, and this coupled network also activates RGCs, producing multiple oscillatory peaks in the electrically evoked response. When the gap junctions were blocked, the RGCs received inputs only from bipolar cells directly, producing a single electrically evoked response (J. Ahn et al., 2022).

On comparing the electrically evoked spikes between the rhythmic and non-rhythmic spiking cells, the cells that have rhythmic firing showed a significantly lower response (Haselier et al., 2017). In our recordings from the *rd10* retina, we observed both rhythmic spiking (referred to as phase-locked spiking cells) and non-rhythmic spiking (referred to as non-phase-locked spiking cells) cells. To get a better stimulation response, we tried targeting the non-phase-locked spiking cells. Here, we showed that this can be achieved by stimulating at the maxima

of the oscillation, when the rhythmic spikes are phase-locked to the minima (Menzler & Zeck, 2011; Zeck, 2016).

The following section shows the results of stimulating the *rd10* retina at the maxima and minima of the oscillation.

4.2. Results

4.2.1. Some cells fire phase-locked to the oscillation in the degenerated retina

In-vitro recordings from five 4-5 months *rd10* mice were collected using 60 electrodes MCS MEA. From these recordings (n=12), oscillations were identified in an average of approximately 33.03 ± 4.89% of the 60 electrodes, with variability across experiments depending on the retinal preparation.

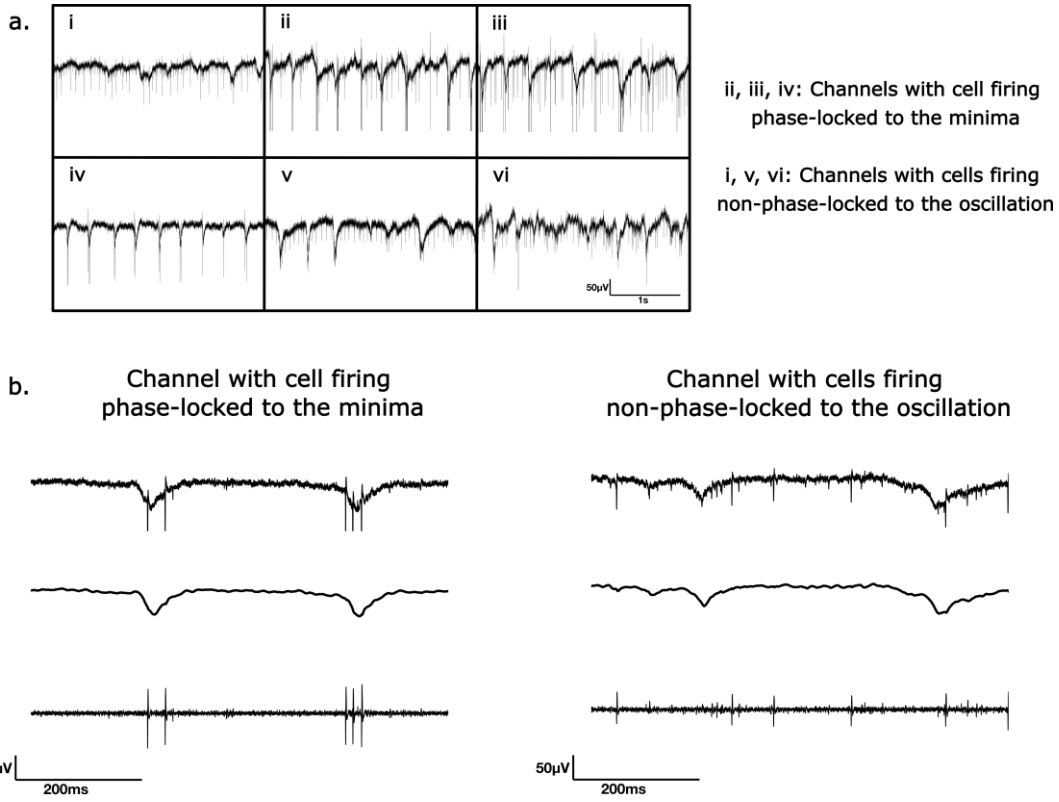

	Condition (out of all channels that show oscillation)	Percentage
1.	Channels with spikes phase locked to the minima	40.52 ± 3.21
2.	Channels with large amplitude spikes phase locked to the minima	19.62 ± 2.92

Fig 4.2.1: Phase-locked spiking in channels: (a) The recording from six MEA electrodes showing oscillations in *rd10* retina. The channels ii, iii and iv have spikes phase-locked to the minima of the oscillation and channels i, v and vi have non-phase-locked spiking cells. (b) One of the channels in (a) has spikes phase-locked to the minima of oscillations (left) and another has continuous spiking (right). Figure b shows top: raw recording, middle: lowpass filtered recordings (0.1-50Hz) to visualise the LFP and bottom: highpass filtered recordings (200-3000Hz) to visualise the spikes. The table gives the percentage of phase-locked spiking cells in the recording.

Among the electrodes that showed oscillations, an average of 40.52 ± 3.21% (from n=12 recordings) had cells with spikes phase-locked to the minima of the oscillation (Fig 4.2.1b). In the rest of the electrodes, the cells showed spikes without any phase-locking. There were very few, around 2-3 electrodes from 12 recordings, that had cells with spikes phase-locked to the maxima of the oscillation. Therefore, this condition was not considered in our analysis.

Each electrode had recordings from multiple cells of varying amplitudes. The phase-locked spiking cells are mostly seen with a larger amplitude than non-phase-locked spiking cells (in 19.62 ± 2.92% cases). Therefore, these cells are separated from the remaining cells by marking the threshold at a larger amplitude.

4.2.2. Stimulating at maxima is preferred over the minima of oscillation

Fig 4.2.2 shows the effect of stimulating at the maxima and minima in all the channels that showed oscillations. We observed that stimulation produced an increase in spike rate at maxima and minima with a larger increase at maxima.

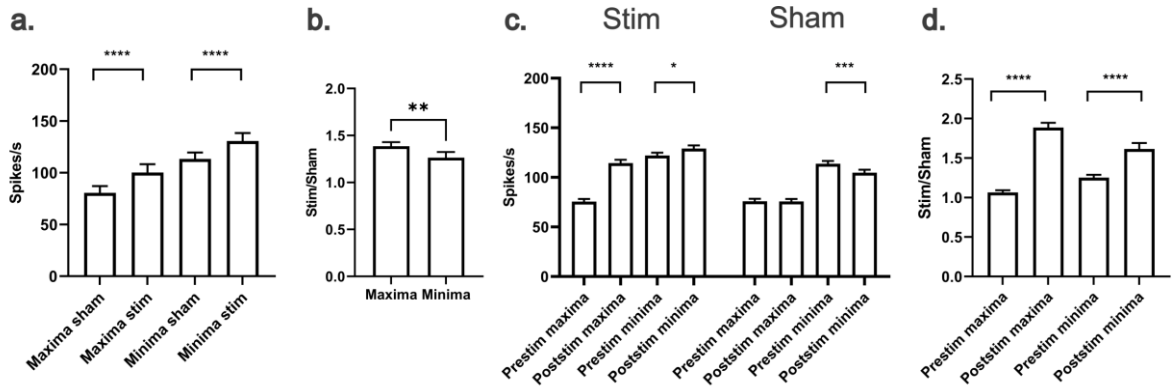

Fig 4.2.2: Stimulating at the maxima and minima: (a) Spike rate comparison between maxima sham, maxima stim, minima sham and minima stim for a window of 130ms. Minima sham has a higher spike rate compared to maxima sham due to the phase-locked spikes. Spike rate increases with stim for both cases. (b) Stim/Sham for maxima is higher than for minima. (c) Spike rate comparison between prestim maxima, poststim maxima, prestim minima, and poststim minima for stim and sham (prestim and poststim spike rate calculated for a window of 65ms). There is excitation at maxima and minima. Spikes reduced in sham minima. (d) Stim/Sham for prestim and poststim shows excitation at both maxima and minima. (A total of 12 retinal pieces from 5 *rd10* mice were analysed. Wilcoxon signed-rank test was used to compare between each group (****: $p<0.0001$; ***: $p\leq0.001$; **: $p\leq0.01$; *: $p\leq0.05$)).

We determined the spike rate at a 130 ms window (Fig 4.2.2 a,b), 65 ms before the stimulus and 65 ms after the stimulus (Fig 4.2.2 c,d). This spike rate was compared for maxima, minima, stim (electrically stimulated) and sham (control) conditions. With electrical stimulation, an increase in spike rate was observed for both maxima and minima (Fig 4.2.2a). In the sham condition, the spike rate was higher at the minima than at the maxima. This difference in spike rate is due to the high incidence of spikes being phase-locked to the minima. To identify the phase that produces a greater increase, we plotted the stim normalised to sham (Fig 4.2.2 b). This ratio was higher for maxima compared to minima (maxima mean= 1.39, minima mean= 1.26).

On comparing the spike rate at 65ms prestim and 65ms poststim (Fig 4.2.2c) for stim, the poststim showed an excitation for both maxima and minima with a higher increase for maxima. In the sham, we observed a decrease in spikes at the minima. This was unexpected because, in the sham condition without electrical stimulation, the spike rate should remain unchanged. Therefore, it was likely due to a calculation artefact (Fig 4.2.3). Applying stim/sham allowed normalisation of the data and reduced the influence of this artefact. Fig 4.2.2d shows the resultant effect of stimulation on prestim and poststim after normalising and we observed a significant increase in both maxima and minima, with slightly higher increase for maxima (prestim maxima mean= 1.07, poststim maxima mean= 1.89, prestim minima mean= 1.25, poststim minima mean= 1.62).

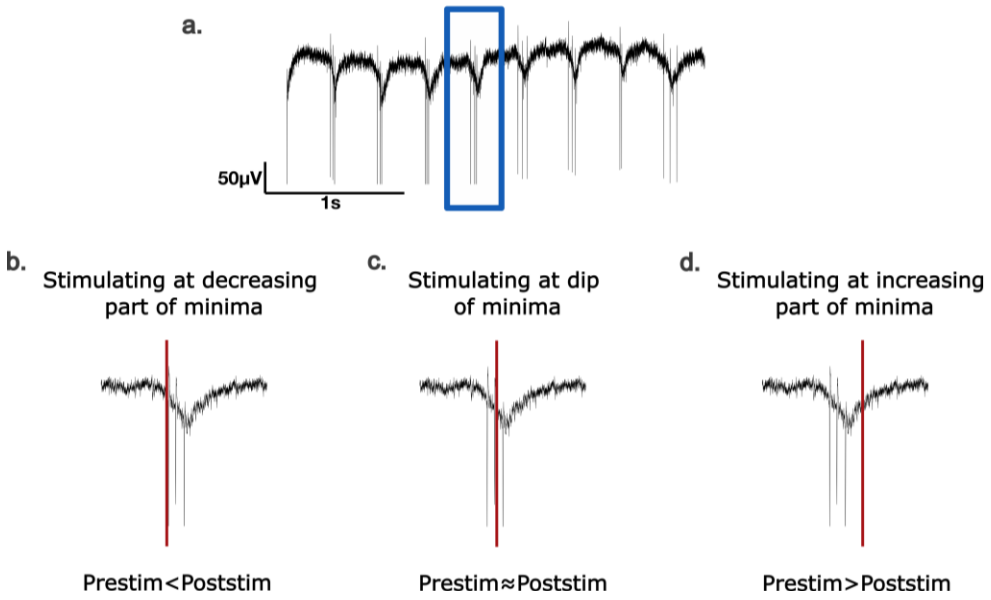

Fig 4.2.3: Artefact in the analysis: recording from *rd10* retina (a) shows spiking phase-locked to the minima of the oscillations. (b-d) One of the minima is enlarged to visualise the drawbacks of variable trigger placement (red) in the minima and the comparison of prestim spikes and poststim spikes. The majority of the analysed samples have the trigger placed in the dip (c) or the increasing part of the minima (d) rather than at the decreasing part of the minima (b).

In the minima sham, the spike rate after stimulation (poststim) is lower than before stimulation (prestim). This difference mainly results from an artefact in the analysis. As described in chapter 2 (section 2.6.3 and 2.6.4), the trigger for electrical stimulation is extracted from analysing the oscillation in one of the channels. In other channels, the oscillation may be slightly shifted in phase. Therefore, in different channels stimulation at the minima may occur the decreasing phase (Fig 4.2.3b), dip (Fig 4.2.3c) or increasing phase (Fig 4.2.3d) of the oscillation, whereas maxima is the flat region between multiple minima. During manual classification, we primarily selected cases where stimulation occurred at the dip or increasing phase of the minima. This choice was made because an electrical stimulation artefact often appears immediately after stimulation, making it difficult to observe the rest of the oscillation. When stimulation occurred at the dip or increasing phase of minima, the segment corresponding to the decreasing phase was still visible before stimulation, making it possible to identify the minima. In contrast, when stimulation occurred at the decreasing phase, the

signal before stimulation did not clearly show the minima and the post-stimulation signal was often dominated by artefact noise. These trials were therefore excluded.

As a result, most of our analysed trials involve dip and increasing phase of minima, where the number of poststim spikes is nearly equal to or lesser than the number of prestim spikes (Fig 4.2.3 c, d). This imbalance explains the lower spike rate observed in poststim compared to prestim when stimulated (the next section confirms this explanation). To rectify this problem, we have compared the ratio of stim by sham for prestim and poststim. Now, the artefact at minima gets normalised and we see the resultant effect of stimulation.

In conclusion (from Fig 4.2.2), we observed that stimulation at maxima produced a higher electrically evoked response than stimulation at minima. In the following sections, we examined the cause of this preference.

4.2.3. Electrical stimulation produces excitation at maxima but phase-locked spiking reduces the excitation at the minima

To determine whether the comparatively weaker electrically evoked spiking at minima results from spikes being phase-locked to the minima, we evaluated the differences in spike rate for the channels that have phase-locked spikes versus the channels that have non-phase-locked spikes. From the previous analysis, we separated the 40.52% of channels that have spikes phase-locked to the minima of the oscillation and the rest of the channels without phase-locked spikes (remaining 59.48%). The spike rates for either case were determined and compared. The results showed that the channels with non-phase-locked firing cells showed excitation when stimulated at maxima and minima whereas the channels with phase-locked firing cells showed a more pronounced excitation when stimulated at the maxima than at the minima.

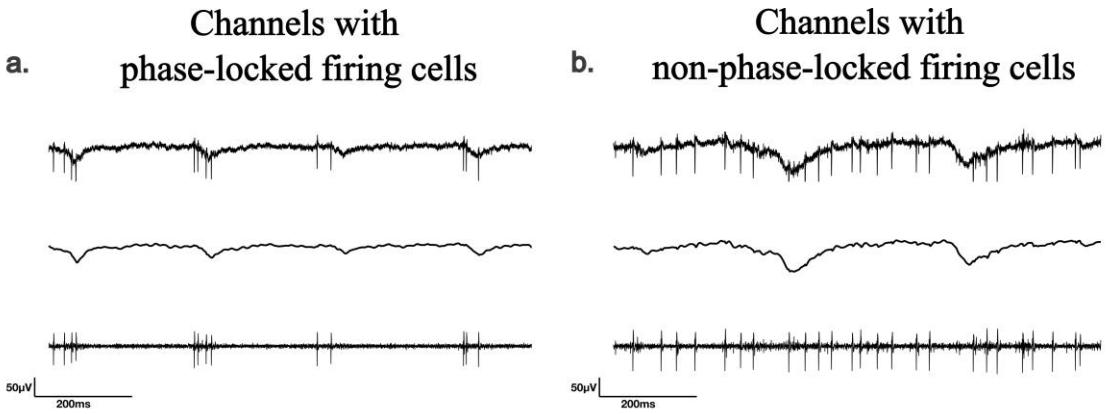

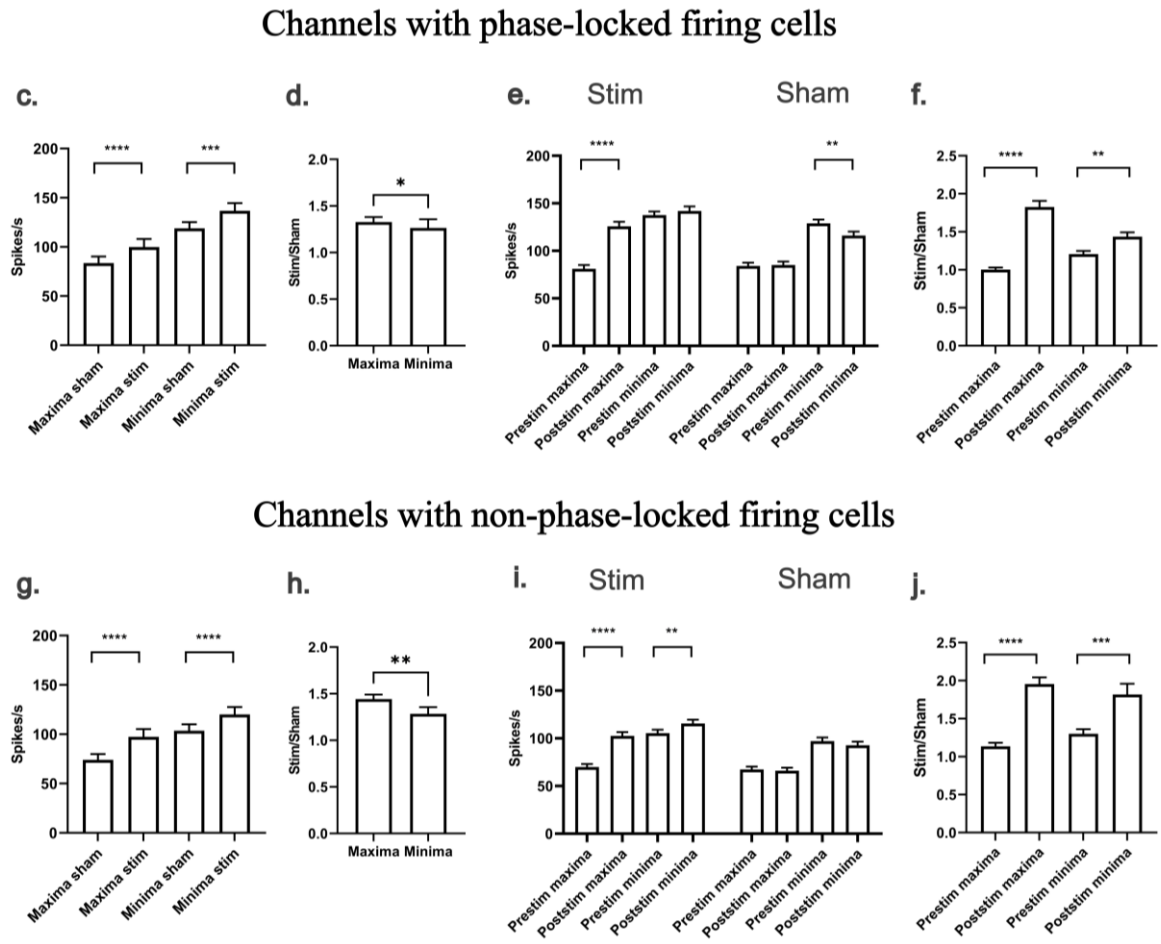

Fig 4.2.4: Channels with phase-locked spikes versus non-phase-locked spikes: the recording of a channel that has cells spiking phase-locked to the minima of the oscillation (a) and channel with non-phase-locked spiking cells (b). The figure shows top: raw recording, middle: lowpass filtered recording (0.1-50Hz) and highpass filtered recording (200-3000Hz). Spike rate (for a window of 130ms) comparison between maxima sham, maxima stim, minima sham and minima stim for channels with phase-locked spikes (c) and channels with non-phase-locked spikes (g). Spike rate increases with stim for both cases. Stim/Sham is higher for maxima than minima for channels with phase-locked spikes (d) and channels with non-phase-locked spikes (h). Spike rate comparison between prestim maxima, poststim maxima, prestim minima, and poststim minima for stim and sham for channels with phase-locked spikes (e) and channels with non-phase-locked spikes (i) (prestim and poststim spike rate calculated for a window of 65ms). There is excitation at maxima for both cases and at minima for non-phase-locked spiking channels. Inhibition in sham minima for phase-locked spiking channels. Stim/Sham of prestim and poststim for channels with phase-locked spikes (f) and non-phase-locked spikes (j). There is excitation at maxima and minima, but the excitation at minima for channels with phase-locking is comparatively lower. (A total of 12 retinal pieces from 5 *rd10* mice were analysed. Wilcoxon signed-rank test was used to compare between each group (****: $p<0.0001$; ***: $p\leq0.001$; **: $p\leq0.01$; *: $p\leq0.05$)).

Fig 4.2.4 c-f show the results for the channels with phase-locked spikes and Fig 4.2.4 g-j for the channels with non-phase-locked spikes. In both cases with electrical stimulation, we observed an increase in spike rate at the maxima and minima (Fig 4.2.4 c,g), though the increase was slightly smaller at minima for the channels with phase-locked spiking cells. The stim/sham ratio was higher for maxima in both cases (Fig 4.2.4 d,h), with a significantly larger increase

for the channels with non-phase-locked spiking cells (channels with phase-locked spikes: maxima mean= 1.33, minima mean= 1.26; channels with non-phase-locked spikes: maxima mean= 1.44, minima mean= 1.28).

On comparing the spike rate at 65ms prestim and 65ms poststim with stimulation, the spike rate increased at maxima and did not change at the minima for the channels with phase-locked spikes (Fig 4.2.4e). For channels with non-phase-locked spikes (Fig 4.2.4i), spike rate increased at both maxima and minima. For sham, there was no change in spike rate at maxima for both cases and at minima for channels with non-phase-locked spikes. For channels with phase-locked spikes, the poststim showed lesser spike rate than prestim, attributed to a calculation artefact (Fig 4.2.3). By normalising stim/sham (Fig 4.2.4f,j), we observed an increase at maxima and minima for both cases, but with a smaller increase at minima for channels with phase-locked spikes. (channels with phase-locked spikes: prestim maxima mean= 1.002, poststim maxima mean= 1.83, prestim minima mean= 1.21, poststim minima mean= 1.44; channels with non-phase-locked spikes: prestim maxima mean= 1.14, poststim maxima mean= 1.96, prestim minima mean= 1.30, poststim minima mean= 1.82).

This result confirms that the calculation artefact (Fig 4.2.3) is caused by a bias in the classification of the minima and maxima. The poststim value is lower than the prestim value because, when more samples from the dip and increasing phase of the oscillation are classified as the minima, the poststim period, which occurs during the increasing phase of the oscillation, contains no spikes, whereas the prestim period contains all the phase-locked spikes. This interpretation is supported by the observation that this difference occurs only in channels with phase-locked spikes. In contrast, non-phase-locked spiking channels show similar spike rates in prestim and poststim periods due to the absence of phase locking.

This artefact-related reduction in spike rates at minima makes it difficult to identify the effect of electrical stimulation, as indicated by the lack of change in spike rate with stimulation (Fig 4.2.4e) for phase-locked spiking channels. Whereas for the channels with non-phase-locked spikes, there was a significant increase in spike rate with stimulation. On normalising the artefact by comparing stim/sham, we observed excitation with stimulation for both cases, but slightly lower excitation for the channels with phase-locked spikes. Therefore, this points to the fact that cells can be stimulated at both maxima and minima but with lesser excitation at the minima for the channel with phase-locked spikes.

Each channel recorded signals from multiple cells; therefore, in most cases, channels classified as phase-locked spiking contained spikes from both phase-locked and non-phase-locked firing cells. In the next section, we separated the phase-locked and non-phase-locked spiking cells from the channels that showed phase-locked spikes only.

4.2.4. Excitation of non-phase-locked spiking cells at maxima and mild inhibition of phase-locked spiking cells at minima

In the previous section (4.2.3), we separated the channels into those that have phase-locked firing cells versus non-phase-locked firing cells. As each channel had recordings from multiple

cells, the channels classified as with phase-locked firing cells may include spikes from non-phase-locked firing cells as well. Therefore, we separated the cells in these channels into phase-locked firing and non-phase-locked firing. This was achieved by using the 19.62% of channels that showed large amplitude spikes phase-locked to the minima. We separated these spikes by marking a threshold at a higher amplitude. This is then compared to all of the spikes (including maximum amplitude spikes) for the same 19.62% of the channels. A representative image of this classification is shown in Fig 4.2.5 a. The results showed that a strong excitation occurs when stimulated at the maxima of non-phase-locked firing cells. For phase-locked firing cells, we observed no change when stimulated at maxima and a mild inhibition when stimulated at the minima.

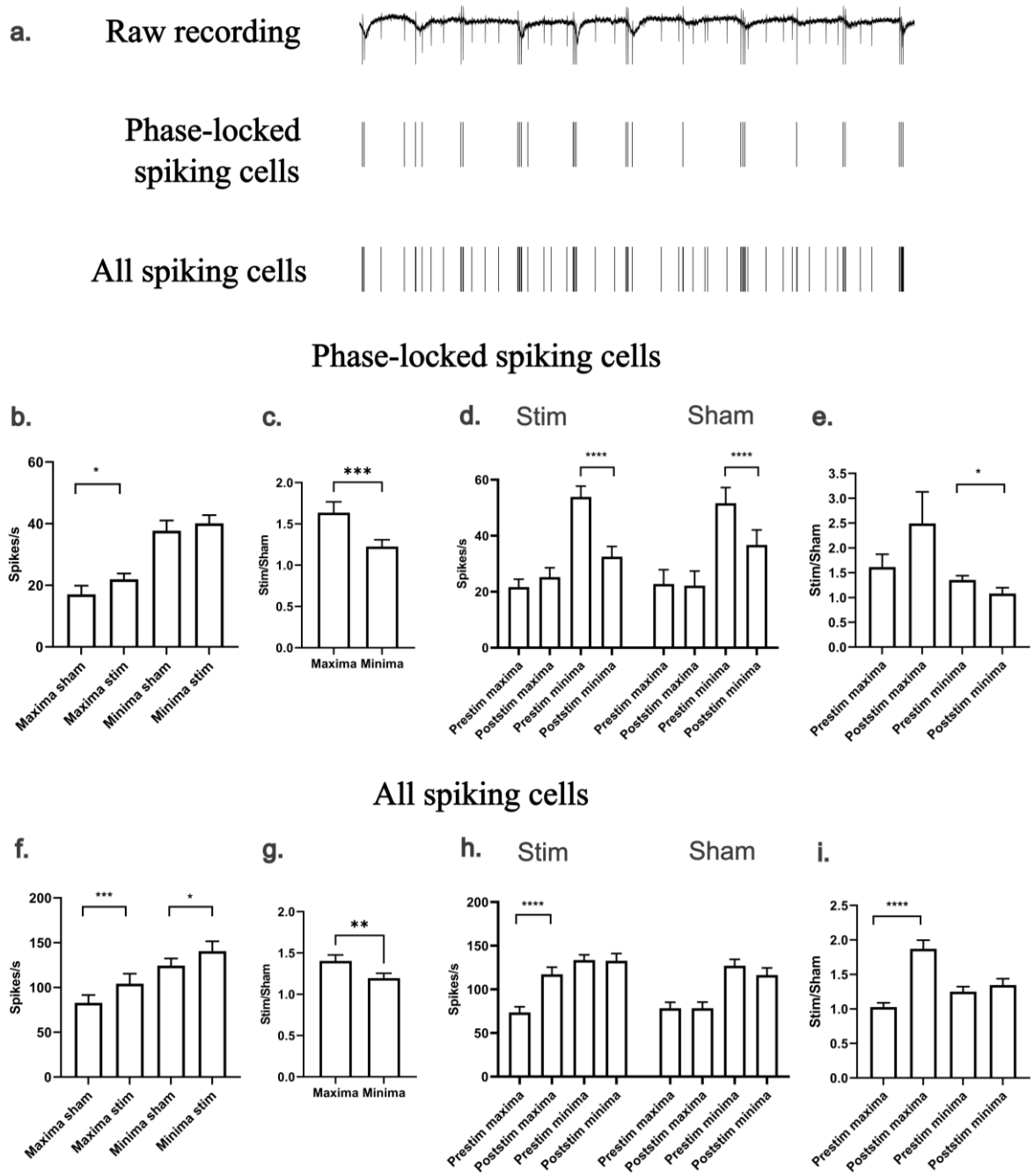

Fig 4.2.5: Phase-locked spiking cells versus non-phase-locked spiking cells: the phase-locked spiking cells were separated from the others by manually marking a threshold and separating them. (a) shows representative recordings of the classification with top: raw recording, middle: separated phase-locked spikes and bottom: all the detected spikes (highpass filter frequency 200-3000Hz). Spike rate (a window of 130ms) comparison between maxima sham, maxima stim, minima sham and minima stim for phase-locked spiking cells (b) and all spiking cells (f). Spike rate increases with stim at maxima for phase-locked spiking cells and all spiking cells. At minima, spike rate increases for all spiking cells. Stim/Sham is higher for maxima than minima for phase-locked spiking cells (c) and all spiking cells (g). Spike rate comparison between prestim maxima, poststim maxima, prestim minima, and poststim minima for stim and sham for phase-locked spiking cells (d) and all spiking cells (h) (prestim and poststim spike rate calculated for a window of 65ms). Reduced spike rate at minima for stim and sham for phase-locked spiking cells. Excitation at maxima for all spiking cells. Stim/Sham for prestim and poststim for phase-locked spiking cells (e) and all spiking cells (i). Inhibition at minima for phase-locked spiking cells and excitation at maxima for all spiking cells. (A total of 5 retinal pieces from 3 *rd10* mice were analysed. Wilcoxon signed-rank test was used to compare between each group (****: $p<0.0001$; ***: $p\leq0.001$; **: $p\leq0.01$; *: $p\leq0.05$)).

Fig 4.2.5 b-e show the results for the phase-locked spiking cells and Fig 4.2.5 f-i for all the spiking cells in the channel (that includes both phase-locked and non-phase-locked spiking cells). In all spiking cells (Fig 4.2.5f), there was a significant increase in spike rate with stimulation at both maxima and minima, though a higher increase at maxima. Therefore, stim/sham showed a preference for maxima (Fig 4.2.5g). For the phase-locked spiking cells, a small increase in spike rate with stimulation was seen at the maxima and no difference at the minima (Fig 4.2.5b). This small increase at the maxima caused a preference for maxima as seen with stim/sham (Fig 4.2.5c; phase-locked spiking cells: maxima mean= 1.64, minima mean= 1.23; all spiking cells: maxima mean= 1.4, minima mean= 1.2).

On comparing the prestim and poststim, we observed no change at maxima and a decrease in spike rate at minima for phase-locked spiking cells (Fig 4.2.5d). However, this decrease was observed in both stim and sham and probably caused by the calculation artefact (Fig 4.2.3). By normalising the artefact, we observed a small inhibition at minima (Fig 4.2.5e). However, phase-locked spiking cells did not show excitation at the maxima. On the other hand, on considering all spiking cells, there was significant excitation at the maxima and no change at minima. Stim/ sham Fig 4.2.5i) also showed a strong excitation at maxima and no change at minima ((phase-locked spiking cells: prestim maxima mean= 1.61, poststim maxima mean= 2.49, prestim minima mean= 1.36, poststim minima mean= 1.08; all spiking cells: prestim maxima mean= 1.03, poststim maxima mean= 1.87, prestim minima mean= 1.25, poststim minima mean= 1.35).

In conclusion, we observed a small inhibition at the minima for the phase-locked spiking cells. At the maxima, there was a strong excitation of non-phase-locked spiking cells.

However, there were some discrepancies in this data. 1) Some cells showed no response to electrical stimulation (Fig 4.2.6a) thereby reducing the effect when averaged. 2) Few cells shifted from phase-locked spiking to non-phase-locked spiking in the middle of the recording (Fig 4.2.6b). This could be attributed to the waxing and waning of the oscillation. It could also

be a result of electrical stimulation or the cells inherently not being phase-locked. These types of cells were removed from the data and the remaining cells were evaluated in the next section.

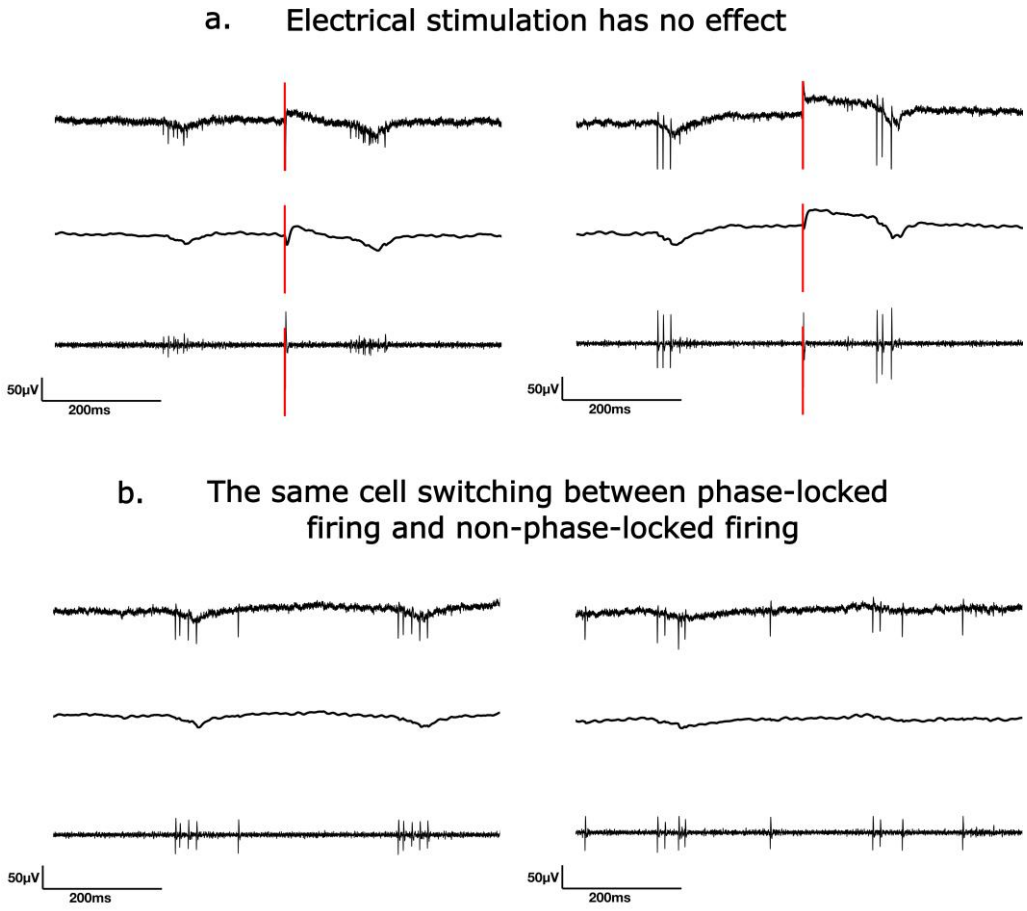

Fig 4.2.6: Inconsistencies in the signal (a) Recording showing no effect in spike rate with electrical stimulation (red) at maxima. (b) Recording of a phase-locked spiking cell (left) which lost its phase-locking after 70s during the recording. The figure shows top: raw recording, lowpass filtered recording (0.1-50Hz) to visualise the LFP and highpass filtered recording (200-3000Hz) to visualise the spikes.

4.2.5. Strong excitation at maxima and inhibition at minima in a subset of cells

This section compares the spike rate of the phase-locked and non-phase-locked spiking cells for a subset of channels that showed a stronger response. Here, we observed phase-locked firing cells getting inhibited when stimulated at minima, whereas the non-phase-locked firing cells were strongly excited when stimulated at maxima.

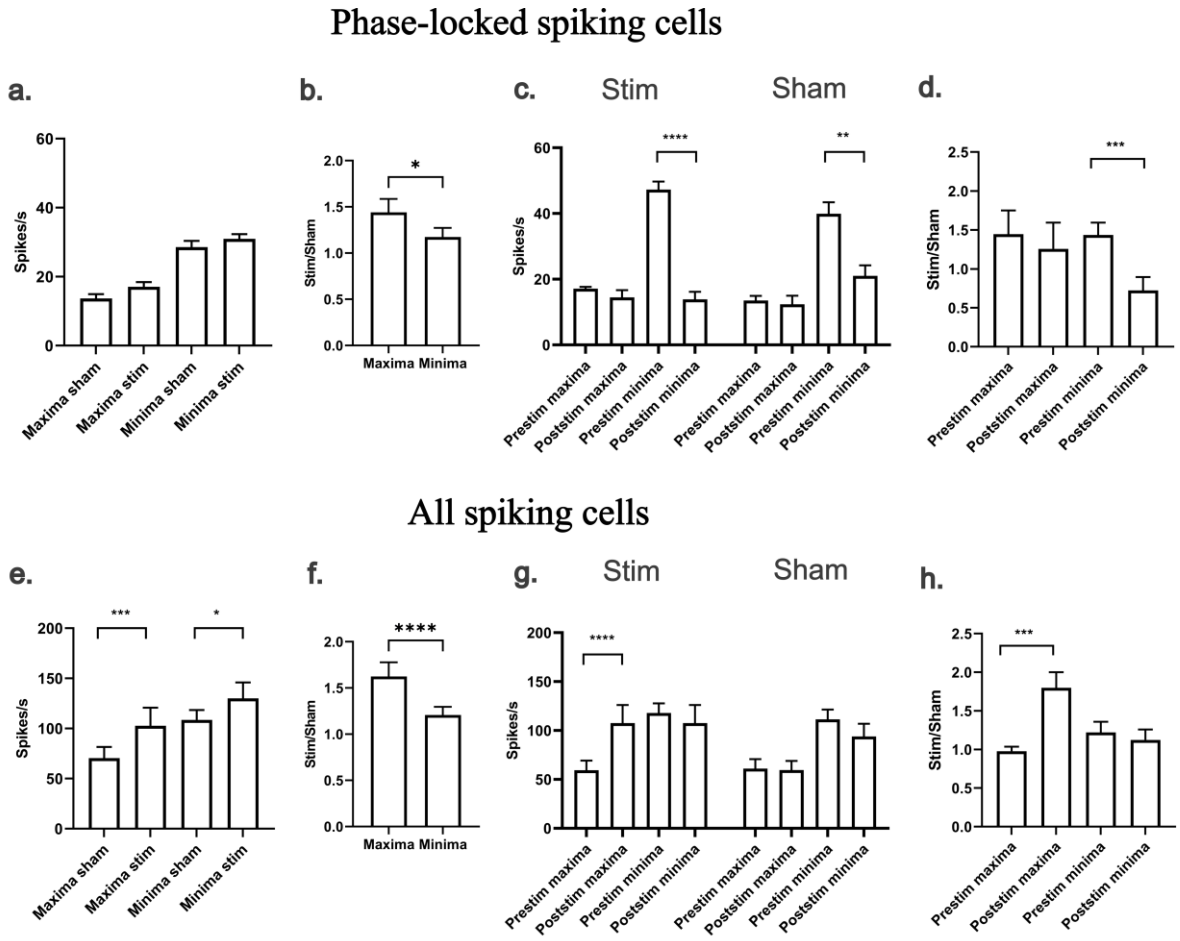

Fig 4.2.7: Subset of cells showing stronger effect: Spike rate (for a window of 130ms) comparison between maxima sham, maxima stim, minima sham and minima stim for phase-locked spiking cells (a) and all spiking cells (e). No change in spike rate with stim for phase-locked spiking cells. Spike rate increases at maxima and minima for all spiking cells. Stim/Sham is higher for maxima than minima for phase-locked spiking cells (b) and for all spiking cells (f). Spike rate comparison between prestim maxima, poststim maxima, prestim minima, and poststim minima for stim and sham phase-locked spiking cells (c) and all spiking cells (g) (prestim and poststim spike rate calculated for a window of 65ms). Reduced spike rate at minima for stim and sham for phase-locked spiking cells. Excitation at maxima for all spiking cells. Stim/Sham for prestim and poststim for phase-locked spiking cells (d) and all cells (h). Inhibition at minima for phase-locked spiking cells and excitation at maxima for all spiking cells. (A total of 4 retinal pieces from 2 *rd10* mice were analysed. Wilcoxon signed-rank test was used to compare between each group (****: $p<0.0001$; ***: $p\leq0.001$; **: $p\leq0.01$; *: $p\leq0.05$)).

Fig 4.2.7 a-d show results for phase-locked spiking cells and e-h for all the spiking cells in the channel (that includes both phase-locked and non-phase-locked spiking cells). For the phase-locked spiking cells, no difference was observed in the spike rate between stim and sham for both maxima and minima (Fig 4.2.7a). For all spiking cells, an increase in spike rate was seen at maxima and minima, with a smaller increase at the minima (Fig 4.2.7e). We observed a preference for maxima compared to minima for both cases (Fig 4.2.7 b,f), with a higher significance for all spiking cells (phase-locked spiking cells: maxima mean= 1.44, minima mean= 1.17; all spiking cells: maxima mean= 1.62, minima mean= 1.21).

On comparing the prestim and poststim, we observed a significant decrease in spike rate at minima in both stim and sham for phase-locked spiking cells (Fig 4.2.7c). The difference was more significant in stim than in sham. On normalising the effect of the calculation artefact (Fig 4.2.3) as stim/sham (Fig 4.2.7d), we observed a decrease in spike rate in poststim compared to prestim, indicating inhibition of phase-locked spiking cells with stimulation. For all spiking cells, we observed excitation at the maxima and no change at the minima (Fig 4.2.7g). From stim/sham (Fig 4.2.7h), we observed similar excitation at maxima and no change at minima (phase-locked spiking cells: prestim maxima mean= 1.45, poststim maxima mean= 1.26, prestim minima mean= 1.44, poststim minima mean= 0.72; all spiking cells: prestim maxima mean= 0.98, poststim maxima mean= 1.8, prestim minima mean= 1.22, poststim minima mean= 1.12).

Therefore, after cleaning up the data, we were able to compare the responses of phase-locked and non-phase-locked spiking cells to electrical stimulation. The cells that have spikes phase-locked to the minima of the oscillation did not get excited; they either showed no response at maxima and minima or were inhibited at minima with stimulation. The inhibition was only observed in a handful of cases. On the other hand, the non-phase-locked spiking cells showed strong excitation at the maxima with electrical stimulation.

4.2.6. Representative example of excitation at maxima and inhibition at minima

The following figure (Fig 4.2.8) is an example of the channels that showed excitation at the maxima and the inhibition at the minima. The excitation at the maxima (note the additional burst of spikes after the stimulus in a) originating from non-phase-locked spiking cells was a consistent response seen in ~70% of the cases. The cell in b fires 4 spikes at the first and the last minimum shown in the recording. Two of the spikes are missing upon stimulation in the middle minimum. This kind of response was observed in a few cases.

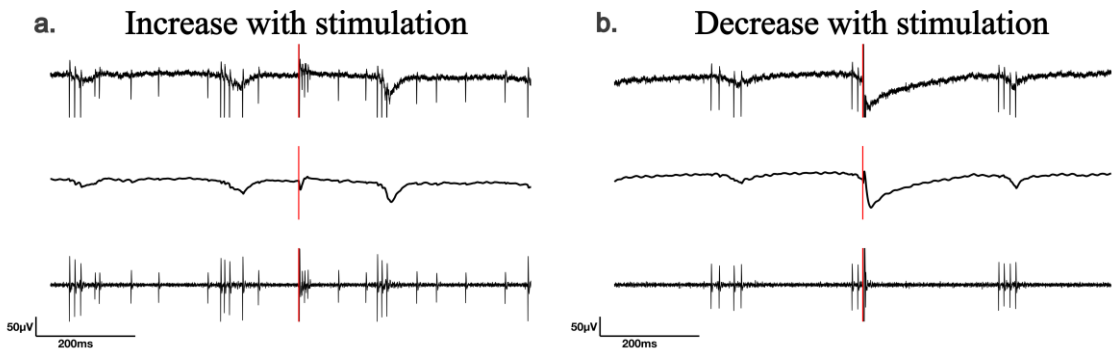

Fig 4.2.8: Example recordings from *rd10* retina showing excitation at maxima and inhibition at minima: (a) Recording showing an increase in spike rate with electrical stimulation (red) at maxima. (b) Recording showing a decrease in spike rate with electrical stimulation (red) at minima. The figure shows top: raw recording, middle: lowpass filtered recording (0.1-50Hz) to visualise the LFP and highpass filtered recording (200-3000Hz) to visualise the spikes.

In conclusion, stimulating the non-phase-locked spiking cells at the maxima seems to be suitable for achieving better stimulation efficiency. The phase-locked spikes were either

inhibited or showed no response and reduced the overall excitability at the minima. Therefore, the maxima of the oscillation is the preferred phase to be electrically stimulated by an implant.

4.3. Discussion

The oscillatory activity found in degenerated retina reduces stimulation efficiency (Gehlen et al., 2020; Haselier et al., 2017; Yoo et al., 2024). In these studies, the electrical stimulation was applied randomly throughout the recording, which yielded a low stimulation efficiency. Here, we tested if stimulating the retina at specific time points in the oscillation, like the different phases, would improve the stimulation response. We found that stimulating at the maxima of the oscillation produced a better response. In this region, the cells that fire non-phase-locked spikes are stimulated and improved the overall response. Stimulating at the minima produced a slightly inhibitory response from the phase-locked spiking cells, thereby reducing the overall excitability at the minima.

The phase-locked spiking cells can be either ON or OFF RGCs as alpha ON, OFF sustained and OFF transient RGCs were shown to fire rhythmically. In our recording, we cannot distinguish the ON and OFF RGCs based on their light responses, as we used 4-5 months *rd10* mice where most of their photoreceptors are lost. However, this age was chosen as regular oscillations can be observed, which was necessary for the identification of the phases. Non-alpha RGCs fire action potentials with no or less rhythmicity (Margolis et al., 2014). Therefore, the non-phase-locked and most excitable cells in this experiment could be of the non-alpha RGCs.

Several studies proposed that oscillations, and possibly the associated rhythmic spiking, occur when the membrane potential of AII amacrine cells remains within a range that enables activation of specific voltage-gated Na^+ channels. Here, electrical coupling between ON bipolar cells and AII amacrine cells modulates this membrane potential (Borowska et al., 2011; Choi et al., 2014; Trenholm et al., 2012; Yee et al., 2012). Another proposed mechanism for the generation of oscillations and rhythmic spiking suggests that retinal patches may exist in which AII amacrine cells and ON bipolar cells are either tightly or weakly coupled via gap junctions (Margolis et al., 2014; Zeck, 2016). The cells with rhythmic firing would be found in a retinal patch with strong coupling. Owing to the strong coupling, the effect of electrical stimulation might spread spatially and temporally in the coupled network (J. Ahn et al., 2022). This is because the electrical stimulation activates the electrically coupled ON bipolar cell AII amacrine cell network, which subsequently activates the RGCs. In contrast, the non-phase-locked spiking cells would belong to a weakly coupled network and might respond more strongly to electrical stimulation. This is through the direct input from the stimulus-activated bipolar cells to the RGCs without any inputs from the other presynaptic cells. Our observation that non-phase-locked spiking cells were excitable at both maxima and minima suggests that they either originate from a weakly coupled network or occur when the membrane potential of AII amacrine cells lies outside the range required to produce oscillations.

In the model from Zeck, 2016, the rhythmic spiking of the RGC is formed by an unidentified GABAergic or glycinergic amacrine cell (Margolis et al., 2014; Zeck, 2016). These amacrine

cells receive oscillatory inputs from bipolar cells and inhibit RGCs in an oscillatory manner. This causes some cells to fire in a phase specific manner. It is then possible that with electrical stimulation, these inhibitory cells also get specifically activated, thereby causing the inhibition of the rhythmic spiking cells at the minima.

In the recordings from five 4-5 month-old *rd10* mice, we found 40.52% of channels showing phase-locking to the minima of the oscillation. Only two or three channels from the recordings from five *rd10* mice showed phase-locking to the maxima. The rhythmic spikes being correlated to the minima of the oscillation have been described previously in the *rd1* retina (Menzler & Zeck, 2011). However, in Biswas et al., 2014, many channels have also shown phase-locking to the maxima of the oscillation. The only difference is that my study used younger *rd10* mice (4-5 months old) while Biswas et al., 2014 used 9-12 months old *rd10* mice. Whether the difference in age is the reason for the difference in phase-locking needs to be addressed in future experiments.

It has been previously shown that stimulating the non-rhythmically firing cells produces a higher response compared to rhythmically firing cells (Haselier et al., 2017). In this study, we found that stimulating at the maxima will specifically activate the non-rhythmically firing cells. This approach shows that stimulation efficiency can be improved without abolishing the oscillations. This finding will be a useful application in a bidirectional implant, that can record and stimulate the retina at the same time. With these implants, stimulating in a phase specific manner can be used to obtain a better electrical stimulation response from the degenerated retina.

5. Identifying the optimal electrical stimulation pulse

5.1. Introduction

One way to treat retinal degeneration diseases is to electrically stimulate the remaining cells in the retina using a retinal implant. Several such implants have been developed and tested in patients, but they produced limited-quality vision (for review, see Tong et al., 2020). There are many aspects of an implant that need to be improved, like the electrode size, number of electrodes, the distance between electrodes and cells, spatial and temporal resolution, safety of stimulation pulse, etc. One such property that needs to be standardised is the stimulation pulse.

Many previous studies have tested different kinds of stimulation pulses. The features of a pulse that are tested are amplitude, duration, frequency, shape and polarity like monophasic vs biphasic, symmetric vs asymmetric and cathodic vs anodic. From these studies, the cathodal first biphasic current pulse required the lowest threshold compared to monophasic pulses to activate RGCs in the wt and *rd1* retina (K. N. Ahn et al., 2015; Hadjinicolaou et al., 2015; Im & Fried, 2016; Jensen et al., 2003; Jensen & Rizzo, 2009). Identifying a suitable pulse amplitude is also crucial for producing better RGC responses. Temporally varying visual inputs can be encoded efficiently by temporally modulated pulse amplitude and this effect was seen to be better in the range of 20-60μA (Ryu, Ye, Lee, Goo, & Kim, 2009). Similarly, the frequency of the pulse also played a very important role in generating RGC responses. This was shown by testing a series of pulse frequencies from 1-9Hz and observing the RGC response increasing linearly with an increase in pulse frequency (Ryu, Ye, Lee, Goo, Kim, et al., 2009).

In RGCs, spikes are initiated at a region on the proximal axon called the axon initial segment (AIS) (Kole & Stuart, 2012; Stuart et al., 1997). This region consists of a dense band of ion channels and cytoskeletal proteins. The high density of sodium channels $Na_v1.6$ in AIS plays an important role in generating action potentials (Fried et al., 2009). A lower stimulation threshold can be achieved by stimulating close to the dense sodium channel band in the AIS. The variability in the AIS properties like the AIS length and distance from the soma, causes or contributes to the variation in the stimulation thresholds in different retinal cells (Fried et al., 2009; Raghuram et al., 2021).

When stimulating epiretinally, RGCs can be activated both directly and indirectly (Fried et al., 2006; Jensen et al., 2003; Raghuram et al., 2021; Sekirnjak et al., 2006; Tong et al., 2020). Direct activation refers to the depolarisation of RGCs as a response to electrical stimulation. Indirect activation refers to the activation of presynaptic cells, thereby activating RGCs through the presynaptic inputs. In this case, the electrical stimulus activates bipolar cells and amacrine cells, causing excitation and inhibition of RGCs, respectively (J. Ahn et al., 2022; Fried et al., 2006). Direct activation produces one action potential immediately after electrical stimulation with a latency of < 0.7 ms, whereas indirect activation produces a cluster of action potentials with longer latency, which can be eliminated by blocking the presynaptic inputs (Fried et al., 2006). Direct activation can be achieved by using a short stimulus pulse and at a higher

stimulation frequency. In contrast, a longer pulse at high amplitude produces a cluster of action potential due to indirect activation (Fried et al., 2006).

Different stimulation pulses were tested in the retinal degeneration animal models like *rd1* and *rd10*. In these animals, the stimulation threshold was found to be higher than in the wt retina (Corna et al., 2021; Goo et al., 2016; Goo, Ye, et al., 2011; Jensen & Rizzo, 2008; Ye et al., 2008). The stimulation efficiency or the evoked spikes and the signal-to-noise ratio are lower in the degenerated retina compared to the wt retina (J. Ahn et al., 2022; Gehlen et al., 2020; Haselier et al., 2017; Nruthyathi et al., 2025; D. J. Park et al., 2015; Yee et al., 2012). The latency of electrically evoked response is also higher in the degenerated retina compared to the wt retina (Ye et al., 2008). It has been observed that the electrically evoked response gets distributed spatially through the strongly coupled retinal network in the degenerated retina and also produces multiple peaks of action potentials, whereas the wt retina shows a strong peak in response to an electrical stimulus (J. Ahn et al., 2022). The presence of oscillatory activity is shown to be a reason for reduced stimulation efficiency in the degenerated retina (Gehlen et al., 2020; Haselier et al., 2017).

There are different types of RGCs in the retina. The two main classes are the OFF RGCs and ON RGCs. OFF RGCs are the cells that get inactive with light stimulation and ON RGCs are the cells that get active with light stimulation. The RGCs that produce a short response to light are called transient RGCs and the cells that produce a longer response are referred to as sustained RGCs. The currently available implant stimulates without distinguishing the different RGCs. As it stimulates ON and OFF RGCs non-selectively, the natural light response is not mimicked. This makes analysis of elicited activity more difficult for the brain. Therefore, selectively stimulating the different cell types, especially the ON RGCs and OFF RGCs, is needed to mimic the natural light response using an implant.

Several studies have identified the specific stimulation amplitude, frequency and duration of the pulse that would stimulate ON RGCs and OFF RGCs differentially. One method is to use high amplitude and high frequency pulses to stimulate ON RGCs and low amplitude pulses at all frequencies to stimulate OFF RGCs (Guo et al., 2018). Another study has shown that on increasing the stimulation pulse duration, ON RGCs produced a lesser number of action potentials while there was limited difference in action potential rate with pulse duration in OFF RGCs (Im et al., 2018). This study also showed that a cathodal pulse showed a better electrically evoked response than an anodal pulse. A diamond pulse with a nonzero baseline increased the activity in ON RGCs and decreased the activity in OFF RGCs, whereas with a pulse of the inverted envelope where the peak of the diamond pulse is lowered and the baseline increased, an opposite effect was observed, where the activity of ON RGCs decreased and OFF RGCs increased (Twyford et al., 2014). The different pulse per second (PPS) pulse trains were shown to modulate different ON RGCs and OFF RGCs efficiently and even modulated further types of RGCs like the brisk transients, local edge detectors and directionally selective RGCs (Cai et al., 2011). The network-mediated responses in ON RGCs were modulated by pulse amplitude and are independent of pulse count and repetition frequency. On the other hand, OFF RGCs were better modulated by the number of stimuli than the pulse amplitude (Roh et al.,

2022). With multiple pulse stimulation, the ON RGCs reset the ongoing response to previous stimuli and produce a response similar to single pulse stimulation. OFF RGCs get desensitised with multiple stimulations (Im & Fried, 2016).

In most of the stimulation studies, a rectangular biphasic stimulation pulse was used. A study showed that in ON RGCs of the wt retina, direct RGC activation was more triggered by an increasing ramp shaped pulse and the indirect activation by variations of triangular shapes rather than a rectangularly shaped pulse (Lee & Im, 2018). However, it is not tested if there is a difference between different pulse shapes for selectively stimulating ON RGCs and OFF RGCs. Therefore, here, we will be testing different stimulus pulse shapes in the wt and *rd10* retina.

5.2. Results

In this experiment, six different shapes of electrical pulses: square, irregular square, triangle, increasing ramp, decreasing ramp and sine (refer Fig 2.7 in materials and methods) were compared in wt and *rd10* retina. These pulses were tested in a combination of four different amplitudes: 50µA, 100µA, 200µA and 300µA and six different durations: 120µs, 200µs, 320µs, 400µs, 640µs and 800µs.

5.2.1. Standardisation of the paradigm

For the pharmacological (chapter 3) and phase stimulation (chapter 4) studies, a cathodic first biphasic square pulse of amplitude 100µA and duration 400µs was applied. This electrical stimulus was shown to increase the spike rate in the wt retina (Gehlen et al., 2020; Haselier et al., 2017). Pulses were separated by a gap of 20s. This gap is necessary to prevent desensitisation of the retinal activity and help the retina return to normal activity. In this study, we will be testing a series of amplitude and duration for each shape of the pulse. This would cause a large number of combinations to be tested in one retinal piece, ending with very long experiments. Two questions had to be solved first. First, would the retinal performance remain constant over long recording periods with repetitive stimulation? Second, could the duration of the experiment be reduced by shortening the gap between each stimulus from 20s to 10s?

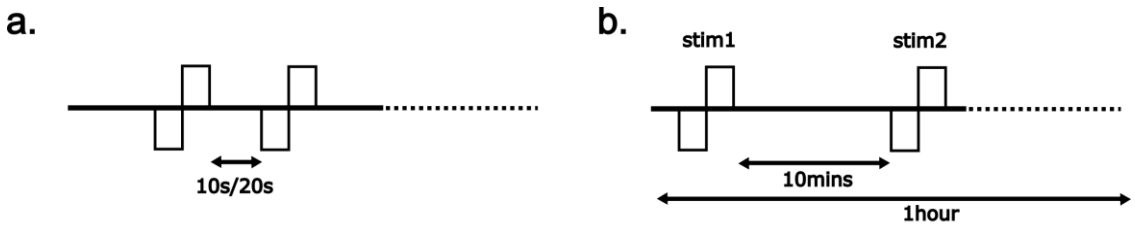

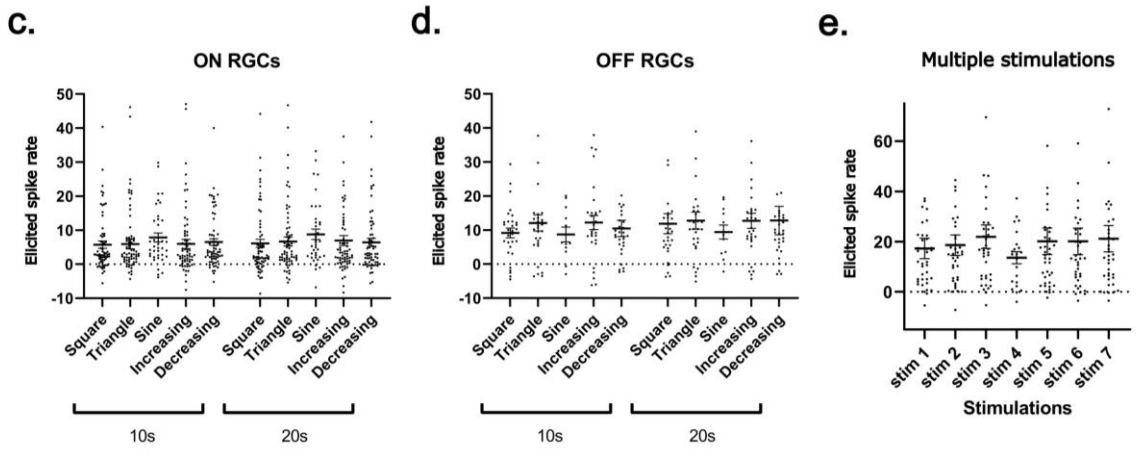

Fig 5.2.1: Standardisation of the experimental paradigm: (a) a gap of 10s and 20s between multiple pulses was tested and results shown in (c) and (d). For every shape tested, there is no difference with either gap. ON and OFF RGCs were separated manually from their response to the light stimuli by adjusting the threshold of spike detection accordingly (Analysed from a total of 7 retinal pieces from 3 wt mice). (b) multiple electrical stimulations given every 10mins for 1hour, result shown in (e). Electrically stimulating for one hour did not produce a significant change in the responses (Analysed from a total of 2 retinal pieces from 1 wt mouse).

To standardise the experiment, we tested a gap of 10s and 20s gap for a series of electrical pulses and compared the response of the retina. The effect of different gaps in ON RGCs and OFF RGCs are shown in Fig 5.2.1c and Fig 5.2.1d, respectively. The ON RGCs and OFF RGCs were separated manually based on their light response. For both ON RGCs and OFF RGCs, we observe no difference between the 10s and 20s gap for each shape. This shows that reducing the gap to 10s will not affect the response of the retina to electrical stimulation and the retina gets sufficient time to return to normal activity. This would allow the different parameters of the pulse to be tested within one hour for each retinal piece.

Another issue with such a long recording is whether the health of the retina lasts for one hour with continuous stimulation. Therefore, in order to find if the activity of the retina changed for the one-hour-long recording, we stimulated the retina every 10 minutes for one hour and looked into the change in retinal response (Fig 5.2.1b). Fig 5.2.1e shows the result of this experiment. We observed the activity to remain constant for each of the stimulation pulses. The first stimulus, stim1 and last stimulus, stim 7, seemed to produce comparable responses, confirming that the health of the retina was not compromised with such a long recording.

There were amplitudes and durations of pulses that were beyond the charge injection limit and would damage the electrodes. Such parameters were not used in our experiment. However, even after removing these parameters, pulses with particularly large amplitude and long duration still elicited saturation of the channels. The saturation of the electrodes was observed when the signal was beyond the amplifier's voltage limit, hence flattening the signal (Venkatachalam et al., 2011). The saturation effect on the channels seemed to be different for different shapes of the pulse. Fig. 5.2.2a-f shows a heatmap with the number of saturated channels for each shape. We can observe that almost every parameter showed a total of 7-8 saturated channels (of a total of 60 recording channels). These were the channels that were used

to stimulate the retina. Since these channels showed saturation for every shape, amplitude and duration of pulse, they were eliminated from the analysis. For the remaining channels, some of the large amplitude and duration seemed to produce saturation and this was seen to be variable among different shapes. Sine and irregular square pulses produced the lowest number of saturated channels with saturation seen at only 300µA- 200µs. Square pulse also showed less saturated channels, saturated at 300µA- 200µs and 300µA- 120µs. Increasing ramp and triangular showed saturation at four combinations of parameters: 300µA- 200µs, 300µA- 120µs, 200µA- 400µs and 200µA- 320µs. The shape, decreasing ramp seemed to produce the most saturated channels and had saturation at five parameters: 300µA- 200µs, 300µA- 120µs, 200µA- 400µs, 200µA- 320µs and 200µA-200µs. The maximum number of saturated channels observed was 57-58 channels out of 60. We eliminated the channels that showed saturation and computed the elicited spike rate from the remaining channels that did not show saturation. Fig. 5.2.2g-h shows the comparison of saturated channels wt retina and *rd10* retina. We observed a similar number of saturated channels in *rd10* retina as in wt retina. Shapes like decreasing ramp, triangular and increasing ramp produced the most saturation of electrodes even in the degenerated retina.

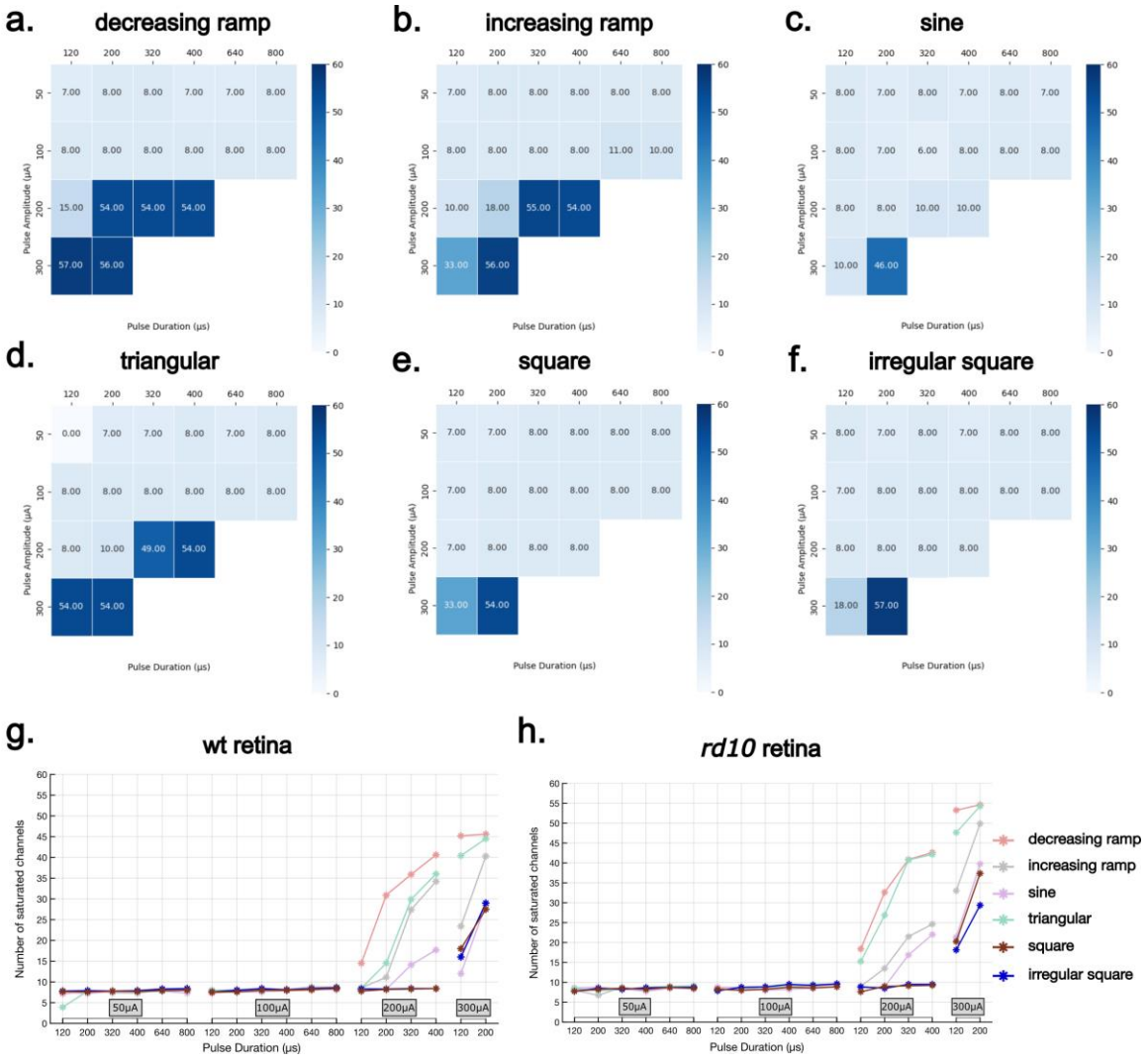

Fig 5.2.2: Saturation of MEA channels: the number of saturated electrodes from one piece of retina for varying amplitudes and durations is represented as a heatmap for each shape: decreasing ramp (a), increasing ramp (b), sine (c), triangular (d), square (e) and irregular square (f). The number on each box of the heatmap gives the number of saturated channels for that particular combination of stimulus parameters. (g) and (h) shows the average number of saturated channels for different stimulus parameters (pulse amplitudes and durations represented on the X-axis and pulse shapes as different coloured lineplots; average from 5 retinal pieces from 2 wt mice and 4 retinal pieces from 2 *rd10* mice).

5.2.2. Certain stimulation pulse parameters elicit slight excitation in ON RGCs, while OFF RGCs are inhibited or are unresponsive

In the following figure, the elicited spike rate, which is the difference between the poststimulus action potential rate and the prestimulus action potential rate, were compared for each of the parameters of electrical pulses in wt retina.

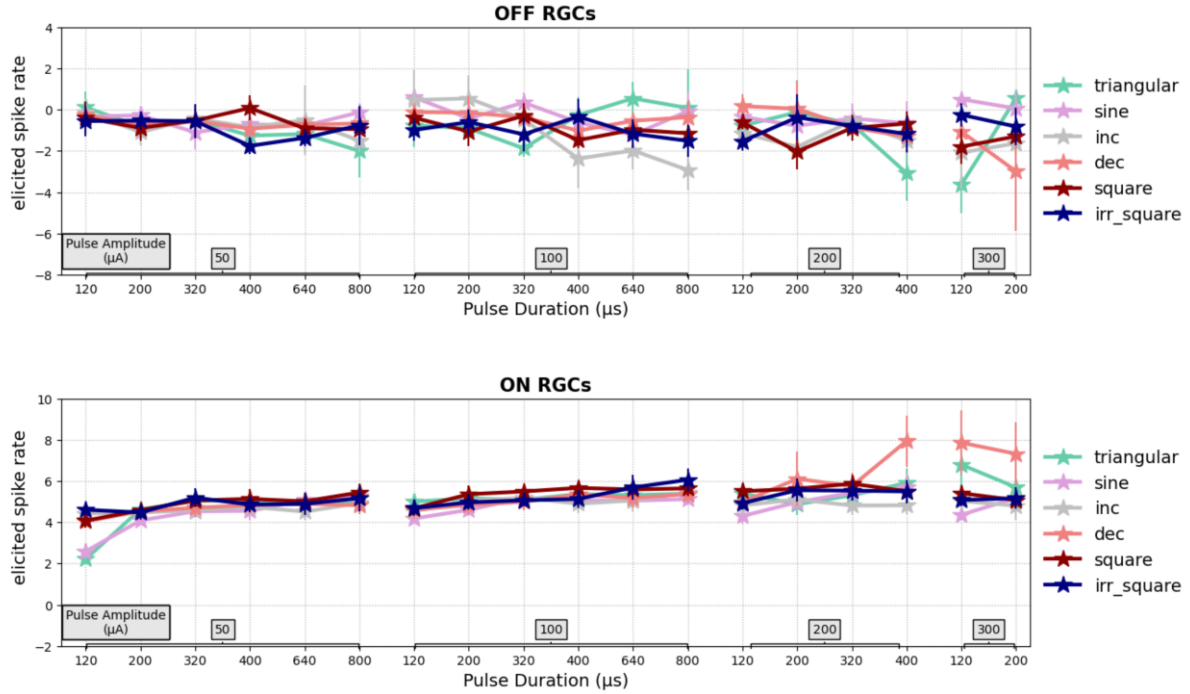

Fig 5.2.3: Elicited spike rate in wt retina: 6 different shapes: square, irregular square, triangle, increasing ramp, decreasing ramp and sine shown as different coloured lines, 4 different amplitudes: 50µA, 100µA, 200µA and 300µA (these amplitudes are for square pulse, for other shapes the amplitudes are modified to keep the net charge similar for all shapes) and 6 different durations: 120µs, 200µs, 320µs, 400µs, 640µs and 800µs are compared in OFF RGCs (top) and ON RGCs (bottom) (Average from 5 retinal pieces from 2 wt mice).

In the wt retina, OFF RGCs produced zero or negative elicited spike rate. There is a trend for an inhibition and that inhibition increases with an increase in pulse amplitude and duration. Therefore, a combination of large amplitude and duration can be used to inhibit OFF RGCs. Differently shaped pulses produced no significant difference in the response of OFF RGCs. ON RGCs, on the other hand, showed excitatory responses with electrical stimulation. The excitation became more pronounced with an increase in stimulus strength. No difference was observed in the response of ON RGCs to different shapes of pulse. Inhibition in OFF RGCs

and excitation in ON RGCs were found to be maximal at 100µA- 800µs and the effect often saturated for higher amplitudes and duration of pulses.

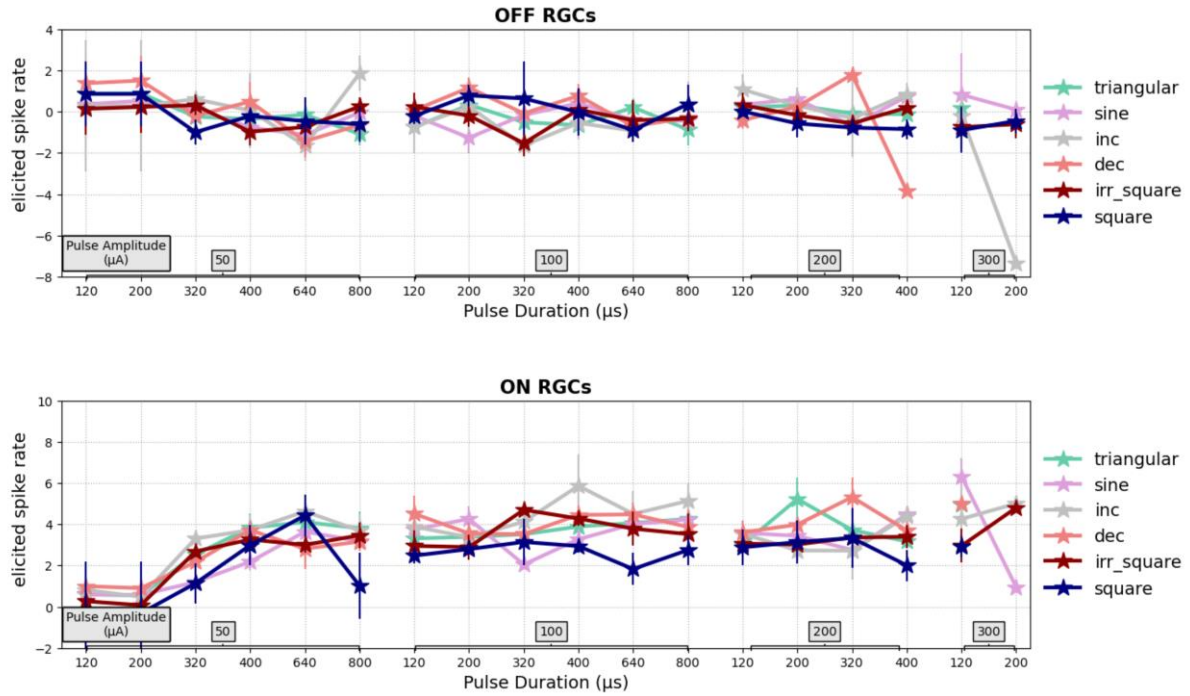

Fig 5.2.4: Elicited spike rate in *rd10* retina: 6 different shapes: square, irregular square, triangle, increasing ramp, decreasing ramp and sine shown as different coloured lines, 4 different amplitudes: 50µA, 100µA, 200µA and 300µA (these amplitudes are for square pulse, for other shapes the amplitudes are modified to keep the net charge similar for all shapes) and 6 different durations: 120µs, 200µs, 320µs, 400µs, 640µs and 800µs are compared in OFF RGCs (top) and ON RGCs (bottom) (Average from 4 retinal pieces from 2 *rd10* mice of age 1 month).

In the *rd10* retina, the OFF RGCs produced a slight excitation (elicited spike rate of 1-2 for some shapes) at the lowest pulse amplitude and duration while, for higher pulse amplitude and duration, a gradually increasing trend of inhibition was observed. However, the inhibition in OFF RGC was lower in the *rd10* retina compared to the wt retina. There was no significant difference in the responses between different shapes of pulses. The ON RGCs showed excitation that increased with stimulus strength. The increasing trend was more pronounced in *rd10* compared to wt because ON RGCs showed no response to the first two parameter pairs- 50µA- 120µs and 50µA- 200µs in *rd10*. Excitatory responses were observed from the later parameters onwards, while, in wt retina, we observed excitatory responses of ON RGCs from the lowest pulse amplitude and duration itself. The different pulse shapes produced varied, but not significant, differences in the elicited spike rate of ON RGCs with increasing stimulus strength. ON RGCs showed the weakest response to electrical stimulation with square shape. Unlike in the wt retina, the elicited spike rate saturated a bit earlier, at 50µA- 800µs, in both OFF RGCs and ON RGCs in the *rd10* retina.

The following figure shows an example of a recording from OFF RGC and ON RGC in wt mouse retina.

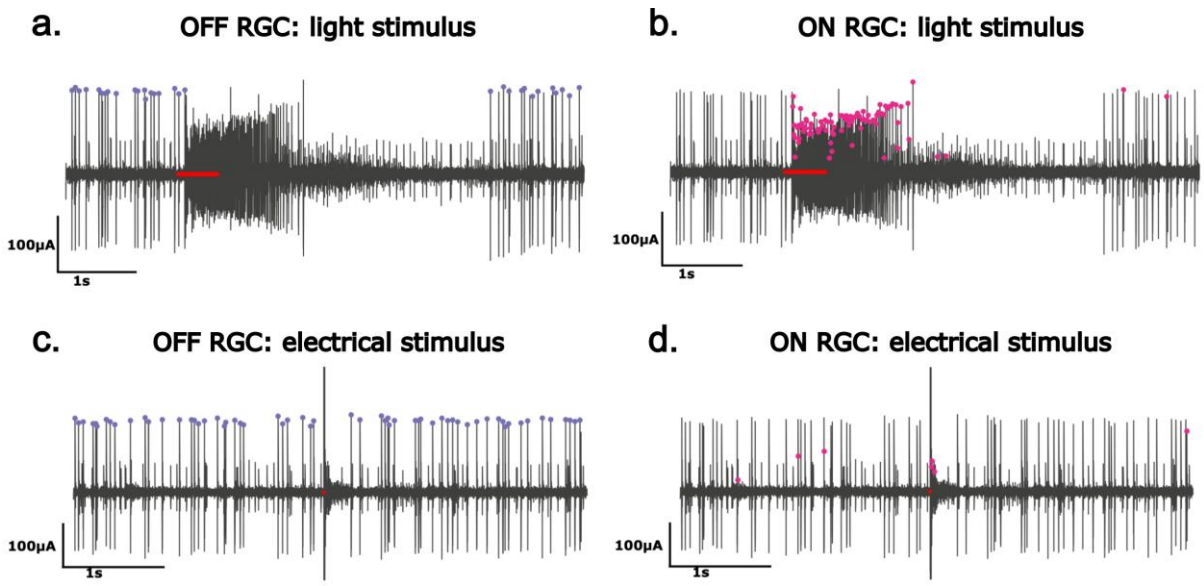

Fig 5.2.5: Effect of light and electrical stimulus in OFF RGC and ON RGC in wt retina: (a) with light stimulation (light stimuli represented by the red line of intensity: 1200mV, duration: 500ms (1405 rhodopsin isomerisations per rod and stimulus)) in OFF RGC, the cell is inhibited for a short time as shown by the decrease in blue dotted spikes with stimulus. (b) ON RGC increases spiking with light stimulus, represented by the pink dotted spikes. (c),(d) similar effect mimicked with electrical stimulus (vertical line) in OFF RGC and ON RGC with irregular square pulse of amplitude and duration 100µA- 800µs.

Multiple ON RGCs and OFF RGCs were recorded at each electrode. Cells were classified based on their light response and were assigned to an ON and an OFF cluster, respectively, for example, in Fig 5.2.5 a,b, OFF RGC spikes were clustered and labelled with blue dots and ON RGC spikes with pink dots. We observed that the OFF RGCs stop spiking after the onset of the light stimuli. In the same manner, with electrical stimuli, we observed the activity of OFF RGCs slightly reduced for appr. 250 ms. For ON RGCs, we observed an increase in spiking with light stimulation and, similarly, an increase with electrical stimulation (note the cluster of spikes labelled with red dots after the stimulus). This shows that the dichotomy in the light response of ON RGCs and OFF RGCs can be recreated with a certain set of our parameters of the electrical stimulation pulse.

The effect of pulse amplitude, duration, charge and shape is analysed in detail in the following sections.

5.2.3. Higher pulse amplitude selectively stimulates ON RGCs over OFF RGCs

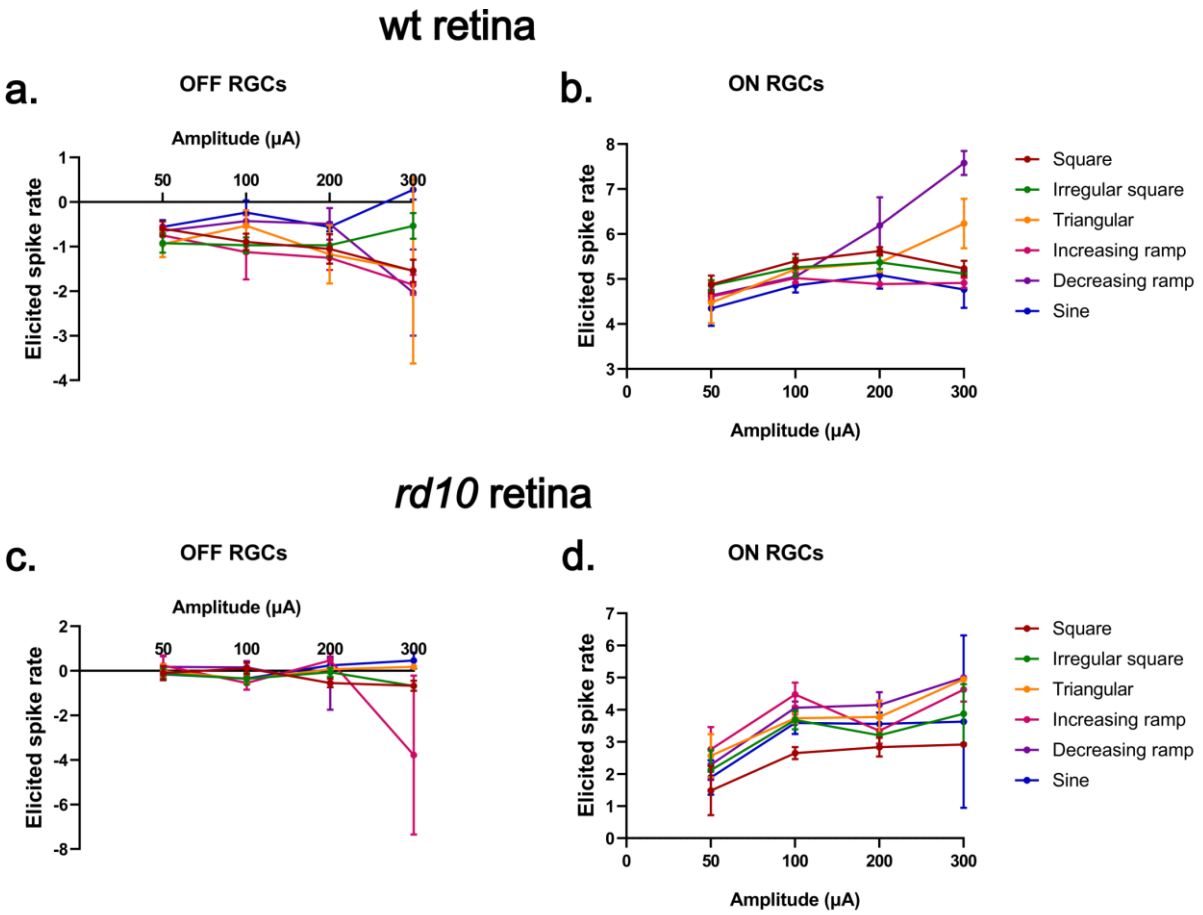

Fig 5.2.6: Elicited spike rate comparison for different amplitudes of electrical pulses in wt and *rd10* retina: 6 different shapes: square, irregular square, triangle, increasing ramp, decreasing ramp and sine shown as different coloured lines and 4 different amplitudes: 50µA, 100µA, 200µA and 300µA compared in OFF RGCs: in wt retina (a) and *rd10* retina (c) and ON RGCs: in wt retina (b) and *rd10* retina (d) (Averaged from 5 retinal pieces from 2 wt mice and 4 retinal pieces from 2 *rd10* mice.).

The elicited spike rates were compared for different amplitudes of the pulse: 50µA, 100µA, 200µA and 300µA. Fig 5.2.6 shows the responses of ON RGCs and OFF RGCs to different pulse amplitudes. In this analysis, the elicited spike rates for all durations were pooled together and the comparisons were made between the amplitudes.

The wt OFF RGCs showed slight inhibition (elicited spike rate < 0) for the different amplitudes of the stimulus pulse. At 50µA, 100µA and 200µA, all shapes showed a similar trend where the elicited spike rate was below 0, indicating a slight inhibition. But at 300µA, there seemed to be variability between different shapes with sine showing an elicited spike rate greater than 0, irregular square showing an elicited spike rate between 0 and -1 and increasing ramp, square, decreasing ramp and triangular pulse showing an elicited spike rate at round -2. ON RGCs, on the other hand, showed excitation (elicited spike rate > 4) with electrical stimulation. For square, irregular square, increasing ramp and sine, there was little to no variation with different amplitudes. But for the triangular and decreasing ramp, the elicited spike rate increased slightly with the amplitude of the pulse, with the decreasing ramp showing the greatest excitation

(elicited spike rate of around 8). Therefore, with the increase in amplitude of the stimulation pulse, decreasing ramp and triangular pulse showed a stronger excitation in ON RGC and stronger inhibition in OFF RGC and can be used to selectively stimulate these cells.

In the *rd10* retina, OFF RGCs showed neither excitation nor inhibition with a change in amplitude of the stimulus pulse for most of the shapes. At 300µA, the increasing ramp seemed to show slight inhibition, although only in a few cases, as the standard error mean was very high. For ON RGCs, the elicited spike rate was lower in *rd10* retina compared to wt (in wt, elicited spike rate = 4-8 and in *rd10*, elicited spike rate = 1-5). The square shaped pulse seemed to produce the lowest elicited spike rate for all the amplitudes. A clear preference for the triangular and decreasing ramp pulse for selectively activating ON RGC and OFF RGC, as observed in the wt retina, was not seen in the *rd10* retina.

A difference in the RGC response between different shapes was seen at the largest amplitude of stimulation pulse tested, 300µA. For other amplitudes, all the shapes showed a similar response. Triangular and decreasing ramp produced the most selective stimulation of ON and OFF RGC in wt retina. In the *rd10* retina, every shape except the square pulse showed similar selective excitation of ON RGCs and no response in OFF RGCs.

5.2.4. Varying pulse duration does not influence ON and OFF RGCs responses

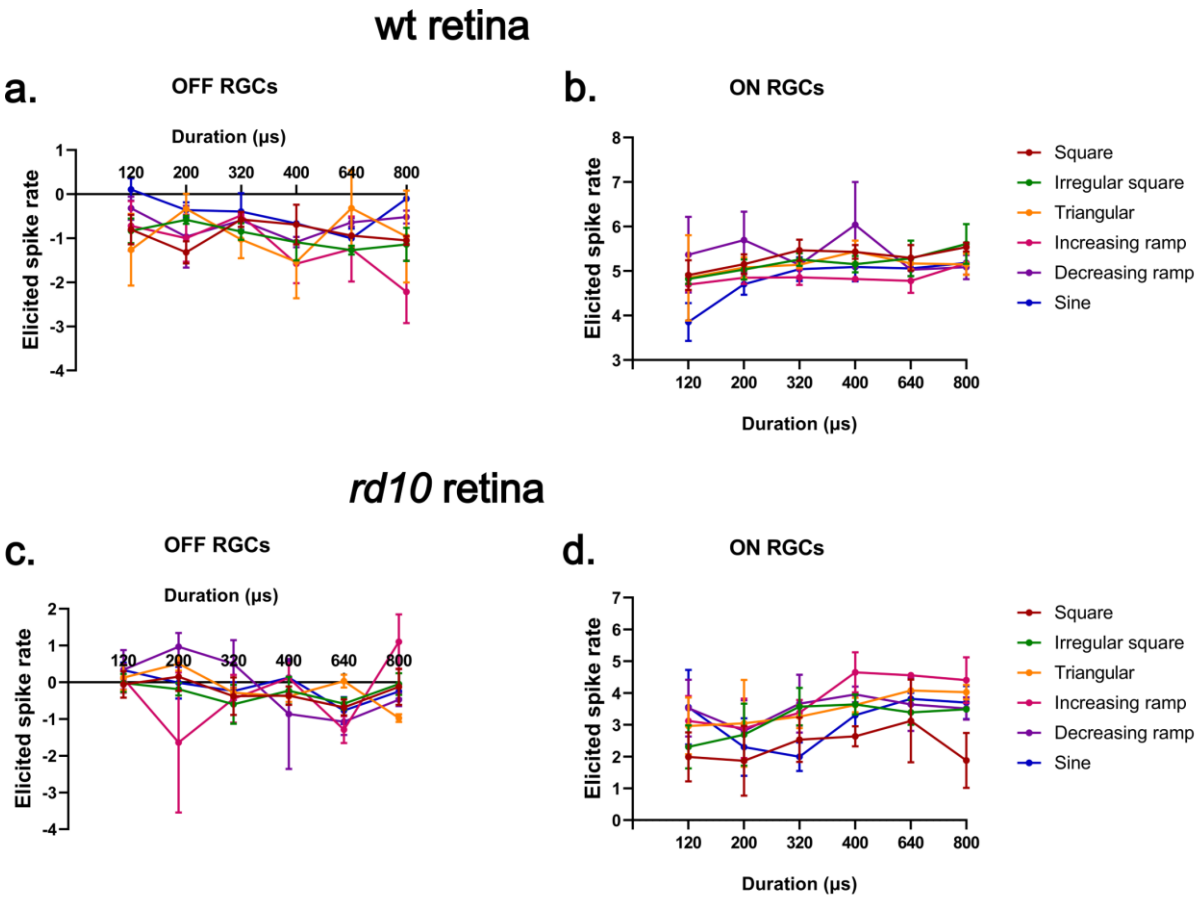

Fig 5.2.7: Elicited spike rate comparison for different duration of electrical pulses in wt and *rd10* retina: 6 different shapes: square, irregular square, triangle, increasing ramp, decreasing ramp and sine shown as different coloured lines and 6 different durations: 120µs, 200µs, 320µs, 400µs, 640µs and 800µs are compared in OFF RGCs: in wt retina (a) and *rd10* retina (c) and ON RGCs: in wt retina (b) and *rd10* retina (d) (Averaged from 5 retinal pieces from 2 wt mice and 4 retinal pieces from 2 *rd10* mice).

The elicited spike rates were compared for the six different durations of pulse: 120µs, 200µs, 320µs, 400µs, 640µs and 800µs. Fig 5.2.7 shows the responses of ON and OFF RGCs to different pulse durations. The elicited spike rates for all amplitudes were pooled together and the comparisons were made between the durations.

The wt OFF RGCs showed elicited spike rates between 0 and -1 indicating a slight inhibition at different durations and for different shapes of pulse. Only increasing ramp produced elicited spike rate of -2 at the longest duration of pulse 800µs. ON RGCs, on the other hand, showed excitation for all durations. The variability between shapes of pulse was seen at 120µs, with sine shape producing the lowest excitation and the decreasing ramp producing the highest excitation. For the rest of the durations, the response was very similar (elicited spike rate = 5-6) for all the shapes of pulse.

In the *rd10* retina, OFF RGCs showed no response for all durations and shapes of pulse. ON RGCs showed excitation and a slight increase in excitation with an increase in duration. The overall excitation in *rd10* (between 1-4, maximum 5 for increasing ramp) was lower compared to wt (between 4-6). The square shape showed the least response for different durations of pulse.

ON RGC and OFF RGC showed milder differences in their response with varying pulse duration. For the OFF RGCs, all shapes produced similar responses (slight inhibition in wt retina and no response in *rd10* retina) whereas with varying amplitude (section 5.2.3), a difference between shapes can be observed at the highest amplitude tested, 300µA. The wt ON RGCs showed excitation that increases with stimulus amplitude whereas there were very small differences with a change in stimulus duration. Variability between shapes occurs at the highest amplitude of 300µA and lowest duration of 120µs in wt retina. In *rd10* retina, excitation increases slightly with an increase in pulse duration and amplitude.

5.2.5. Pulse charge strongly modulates the selective stimulation of ON RGCs over OFF RGCs

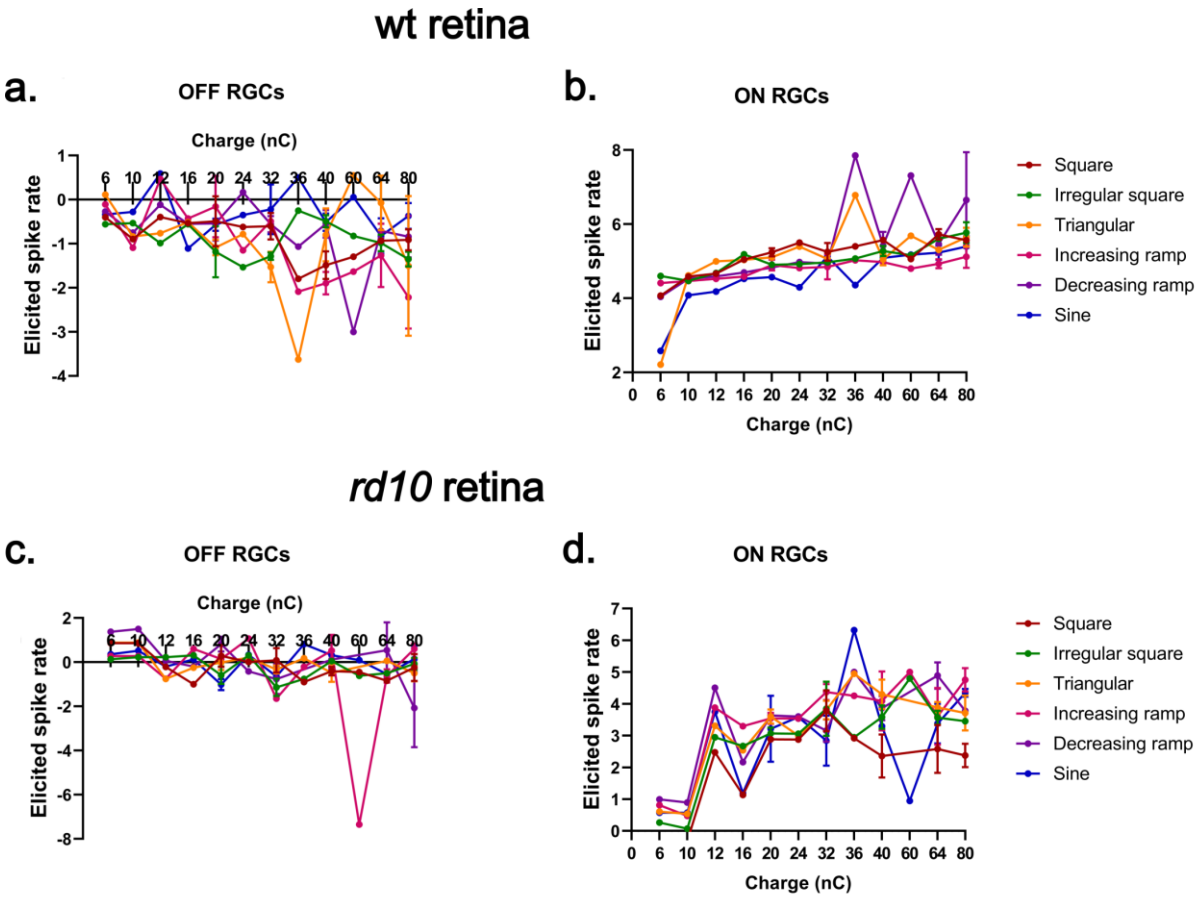

Fig 5.2.8: Elicited spike rate comparison for different charges of electrical pulses in wt and *rd10* retina: 6 different shapes: square, irregular square, triangle, increasing ramp, decreasing ramp and sine shown as different coloured lines and 12 different charges: 6nC, 10nC, 12nC, 16nC, 20nC, 24nC, 32nC, 36nC, 40nC, 60nC, 64nC and 80nC are compared in OFF RGCs: in wt retina (a) and *rd10* retina (c) and ON RGCs: in wt retina (b) and *rd10* retina (d) (Averaged from 5 retinal pieces from 2 wt mice and 4 retinal pieces from 2 *rd10* mice).

The charge of the pulse was computed as the product of the amplitude and duration of the pulse. In this manner, there will be twelve different charges of the pulse: 6nC, 10nC, 12nC, 16nC, 20nC, 24nC, 32nC, 36nC, 40nC, 60nC, 64nC and 80nC. The charge is kept constant between different shapes by varying the amplitude of the pulse. Therefore, the different shapes represent different patterns of the same charge injection. By comparing the different shapes for various charges, we could identify which pattern is most suitable for achieving the best response.

In wt retina, OFF RGCs showed inhibition and the inhibition mildly increased with an increase in charge of the stimulation pulse. At the lowest charge, there was very little variation between different shapes but as the charge increased, the variability in response increased between shapes. The increasing ramp produced the highest inhibition and the rest of the shapes produced a variable effect. On the contrary, ON RGCs showed excitation that increased with an increase in charge. The sine and triangular stimuli produced only 2 elicited spikes at 6nC but the

response increased for higher charges. From 10nC onwards, all the shapes produced nearly similar responses. The maximum elicited spike rate was around 6 for all the shapes except for the decreasing ramp where 8 spikes were elicited at certain times.

OFF RGCs in retina did not respond to differently charged electrical stimulation except decreasing ramp (small inhibition at 80nC) and increasing ramp (small inhibition at 60nC). ON RGCs, on the other hand, showed no response at 6 and 10nC, but as the charge increased, excitatory responses were seen. The square pulse produced the least response at all charges.

We observed a strong modulation of ON RGCs response with an increase in pulse charge in both wt and *rd10* retina, but pulse charge showed only a slight inhibition in wt retina and no effect in *rd10* retina in the OFF RGCs response.

5.2.6. Which pulse shape produces the highest selectivity of ON and OFF RGCs?

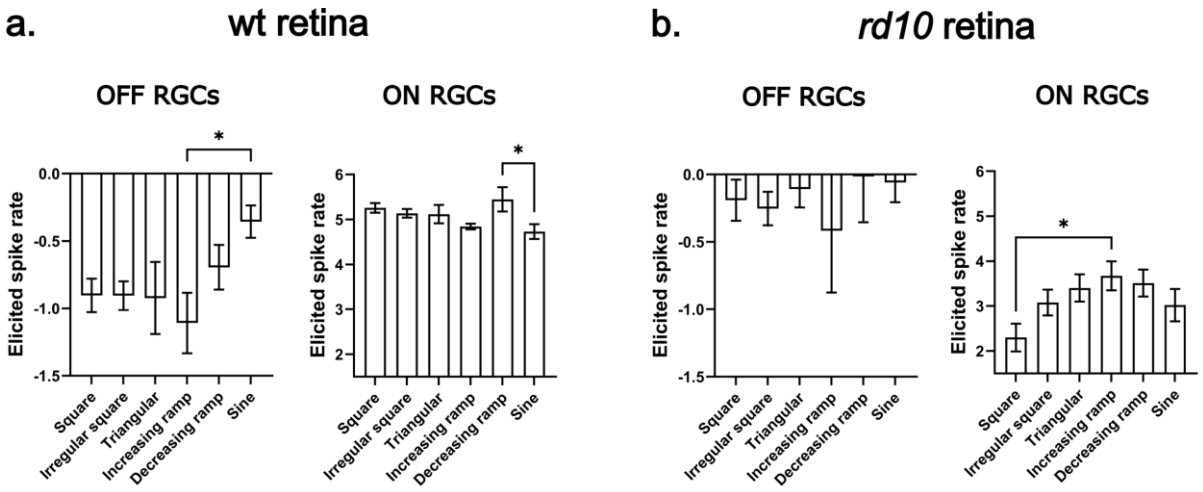

Fig 5.2.9: Elicited spike rate comparison for different shapes of electrical pulses in wt and *rd10* retina: 6 different shapes: square, irregular square, triangle, increasing ramp, decreasing ramp and sine are compared in OFF RGCs and ON RGCs for wt retina (a) and *rd10* retina (b) (Averaged from 5 retinal pieces from 2 wt mice and 4 retinal pieces from 2 *rd10* mice; significance was tested using one-way ANOVA (*: $p \leq 0.05$)).

Fig 5.2.9 compares the different shapes of pulses, pooled together for all amplitudes and durations of pulse.

In the wt retina, OFF RGCs showed slight inhibition for different shapes of pulse, with the highest inhibition produced by the increasing ramp and the least by the sine pulse. ON RGCs showed excitation with stimulation with the highest excitation produced by the decreasing ramp and the least by the sine. Therefore, pulse shapes like increasing ramp and decreasing ramp can be used to selectively excite ON RGCs and inhibit OFF RGCs whereas a sine pulse is least preferred for selective electrical stimulation as it produced least excitation in ON RGCs and the least inhibition in ON RGCs.

In the *rd10* retina, all shapes produced lower inhibition in OFF RGCs and lower excitation in ON RGCs in comparison to the wt retina. OFF RGCs showed very low to no inhibition with

electrical stimulation and there was no significant difference seen between different shapes. In ON RGCs, an excitation of the cells was observed with the increasing ramp showing the highest excitation and the square pulse the least.

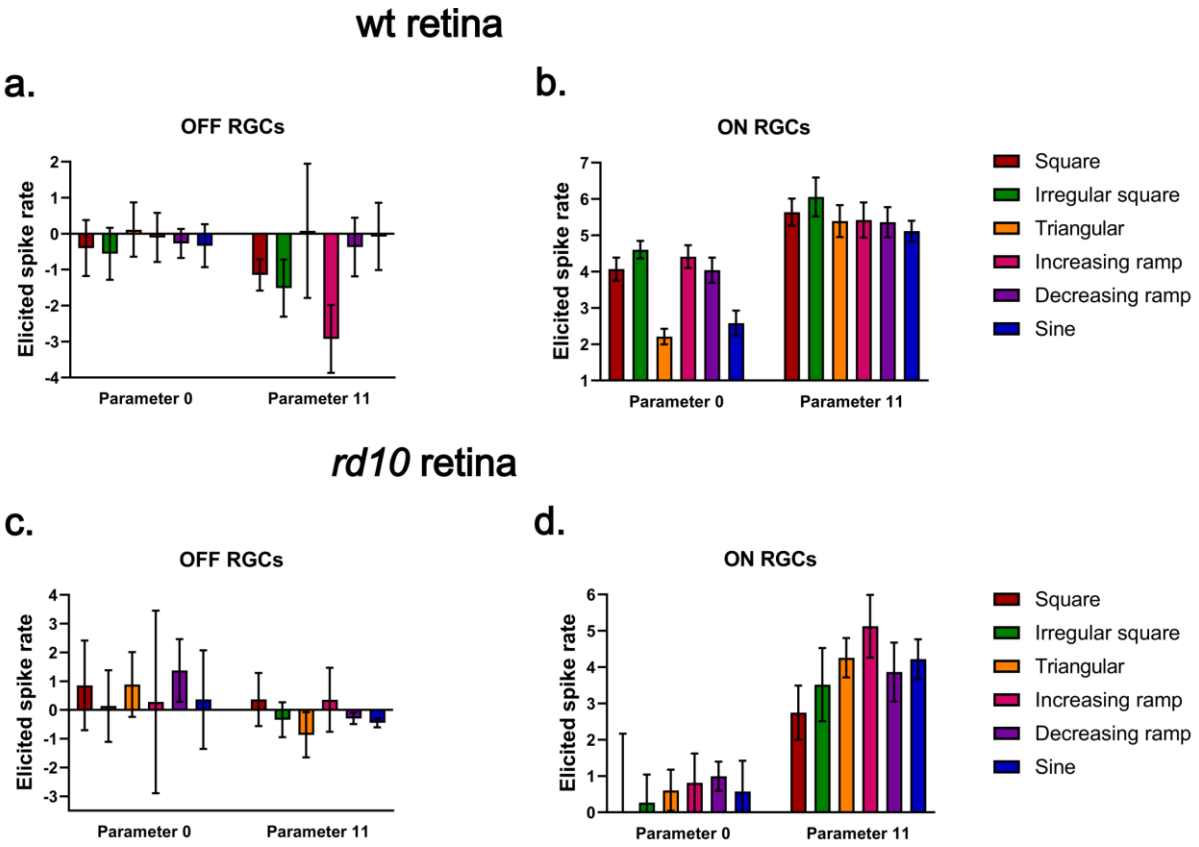

Fig 5.2.10: Elicited spike rate comparison for parameter 0 and parameter 11 in wt and *rd10* retina: 6 different shapes: square, irregular square, triangle, increasing ramp, decreasing ramp and sine shown as different coloured bars compared for parameter 0: 50µA, 120µs and parameter 11: 100µA, 800µs in OFF RGCs: in wt retina (a) and *rd10* retina (c) and ON RGCs: in wt retina (b) and *rd10* retina (d) (Averaged from 5 retinal pieces from 2 wt mice and 4 retinal pieces from 2 *rd10* mice).

Fig 5.2.10 shows the comparison of different shapes between two parameter combinations: 1) parameter 0: 50µA- 120µs, which produced the least response to stimulation and 2) parameter 11: 100µA- 800µs, which produced the strongest response to stimulation.

At parameter 0 in the wt retina, the OFF RGCs showed little to no response with all pulse shapes. At parameter 11, pulse shapes like square, irregular square and increasing ramp produced increase in inhibition. The remaining pulse shapes, triangular, decreasing ramp and sine, produced no response to electrical stimulation. In ON RGCs, both parameters produced excitation. Parameter 0 elicited around 4 spikes in response to the stimulation for all pulse shapes except triangular and sine, which elicited only around 2 spikes. With parameter 11, the excitation increased and around 5-6 spikes were elicited with all different shapes of pulse, with irregular square producing the highest excitation. Square, irregular square and increasing ramp seemed to be the preferred shapes as they selectively excited ON RGCs and at the same time inhibited OFF RGCs. Among these, increasing ramp will be the best choice. The other three

shapes, triangular, sine and decreasing ramp also produced good excitation at parameter 11 but they did not inhibit OFF RGCs.

In the *rd10* retina, OFF RGCs showed slight excitation with stimulation with parameter 0 in the case of square, triangular and decreasing ramp, while irregular square, increasing ramp and sine produced no response to stimulation. With parameter 11, the response was reduced where irregular square, triangular, decreasing ramp and sine showed little inhibition, and square and increasing ramp showed slight excitation to no response. Therefore, on changing from parameter 0 to parameter 11, the OFF RGCs responses showed lesser excitation and sometimes slight inhibition with electrical stimulation. ON RGCs, on the other hand, showed excitation to electrical stimulation. At parameter 0, the excitation was very low, with around 0-1 elicited spikes, but at parameter 11, the excitation was stronger, with around 3-5 elicited spikes. Therefore, in the *rd10* retina, parameter 11 with pulse shapes like irregular square, triangular, decreasing ramp and sine seemed to be preferred to selectively excite ON RGCs and inhibit OFF RGCs. Increasing ramp produced the highest excitation with stimulation in ON RGCs, but it also produced slight excitation in OFF RGCs as well, making it less preferred for selective stimulation. Similarly, the square shape also produced slight excitation in ON RGCs and OFF RGCs.

5.2.7. The preferred parameters for selectivity of ON RGCs over OFF RGCs

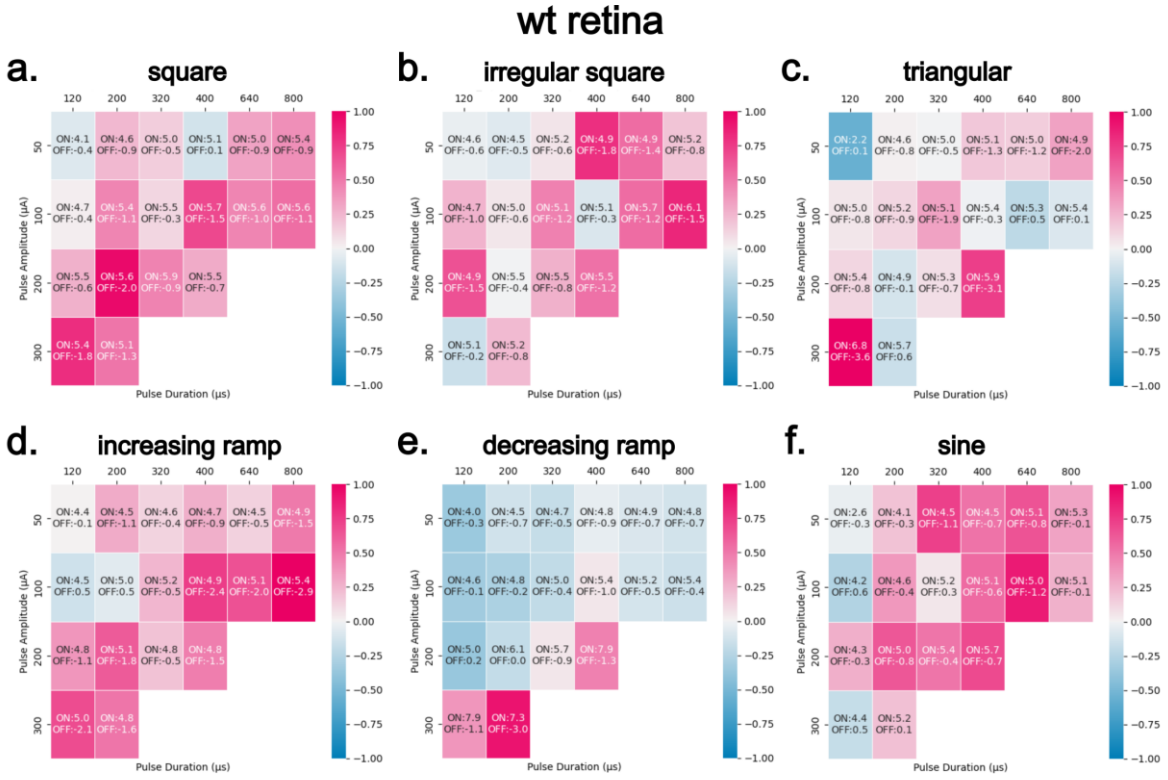

Fig 5.2.11: Selectivity heatmap for different parameters of electrical pulses in wt retina: 6 different shapes: square, irregular square, triangle, increasing ramp, decreasing ramp and sine shown as different plots (a-f), 4 different amplitudes: 50µA, 100µA, 200µA and 300µA (y-axis) and 6 different durations: 120µs, 200µs, 320µs, 400µs, 640µs and 800µs (x-axis). The scale bar is the selectivity metric as calculated in 2.7.3.5 in materials and methods section that shows strong excitation of ON RGCs and strong inhibition of OFF

RGCs as bright pink colour and weak excitation of ON RGCs and weak inhibition of OFF RGCs as blue. The numbers in each block of the heatmap are the elicited spike rate of ON RGCs and OFF RGCs at the respective parameter combination. The white blocks in the heatmap depict the parameters that are beyond the charge injection limit of the MEA electrodes and not tested (Analysed from 5 retinal pieces from 2 wt mice).

In the wt retina, the higher amplitude and duration of pulses produced the highest selectivity for ON RGCs. This was evident for square, irregular square, increasing ramp and sine, where we see the highest selectivity (pink blocks in Fig 5.2.11) along the diagonal of the heatmap, which is the highest duration and amplitude tested. For triangular and decreasing ramp, the selectivity was seen in very few parameters, mainly with amplitude 200µA and 300µA.

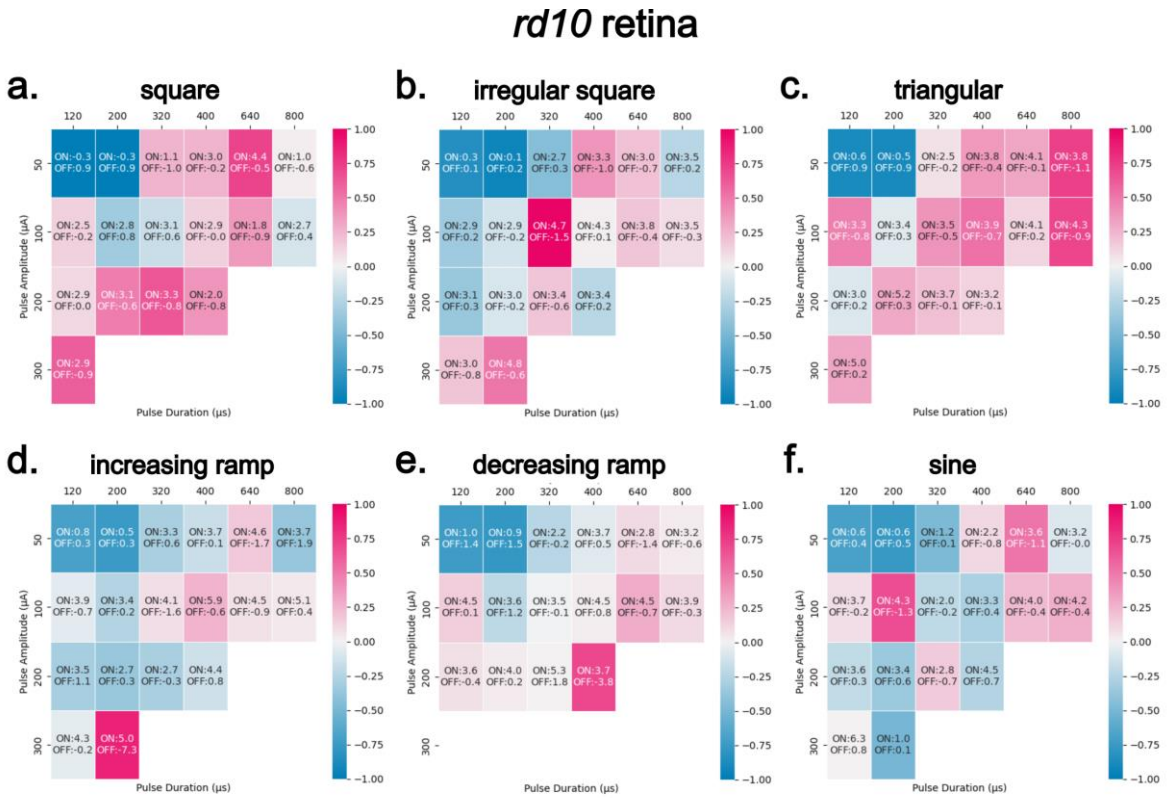

Fig 5.2.12: Selectivity heatmap for different parameters of electrical pulses in *rd10* retina: 6 different shapes: square, irregular square, triangle, increasing ramp, decreasing ramp and sine shown as different plots (a-f), 4 different amplitudes: 50µA, 100µA, 200µA and 300µA (y-axis) and 6 different durations: 120µs, 200µs, 320µs, 400µs, 640µs and 800µs (x-axis). The scale bar is the selectivity metric as calculated in 2.7.3.5 in the materials and methods section that shows strong excitation of ON RGCs and strong inhibition of OFF RGCs as bright pink colour and weak excitation of ON RGCs and weak inhibition of OFF RGCs as blue. The numbers in each block of the heatmap are the elicited spike rate of ON RGCs and OFF RGCs at the respective parameter combination. The white blocks in the heatmap depict the parameters that are beyond the charge injection limit of the MEA electrodes and not tested (Analysed from 4 retinal pieces from 2 *rd10* mice).

The different shapes showed selectivity at variable points without a specific trend in the *rd10* retina. For every shape, most of the stimulation parameters showed lower selectivity in *rd10* retina (Fig 5.2.12) in comparison to wt (Fig 5.2.11). This is because of two reasons: 1) the excitation of ON RGCs with electrical stimulation was lower in *rd10* retina compared to wt, 2)

OFF RGCs showed little to no response in *rd10* retina while it showed inhibitory responses in wt retina.

The stimulation amplitude and duration that produced the highest selective excitation of ON RGCs and inhibition of OFF RGCs for each pulse shape is listed in Table 5.2.1. Selecting the pulse parameters that produce highest excitation of ON RGCs, represented by larger and positive elicited spike rate (ESR) and highest inhibition of OFF RGCs, represented by the most negative ESR, is essential to mimic the natural light response.

Table 5.2.1: Selective stimulation of ON RGCs over OFF RGCs

wt retina				
Shape	**Preferred amplitude**	**Preferred duration**	**ESR of ON RGCs**	**ESR of OFF RGCs**
Square	200µA	200µs	5.6	-2
Irregular square	100µA	800µs	6.1	-1.5
Triangular	300µA	120µs	6.8	-3.6
Increasing ramp	100µA	800µs	5.4	-2.9
Decreasing ramp	300µA	200µs	7.3	-3
Sine	100µA	640µs	5	-1.2
***rd10* retina**				
Shape	**Preferred amplitude**	**Preferred duration**	**ESR of ON RGCs**	**ESR of OFF RGCs**
Square	50µA	640µs	4.4	-0.5
Irregular square	100µA	320µs	4.7	-1.5
Triangular	100µA	800µs	4.3	-0.9
Increasing ramp	300µA	200µs	5	-7.3
Decreasing ramp	200µA	400µs	3.7	-3.8
Sine	100µA	200µs	4.3	-1.3

5.3. Discussion

Selective stimulation of ON RGCs and OFF RGCs was tested with six different shapes of electrical pulses for a series of amplitudes and durations. The ON RGCs showed a trend for excitation in both wt and *rd10* retina whereas OFF RGCs showed slightly inhibitory response to the stimulation pulses in wt retina and no response in *rd10* retina. The trend for excitation and inhibition increases with an increase in pulse amplitude and duration in both the strains. However, the responses of ON and OFF RGCs to electrical stimulation were more pronounced in wt than in *rd10* retina. The shapes like the increasing ramp and irregular square, produced better response and better selectivity to electrical stimulation compared to the commonly used, square pulse.

The study Lee & Im, 2018 showed that on comparing rectangular, triangular, increasing ramp and decreasing ramp shapes of pulse in alpha ON RGCs, the increasing ramp produced the most direct activation response and all other non-rectangular shapes produced a better indirect activation response. Similar to this, we observed that the square pulse produced the least response to electrical stimulation compared to all the other shapes, especially in the *rd10* retina. In ON RGCs, the decreasing ramp (Fig 5.2.9) and irregular square (Fig 5.2.10) showed the highest response in wt and the increasing ramp (Fig 5.2.9 and Fig 5.2.10) in the *rd10* retina. Whereas in OFF RGCs, the highest inhibition was seen with increasing ramp pulse in both wt and *rd10* retina (Fig 5.2.9 and Fig 5.2.10). Therefore, shapes like increasing ramp, decreasing ramp and irregular square are most suitable for selective excitation of ON RGCs and inhibition of OFF RGCs.

In this experiment, the stimulus elicited spikes could result from the indirect stimulation of RGCs through the presynaptic network. The spikes produced from direct stimulation are very likely masked by the stimulation artefact due to their short latency (Goo, Ye, et al., 2011; Jensen & Rizzo, 2008). The stimulation responses in the *rd10* retina are also found to be mainly caused by the indirect stimulation of the RGCs (J. Ahn et al., 2022). Therefore, in our experiment, the response from both wt and *rd10* is more likely caused by the indirect stimulation of the RGCs.

With an increase in the amplitude of the stimulation pulse, we observed an increase in excitation of ON RGCs in the wt and *rd10* retina (Fig 5.2.6). This is similar to the amplitude modulation reported in previous studies (Cai et al., 2011; Roh et al., 2022). In OFF RGCs, with increase in stimulus amplitude, we see an increase in inhibitory responses in wt retina. In *rd10* retina, almost all stimulus amplitudes produced no response (Fig 5.2.6). With the change in stimulus duration, ON RGCs and OFF RGCs showed little to no change in their responses (Fig 5.2.7). On the contrary, in Im et al., 2018, they observed no change in the stimulus elicited responses of OFF RGCs with a change in the pulse duration but a decrease in stimulus elicited spikes in ON RGCs. The difference between this study and the result we observed could be caused by the difference in the range of pulse durations tested, they used pulse durations in the ms range, whereas we tested it in the µs range. With the increase in charge, we observed a monotonic increase in the response of ON RGCs, with the response reaching saturation at 10nC in the wt retina and at 12nC in the *rd10* retina (Fig 5.2.7). The pulse charge causes stronger modulation of RGC responses. A similar increasing trend with charge has been reported earlier

(Lee & Im, 2018), but due to the difference in the charge ranges tested, the study does not report saturation of responses for higher pulse charges.

The electrical stimulation elicits a change in spike rate by influencing the membrane potential of the cells (Lee et al., 2023, 2024). Using different frequencies of stimulation pulses, the authors argue that low frequency stimulation hyperpolarises the membrane potential, thereby releasing voltage-activated sodium channels from inactivation and producing a monotonically increasing spiking response (spiking response increases and then saturates). Whereas high frequency stimulation depolarises the membrane potential producing a non-monotonic spiking response (spiking response increases and after a certain pulse parameter, it decreases). This has been shown for ON RGCs and OFF RGCs, with ON RGCs showing higher sensitivity and spiking. In our case, we see monotonically increasing spiking responses for ON RGCs, similar to the response to low frequency stimulation. This means that the response of ON RGCs is likely mediated by the hyperpolarisation of the membrane potential of ON RGCs with electrical stimulation. For OFF RGCs, we observed a decrease or no response to electrical stimulation. But in Lee et al., 2023, 2024, they observed monotically or non-monotonic change in spike rate. This difference may be due to the use of a single-pulse stimulation in this study, which likely elicited a lower cellular response because OFF RGCs have lower sensitivity. In contrast, Lee et al., 2023, 2024 used high frequency stimulation pulses.

ON RGCs exhibited stronger stimulation elicited responses than OFF RGCs in both wt and *rd10* retina. This may be because ON RGCs are more sensitive to electrical stimulation (Lee et al., 2023, 2024). In addition, the lower level of background activity in ON RGCs may facilitate the generation of robust electrically evoked spikes. In contrast, OFF RGCs show high background spontaneous firing, which may result in poorer responses to electrical stimulation.

The selective excitation of ON RGCs and inhibition of OFF RGCs through subretinal stimulation was observed by Carleton & Oesch, 2024. In their study, they identified the mechanisms responsible for the selective inhibition of OFF RGCs. They observed that OFF RGCs received direct or presynaptic inhibition from AII or other amacrine cells, which gets blocked with the application of inhibitory blockers or strychnine. The crossover inhibition through the ON bipolar cells- AII amacrine cells pathway and the rod bipolar cells input to the AII or any other amacrine cells together activate the amacrine cells, thereby producing the inhibition of OFF RGCs (Demb & Singer, 2012; Hoon et al., 2014; Masland, 2012; McGuire et al., 1984; Wässle, 2004; Wässle et al., 1986). The remaining cones were shown to not influence this selective inhibition of OFF RGCs. Therefore, in this experiment, the selectivity could also be produced by the same mechanism where the electrical stimulation directly or indirectly activates ON RGCs through ON bipolar cells and at the same time, inhibits OFF RGCs by activating amacrine cells or by activating cells presynaptic to amacrine cells like the rod bipolar or ON bipolar cells.

In wt retina, we observed excitation of ON RGCs and inhibition of OFF RGCs (albeit much weaker) with electrical stimulation. In *rd10* retina, both ON RGCs excitation and OFF RGCs inhibition are weaker with the inhibition no longer visible in most of the cases. This difference between wt and degenerated retina has been shown by several studies where the degenerated

retina seems to require a higher stimulation threshold (Corna et al., 2021; Goo et al., 2016; Goo, Ye, et al., 2011; Jensen & Rizzo, 2008; Ye et al., 2008) and the stimulation efficiency or the evoked spikes and the signal-to-noise ratio are lower in the degenerated retina compared to the wt retina (J. Ahn et al., 2022; Gehlen et al., 2020; Haselier et al., 2017; D. J. Park et al., 2015; Yee et al., 2012).

Different shapes of stimulation pulse inject and remove charge in different ways that could affect the sustainability of the electrodes. In this experiment, this is quantified in the means of stimulation artefact or the saturation of the channels. Irregular square, square and sine produced the least number of saturated channels. Decreasing ramp, on the other hand, produced the most saturation of electrodes. The benefit of using shapes like the irregular square, which is an asymmetric pulse, is that as the second phase of the irregular square pulse is longer it would balance the charge over longer time periods, thereby reducing the impact of stimulation on the electrodes (K. N. Ahn et al., 2015). Therefore, selecting the best shapes of electrical pulse is not only required to obtain better response and better selectivity but also to reduce the damage to the electrodes.

In this study, we stimulated the retina epiretinally with different stimulation pulses of varying amplitude, duration and shape. We found that shapes like irregular square and increasing ramp produced selective stimulation of ON RGCs over OFF RGCs and this effect was more pronounced at a certain amplitude and duration of the pulse. These stimulation pulses were able to elicit differential ON and OFF RGC stimulation in both wt and *rd10* retina. The traditionally used square pulse produced the least response, especially in the *rd10* retina. Pulse shapes like irregular square, square and sine also produced fewer saturated electrodes. Thus, we were able to identify optimal stimulation pulses that selectively stimulate ON RGCs over OFF RGCs in both wild-type and the degenerated retina. These pulse parameters may therefore be applied in epiretinal implant to improve performance in patients with retinal degeneration.

6. Discussion

Degeneration of photoreceptors causes loss of vision in patients with RP or AMD. Retinal implants are used to restore vision in these patients by electrically stimulating the remaining cells in the retina. However, the implants are seen to be successful in very few patients. One reason for the low performance may be the low efficiency of electrical stimulation of RGCs by the implant. In my thesis, I have found the following ways to improve the electrical stimulation of an implant.

1. A pathological oscillatory activity has been identified in the degenerated retina, which is responsible for reducing the stimulation efficiency. Pharmacological drugs can be used to abolish these oscillations. Among the drugs tested, THIP ($GABA_A$ receptor agonist), memantine (NMDA antagonist) and carbenoxolone (gap junction antagonist) abolished oscillations and increased the stimulation efficiency.

2. The oscillations are often accompanied by rhythmic spiking in the *rd10* retina. In certain cells, most of the action potentials occur phase-locked to the minima of the oscillation. We found out that stimulating specifically at the minima inhibits spiking in some of these cells. Stimulating at the maxima, where the action potentials are not phase-locked, causes an excitatory response from the non-phase locked cells. Therefore, stimulating at the maxima seems to be beneficial to achieve a better response.

3. We tested a series of electrical pulses of varying amplitude, duration and shape and found that an asymmetric square pulse or triangularly shaped pulses at certain amplitudes and durations produce better RGC response. Differential stimulation of ON and OFF RGCs was observed, where ON RGCs are seen to be excited and OFF RGCs are inhibited at certain pulse parameters. Shapes like irregular square, square and sine also cause less stimulation artefact and saturation of the electrodes, making these shapes ideal for long-term use in an implant.

6.1. Application of the findings in humans

6.1.1. Pharmacologically abolishing oscillations

An oscillatory activity is identified in several retinal degeneration animal models. Although the presence of oscillations in RP patients is still under investigation, the patients have reported seeing phosphenes, which could be caused by the hyperactivity associated with the oscillations (Bittner et al., 2009; Brown et al., 2015; Heckenlively et al., 1988). These oscillations are affecting the electrical stimulation produced by an implant in two ways: 1) by interfering with the stimulation by adding high background noise from the oscillations and the associated spontaneous spiking (Yee et al., 2012), and 2) by reducing the stimulation elicited spikes (J. Ahn et al., 2022; Gehlen et al., 2020; Goo, Ahn, et al., 2011; Haselier et al., 2017; Menzler & Zeck, 2011; Nruthyathi et al., 2025; D. J. Park et al., 2015; Rincón Montes et al., 2019). Abolishing the oscillations seems to be a way to counteract these problems, as shown previously with benzodiazepines (Gehlen et al., 2020). However, the drugs tested in their study, benzodiazepines, show several side effects and are not suitable for chronic use (Fraser, 1998). From previous studies (see chapter 3 for details), it was hypothesised that the absence of glutamate inputs from photoreceptors during retinal degeneration causes a change in the membrane potential of ON bipolar cells and AII amacrine cells. This opens certain voltage-gated Na^+ channels in AII amacrine cells, producing oscillations (Borowska et al., 2011; Choi et al., 2014; Trenholm et al., 2012). Based on this pathway, we tested several targets and found a few pharmacological drugs that would abolish oscillations. THIP ($GABA_A$ receptor agonist), memantine (NMDA antagonist) and carbenoxolone (gap junction antagonist) have abolished oscillations and at the same time improved stimulation efficiency. Therefore, these drugs can be used to improve the performance of the implant.

THIP (gaboxadol), memantine and carbenoxolone abolished oscillations but the effect was only reversible with THIP and memantine. Both THIP and memantine are clinically approved drugs and can be taken orally. However, the suitability of these drugs for chronic use remains uncertain. We observed that memantine affects spike frequency and spike amplitude; the effect on spike frequency can be attributed to the blockade of the excitatory input through NMDA receptors but the effect on the spike amplitude could be due to non-specific binding of memantine, making the drug questionable for long-term use by patients with implants. THIP, on the other hand, has comparatively fewer tolerance and addiction side effects (Drasbek & Jensen, 2006) compared to benzodiazepines but neither of them are approved for chronic use. A new $GABA_A$ receptor agonist, ganaxolone, has been discovered and approved recently by the FDA and the EU. This drug is given to epileptic patients and has fewer side effects, making it suitable for chronic use (Knight et al., 2022; Monaghan et al., 1999). Ganaxolone can be orally administered and is metabolised and distributed into tissues quickly, reaching maximum plasma concentration within 2-3 hours (https://go.drugbank.com/drugs/DB05087). Therefore, this drug could be a possible alternative to be given to patients once its effect on oscillations is determined.

One possibility to avoid systemic effects of benzodiazepines or other drugs would be to employ local targeted drug delivery. This technique has been used to deliver steroids as an anti-inflammatory agent to treat several eye diseases (Ham et al., 2023; Kim & Woo, 2021). To target the retina, the drugs are either injected intravitreally or administered using a slow-release implant. With intravitreal injections, the drug dissolves in the vitreous and is slowly diffused and absorbed in the retina. Such injections, however, must be repeated at short intervals, making this treatment cumbersome for the patients and increasing the risk for infections (Morioka et al., 2020; Urbańska et al., 2023). Alternatively, the drugs can be applied by injecting an implant which can either be a biodegradable implant that dissolves and slowly releases the drug in a span of 3-6 months or a nonbiodegradable implant that releases the drug for a longer period, 18-36 months (Fung et al., 2020; Ham et al., 2023). Targeted drug delivery combined with a retina prosthesis is a new area of research that is being explored. There have been studies done in developing a MEA implant that also contains microfluidic structures or ionic pumps that could electrically stimulate the retina and at the same time deliver drugs into the retina (Deubel et al., 2023). Therefore, drugs like THIP or benzodiazepines could be administered locally to the retina without having long-term systemic side effects.

6.1.2. Phase specific stimulation

The oscillations in the degenerated retina are often accompanied by phase-locked spikes, most often phase-locked to the minima of the oscillation. In this study, we found out that stimulating the retina specifically at the minima did not produce excitation, but rather no response or an inhibitory response. On the other hand, stimulation at the maxima where the phase-locked spikes are absent produced excitation. Therefore, an alternative way to achieve better stimulation efficiency without abolishing oscillations is by stimulating phase-specifically.

It was suggested that the oscillations and the phase-locked spiking in the degenerated retina are formed by the strongly electrically coupled network of the AII amacrine cells and ON bipolar cells (Borowska et al., 2011; Trenholm et al., 2012; Zeck, 2016). With electrical stimulation, the degenerated retina produces a response that has fewer evoked spikes compared to wt retina, and is more spatially and temporally dispersed, mediated through the strong gap-junction coupling (J. Ahn et al., 2022). Such dispersion may affect the spatial and temporal resolution of the electrical stimulation produced by an implant and could be a contributing factor to its low performance. Here, stimulating at the maxima excites only the non-phase-locked spiking cells, that are hypothetically formed in a region of weakly coupled AII amacrine cells and ON bipolar cells (Zeck, 2016) and produces better evoked spikes. As non-phase-locked spiking cells are from a weakly coupled region, targeting them would prevent the dispersion of the evoked response and could improve the spatial and temporal resolution of the electrical stimulation by an implant.

To stimulate in a phase-specific manner, the phases of the oscillation have to be determined. For this, a bidirectional implant would be necessary, that can record the activity of the cells, process it in real-time and stimulate in a phase-specific manner. This involves a real-time closed-loop algorithm that is a field of much interest recently (more on this in section 6.2).

6.1.3. Identifying the optimal electrical stimulation pulse

There are two main classes of retinal ganglion cells: OFF RGCs and ON RGCs. OFF RGCs are inhibited with light and ON RGCs are excited with light. Under natural conditions, at any given retinal location only ON or OFF RGCs are activated by a light stimulus. An implant that does not discriminate between ON and OFF cells during stimulation would elicit conflicting neuronal activity that would be difficult for the brain to analyse. Therefore, a cell-specific stimulation would be a great advantage. In this study, we tested different shapes, amplitudes and durations of stimulation pulses. With certain combinations of parameters, the ON RGCs were getting excited, whereas the OFF RGCs were partially inhibited. This effect was moderate but similar to stimulation with low light intensities. Therefore, these parameters can be used to selectively stimulate ON and OFF RGCs and mimic the natural light response using an implant.

In this study, this method has been tested in young *rd10* retina where oscillations were seen, although irregularly, in a few channels. In this case, the excitation of ON RGCs and inhibition of OFF RGCs were reduced compared to the wt retina. One of the reasons causing the difference in the responses of ON and OFF RGCs between wt and *rd10* could be the oscillations which are seen in a few channels. If that is the case, abolishing oscillation or stimulating at the maxima of the oscillation could be ways to obtain better responses and better selective stimulation in the degenerated retina.

There are several implants that have been developed and tested in patients. Epiretinal and suprachoroidal implant systems consist of a camera that captures the image of the environment, which is then converted into electrical signals to stimulate the retina in a specific pattern, that is supposed to mimic the shape of the object recognised (Weiland & Humayun, 2014). These implants produced partial vision in patients. An example of this is the case with Argus II, an epiretinal implant that was tested in nearly 200 patients and showed improvement in the performance of simple tasks like object localisation and letter reading (Palanker, 2023; Weiland & Humayun, 2014). The reported effectiveness of these implants may be attributable to pulse parameters that lie within a range capable of selectively activating ON RGCs and suppressing OFF RGCs, similar to this study. Therefore, the stimulations given through multiple electrodes in a specific pattern, resembling the detected object, would have activated ON RGCs and at the same time inhibited OFF RGCs, similar to light stimulation, thereby aiding in the recognition of the object. The selective stimulation of each cell without activating surrounding cells is also necessary to improve the spatial and temporal resolution of the image produced from the electrical stimulation of an implant.

To selectively stimulate, we need to recognise the ON RGCs and OFF RGCs. This requires recording the cell activity, analysing and stimulating the retina in a closed-loop manner. Therefore, a closed-loop stimulation approach is also necessary to apply this finding (more on this in section 6.2).

6.2. Bidirectional implant

The phase specific stimulation and selective stimulation of ON RGC and OFF RGC are only possible with a closed-loop approach. This involves developing an implant that could record and stimulate the retina at the same time, i.e. a bidirectional implant. There are several benefits on using a bidirectional implant: 1) it helps to stimulate at certain phases of the oscillation at which the response of the degenerated retina gets better (chapter 4), 2) it helps to identify optimal stimulation pulses that can selectively stimulate different RGCs (chapter 5), 3) as the degenerated retina undergoes remodelling which causes a reduced stimulation efficiency, a bidirectional implant would help us identify the optimal stimulation needed for each stage of degeneration in a patient (K. Y. Wu et al., 2023) and 4) as the signals from the cells vary based on the electrode-retina distance, it could similarly compensate for the stimulation by applying higher pulses for farther cells and lower pulses for closer cells (K. Y. Wu et al., 2023).

A closed-loop optimisation system that optimises the stimulation pulses to selectively stimulate specific RGCs in real time has been developed (Ghaffari et al., 2021; Löhler et al., 2024). These systems were tested in an *in vitro* environment and shown to record and stimulate efficiently. The next step will be to incorporate such a system in an implant. A 3D bidirectional implant that could record from the RGCs and stimulate the inner retina is currently being developed (Rincón Montes et al., 2019). The 3D nature of this implant also helps in achieving better contact with the retina.

A limitation of the current closed- loop approach is that the cell-specific stimulation is only feasible in the retina with preserved light responses, where RGC types have been identified based on their responses to light stimulation (Ghaffari et al., 2021; Löhler et al., 2024). In this thesis, the experiments on cell specific stimulation were conducted in wild-type and young *rd10* mice, both of which retain functional vision. However, this approach may not apply to patients with advanced retinal degeneration, in whom light responses are often severely reduced or entirely absent. In such cases, identifying cell types based on light-evoked activity would no longer be possible. One way to solve this is to use their electrical stimulation responses to identify the cells. Here, we showed that certain stimulation pulses activate ON RGCs and inhibit OFF RGCs. Therefore, it will be interesting to look at whether the classification can be achieved based on their responses to electrical stimulation. With this approach, a closed-loop system can be made to identify the cells and send stimulation triggers accordingly. This stimulates the cells specifically without activating the nearby cells, thereby improving the resolution of the electrically evoked response in a degenerated retina.

6.3. Current status of retinal implants

The only FDA-approved implant is Argus II, an epiretinal implant developed by Second Sight Medical Products, Sylmar, USA. This implant consists of 60 electrodes of 200µm diameter, arranged in a flexible array with a 575µm pitch. This implant was placed in more than 200 RP patients, with almost all of the patients being able to perceive light. Some patients showed improvement in tasks like the square localisation test and identifying the direction of motion. The overall orientation and mobility were improved in many cases but it wasn't enough for the

patients to move around freely without any guidance (Humayun et al., 2009). Therefore, as the success rate of Argus II was limited and due to it being suitable for only retinal degeneration diseases, the company decided to shift its focus to developing a cortical implant named Orion (for review, see Palanker, 2023).

The Alpha IMS is a subretinal implant with CE mark developed by Retina Implant AG, Reutlingen, Germany. The implant contains 1600 pixels each with a photodiode that responds to natural light, an amplifier to amplify the signal generated by the photodiode and electrodes to stimulate the retina in response to the signal generated by the photodiode (Stingl et al., 2015). The implant was tested in some patients; the results showed improvements in the detection and counting of objects. The foveal placement of the implant showed better improvements in visual tasks than parafoveal placement. Unfortunately, the implant failed to function after one year of implantation. After tweaking the materials and design, the Alpha AMS implant was developed which had a longer durability of 40 months (Daschner et al., 2018; Palanker, 2023). Unfortunately, the company Retina Implant AG had been closed by March 2019.

The PRIMA implant developed by Pixium Vision, Paris, is a photovoltaic implant that can convert light into a biphasic electrical pulse (Palanker et al., 2020). The image from the environment is captured by a camera, processed and projected onto the retina with photodiodes in 378 pixels of 100µm size. This implant was tested in five subjects and all five subjects perceived brightness. The patients were subjected to several other tasks like letter recognition, word reading and several Landolt C tests, where they performed extremely well (Palanker, 2023; Palanker et al., 2022). Further studies focus on improving the implant by varying electrode pitch and pixel size to enhance resolution and by testing new image processing algorithms.

POLYRETINA is another epiretinal implant developed by Prof. Diego Ghezzi's group in Switzerland. This is a foldable photovoltaic device that contains 10,498 densely packed pixels. The photovoltaic elements are composed of light-sensitive polymers that directly convert light into electrical signals and therefore do not require wires (Ferlauto et al., 2018). Due to this, a larger number of electrodes can be used in this implant, which would lead to a larger visual angle size and better resolution. The implant is also foldable, which makes it easier for the large implant with many electrodes to be inserted into the eye (Palanker, 2023; K. Y. Wu et al., 2023).

Several other implants were developed and tested in patients. EPIRET3 is an epiretinal implant that has 25 electrodes of diameter 100µm and pitch 500µm. This was tested in six patients and the patients were able to perceive light (Menzel-Severing et al., 2012). Another epiretinal implant, IRIS II, which has 150 electrodes, was developed by Pixium Vision. These implants were also shown to elicit visual percepts ('MHRA Approves Bionic Vision System Clinical Trial', n.d. or review, see Palanker, 2023). Unfortunately, the studies on both implants are currently discontinued. NR600 is an epiretinal implant developed by Nano Retina and this is a wireless implant that contains 600 3D electrodes. The glasses that the patient wore had a camera that detects the image, converts it into infrared light and powers the implant. The first few tests showed success in most of the visual tasks (Charters, 2026). Suprachoroidal implants are being

developed by Bionic Vision Australia and by a group at Osaka University. During clinical trials, patients reported perceiving phosphenes but the overall vision was not improved (Ayton et al., 2014; Endo et al., 2018; Palanker, 2023; Petoe et al., 2024).

6.4. Overcoming the limitations of the implant

Several unresolved challenges limit the performance and functionality of implants. These include constraints related to electrode size and number, electrode cell spacing, spatial and temporal resolution, the efficiency of electrical stimulation, and stimulation safety. These issues are being addressed by several research consortia and commercial companies. An overview of recent advances towards overcoming these challenges is presented in Palanker, 2023. In this thesis, we looked for ways to optimise the electrical stimulation produced by an implant.

The first two approaches in this thesis, pharmacologically abolishing oscillations (chapter 3) and phase specific stimulation (chapter 4), deal with the pathological oscillatory activity. Both methods show how to improve the stimulation efficiency of the implant, with the first method by abolishing oscillations with drugs and the second method by stimulating at certain phases. In the third approach (chapter 5), we look into ways to selectively target different RGCs that help us obtain better and well-resolved responses.

High-frequency electrical stimulation can also be used to selectively stimulate ON RGCs and OFF RGCs (Guo et al., 2018; Löhler et al., 2024). However, the continuous high-frequency stimulation poses a problem in that the responses of the RGCs reduce when it is stimulated repeatedly. This phenomenon is called desensitisation which causes fading of the phosphenes generated by the implant. To overcome this, a spatially and temporally modulated pulse train (time-varied, non-stationary or interrupted) that mimics the involuntary microsaccades can be used and this would generate visual perception without the fading (Chenais et al., 2021).

Another approach to improve the electrical stimulation is by using a microcoil array that produces magnetic stimulation to stimulate the retina (Raghuram et al., 2024). The authors developed a flexible and transparent bioelectronic device that contains four micromagnetic stimulation (μMS) elements and is encapsulated in a bioinert material. Micromagnetic stimulation using this device is shown to produce less damage to the cells and more spatially selective and confined responses of the neurons, better than MEA stimulations. This device has been tested in the retina and cortex; further studies on adding more μMS elements are currently being explored. Along this line, another technique that is being developed and tested in the retina is the ultrasonic stimulation. Ultrasound or ultrasonic stimulations are the stimulations in the acoustic range of frequencies which is higher than the upper limit of human perception, 20kHz. They are shown to produce spatially precise stimulations and differential activation of ON and OFF pathways similar to light stimulations (Lo et al., 2020).

Retinal implant research is also expanding beyond conventional performance improvements to include novel concepts such as colour perception and artificial intelligence driven strategies.

6.4.1. Colour perception

The visual percepts formed by the current retinal implants are usually described as being in black and white. There are very few studies that looked into colour perception, but adding colour to an image is shown to help identify objects easily, especially when the resolution of the image is poor, as is the case with the implants. On testing in patients with Argus II, patients reported seeing phosphenes in white/yellow colour at low stimulation frequency and blue/purple at high stimulation frequency (Yue et al., 2021). Similarly, on testing trains of cathodic and anodic pulses in a few other subjects with Argus II, they reported seeing seven combinations of colours: gray-white, yellow-grey, orange-white, white-blue, brown-white, yellow-white, yellow-blue (Stanga et al., 2012). The perception of blue-yellow colour by epiretinal stimulation is thought to occur by stimulating the small bistratified RGCs or midget RGCs that is shown to be involved in blue-yellow colour opponency (Yue et al., 2021). Another method to produce colour perception is by developing a subretinal implant with electrodes, made from polymers that respond to light of different wavelengths, which could replace the photoreceptors (Askew et al., 2024).

6.4.2. Artificial Intelligence

Advancements in artificial intelligence (AI) have significantly contributed to the enhancement of retinal prosthetic technologies. AI algorithms are used for image processing and maximise the information obtained from the recording of the camera (K. Y. Wu et al., 2023). An AI system called NeuCube has been developed to process images and avoid obstacles with high accuracy (Ge et al., 2017). DeepGaze II is an AI algorithm that uses deep neural networks to recognise objects and improve saliency prediction (Kümmerer et al., 2016). AI has proven effective in enhancing face recognition capabilities, a potential that was explored by simulating responses from PRIMA implants and identifying the most suitable machine learning algorithms for this task (J. Park et al., 2025). Another AI-driven image processing framework, *pulse2percept*, was developed by analysing the phosphenes generated by an in-silico retinal implant, further demonstrating the potential of artificial intelligence in simulating and optimising visual perception in prosthetic vision systems (Y. Wu et al., 2023). Retinal stimulation can also be optimised using AI in a closed-loop approach, enabling real-time identification of optimal stimulation parameters and the selective activation of specific RGCs (Ghaffari et al., 2021; Löhler et al., 2024).

6.5. Future prospects

Overall, significant progress has been made in the field of artificial vision through the development of innovative strategies and the clinical testing of retinal implants in patients. However, several challenges remain, including limitations in image processing, spatial and temporal resolution, cell-selective stimulation, efficient electrical activation, and surgical complexity. Despite these hurdles, ongoing advancements continue to address these issues, highlighting the strong potential of retinal prostheses as a promising approach for treating retinal degeneration diseases.

In this work, we have demonstrated several ways to optimise the electrical stimulation of the retina by an implant. To achieve higher stimulation efficiency, abolishing the pathological oscillations using pharmacological drugs like THIP or stimulating at the phase maxima of the oscillation is shown to be beneficial. We also identified the preferred pulse stimulus amplitude, duration and shape that would selectively stimulate ON RGCs over OFF RGCs, thereby mimicking a light response with electrical stimulation. These approaches have the potential to generate responses with greater efficiency and enhanced resolution.

The implementation of these findings in a functional implant requires the development of closed-loop stimulation approaches, such as bidirectional implants capable of both recording and stimulating the retinal activity. Achieving this goal necessitates a collaborative, multidisciplinary effort involving electrophysiology, electronics, materials science, computer science, and surgical expertise. Addressing each challenge through coordinated research is essential for advancing artificial vision technologies and ultimately improving the quality of life for individuals with visual impairments.

7. References

- Ahn, J., Cha, S., Choi, K.-E., Kim, S.-W., Yoo, Y., & Goo, Y. S. (2022). Correlated Activity in the Degenerate Retina Inhibits Focal Response to Electrical Stimulation. *Frontiers in Cellular Neuroscience*, *16*, 889663. https://doi.org/10.3389/fncel.2022.889663

- Ahn, K. N., Ahn, J. Y., Kim, J., Cho, K., Koo, K., Senok, S. S., & Goo, Y. S. (2015). Effect of Stimulus Waveform of Biphasic Current Pulse on Retinal Ganglion Cell Responses in Retinal Degeneration (*rd1*) mice. *The Korean Journal of Physiology & Pharmacology*, *19*(2), 167. https://doi.org/10.4196/kjpp.2015.19.2.167

- Askew, L., Sweeney, A., Cox, D., & Shkunov, M. (2024). Toward Full-Color Vision Restoration: Conjugated Polymers as Key Functional Materials in Artificial Retinal Prosthetics. *Advanced Materials Interfaces*, *11*(29), 2400128. https://doi.org/10.1002/admi.202400128

- Ayton, L. N., Blamey, P. J., Guymer, R. H., Luu, C. D., Nayagam, D. A. X., Sinclair, N. C., Shivdasani, M. N., Yeoh, J., McCombe, M. F., Briggs, R. J., Opie, N. L., Villalobos, J., Dimitrov, P. N., Varsamidis, M., Petoe, M. A., McCarthy, C. D., Walker, J. G., Barnes, N., Burkitt, A. N., … Bionic Vision Australia Research Consortium. (2014). First-in-human trial of a novel suprachoroidal retinal prosthesis. *PloS One*, *9*(12), e115239. https://doi.org/10.1371/journal.pone.0115239

- Azarashvili, T., Baburina, Y., Grachev, D., Krestinina, O., Evtodienko, Y., Stricker, R., & Reiser, G. (2011). Calcium-induced permeability transition in rat brain mitochondria is promoted by carbenoxolone through targeting connexin43. *American Journal of Physiology-Cell Physiology*, *300*(3), C707–C720. https://doi.org/10.1152/ajpcell.00061.2010

- Baden, T., Berens, P., Franke, K., Román Rosón, M., Bethge, M., & Euler, T. (2016). The functional diversity of retinal ganglion cells in the mouse. *Nature*, *529*(7586), 345–350. https://doi.org/10.1038/nature16468

- Biswas, S., Haselier, C., Mataruga, A., Thumann, G., Walter, P., & Müller, F. (2014). Pharmacological Analysis of Intrinsic Neuronal Oscillations in rd10 Retina. *PLoS ONE*, *9*(6), e99075. https://doi.org/10.1371/journal.pone.0099075

- Bittner, A. K., Diener-West, M., & Dagnelie, G. (2009). A Survey of Photopsias in Self-reported Retinitis Pigmentosa: Location of Photopsias is related to Disease Severity. *Retina (Philadelphia, Pa.)*, *29*(10), 1513–1521. https://doi.org/10.1097/IAE.0b013e3181af0d57

- Bloomfield, S. A., & Völgyi, B. (2009). The diverse functional roles and regulation of neuronal gap junctions in the retina. *Nature Reviews Neuroscience*, *10*(7), 495–506. https://doi.org/10.1038/nrn2636

- Borowska, J., Trenholm, S., & Awatramani, G. B. (2011). An Intrinsic Neural Oscillator in the Degenerating Mouse Retina. *The Journal of Neuroscience*, *31*(13), 5000–5012. https://doi.org/10.1523/JNEUROSCI.5800-10.2011

- Bovi Dos Santos, G., de Lima-Vasconcellos, T. H., Móvio, M. I., Birbrair, A., Del Debbio, C. B., & Kihara, A. H. (2024). New Perspectives in Stem Cell Transplantation and Associated Therapies to Treat Retinal Diseases: From Gene Editing to 3D Bioprinting. *Stem Cell Reviews and Reports*, *20*(3), 722–737. https://doi.org/10.1007/s12015-024-10689-4

- Bowery, N. G., HiD, D. R., Hudson, A. L., Doble, A., Middlemiss, D. N., Shaw, J., & TurnbuU, M. (1980). *(-)Baclofen decreases neurotransmitter release in the mammalian eNS by an action at a novel GABA receptor*. *283*.

- Brown, G. C., Brown, M. M., & Fischer, D. H. (2015). Photopsias: A Key to Diagnosis. *Ophthalmology*, *122*(10), 2084–2094. https://doi.org/10.1016/j.ophtha.2015.06.025

- Cai, C., Ren, Q., Desai, N. J., Rizzo, J. F., & Fried, S. I. (2011). Response variability to high rates of electric stimulation in retinal ganglion cells. *Journal of Neurophysiology*, *106*(1), 153–162. https://doi.org/10.1152/jn.00956.2010

- Carleton, M., & Oesch, N. W. (2024). Asymmetric Activation of ON and OFF Pathways in the Degenerated Retina. *eNeuro*, *11*(5), ENEURO.0110-24.2024. https://doi.org/10.1523/ENEURO.0110-24.2024

- Carter-Dawson, L. D., LaVail, M. M., & Sidman, R. L. (1978). Differential effect of the rd mutation on rods and cones in the mouse retina. *Vision Research*, *18*(9), 1175–1183. https://doi.org/10.1016/0042-6989(78)90104-3

- Cembrowski, M. S., Logan, S. M., Tian, M., Jia, L., Li, W., Kath, W. L., Riecke, H., & Singer, J. H. (2012). The mechanisms of repetitive spike generation in an axonless retinal interneuron. *Cell Reports*, *1*(2), 155–166. https://doi.org/10.1016/j.celrep.2011.12.006

- Cha, S., Ahn, J., Jeong, Y., Lee, Y. H., Kim, H. K., Lee, D., Yoo, Y., & Goo, Y. S. (2022). Stage-Dependent Changes of Visual Function and Electrical Response of the Retina in the rd10 Mouse Model. *Frontiers in Cellular Neuroscience*, *16*, 926096. https://doi.org/10.3389/fncel.2022.926096

- Chang, B., Hawes, N. L., Hurd, R. E., Davisson, M. T., Nusinowitz, S., & Heckenlively, J. R. (2002). Retinal degeneration mutants in the mouse. *Vision Research*, *42*(4), 517–525. https://doi.org/10.1016/S0042-6989(01)00146-8

- Chang, B., Hawes, N. L., Pardue, M. T., German, A. M., Hurd, R. E., Davisson, M. T., Nusinowitz, S., Rengarajan, K., Boyd, A. P., Sidney, S. S., Phillips, M. J., Stewart, R. E., Chaudhury, R., Nickerson, J. M., Heckenlively, J. R., & Boatright, J. H. (2007). Two mouse retinal degenerations caused by missense mutations in the β-subunit of rod cGMP phosphodiesterase gene. *Vision Research*, *47*(5), 624–633. https://doi.org/10.1016/j.visres.2006.11.020

- Charters, L. (2026, January 31). *NR600 retinal prosthesis: Safe with promising visual results | Modern Retina*. https://www.modernretina.com/view/nr600-retinal-prosthesis-safe-with-promising-visual-results

- Chenais, N. A. L., Airaghi Leccardi, M. J. I., & Ghezzi, D. (2021). Naturalistic spatiotemporal modulation of epiretinal stimulation increases the response persistence of retinal ganglion cell. *Journal of Neural Engineering*, *18*(1), 016016. https://doi.org/10.1088/1741-2552/abcd6f

- Choi, H., Zhang, L., Cembrowski, M. S., Sabottke, C. F., Markowitz, A. L., Butts, D. A., Kath, W. L., Singer, J. H., & Riecke, H. (2014). Intrinsic bursting of AII amacrine cells underlies oscillations in the rd1 mouse retina. *Journal of Neurophysiology*, *112*(6), 1491–1504. https://doi.org/10.1152/jn.00437.2014

- Clark, S., Antell, A., & Kaufman, K. (2015). New antiepileptic medication linked to blue discoloration of the skin and eyes. *Therapeutic Advances in Drug Safety*, *6*(1), 15–19. https://doi.org/10.1177/2042098614560736

- Cooper, E. C., & Jan, L. Y. (2003). M-Channels: Neurological Diseases, Neuromodulation, and Drug Development. *Archives of Neurology*, *60*(4), 496. https://doi.org/10.1001/archneur.60.4.496

- Corna, A., Ramesh, P., Jetter, F., Lee, M.-J., Macke, J. H., & Zeck, G. (2021). Discrimination of simple objects decoded from the output of retinal ganglion cells upon sinusoidal electrical stimulation. *Journal of Neural Engineering*, *18*(4), 046086. https://doi.org/10.1088/1741-2552/ac0679

- Daschner, R., Rothermel, A., Rudorf, R., Rudorf, S., & Stett, A. (2018). Functionality and Performance of the Subretinal Implant Chip Alpha AMS. *Sensors and Materials*, 179. https://doi.org/10.18494/SAM.2018.1726

- Demb, J. B., & Singer, J. H. (2012). Intrinsic properties and functional circuitry of the AII amacrine cell. *Visual Neuroscience*, *29*(1), 51–60. https://doi.org/10.1017/S0952523811000368

- Deubel, R., Hegel, L., Kauth, A., Ghosh, E., Pachauri, V., Vu, X. T., Johnen, S., & Ingebrandt, S. (2023). Transparent microfluidic MEAs with organic electronic ion pumps for in vitro studies of the pathological retina. . . *Oktober*.

- Drasbek, K. R., & Jensen, K. (2006). THIP, a Hypnotic and Antinociceptive Drug, Enhances an Extrasynaptic GABAA Receptor-mediated Conductance in Mouse Neocortex. *Cerebral Cortex*, *16*(8), 1134–1141. https://doi.org/10.1093/cercor/bhj055

- Du, Y., & Shen, Y. (2025). Progress in photoreceptor replacement therapy for retinal degenerative diseases. *Cell Insight*, *4*(1), 100223. https://doi.org/10.1016/j.cellin.2024.100223

- Endo, T., Fujikado, T., Hirota, M., Kanda, H., Morimoto, T., & Nishida, K. (2018). Light localization with low-contrast targets in a patient implanted with a suprachoroidal-transretinal stimulation retinal prosthesis. *Graefe's Archive for Clinical and Experimental Ophthalmology = Albrecht Von Graefes Archiv Fur Klinische Und Experimentelle Ophthalmologie*, *256*(9), 1723–1729. https://doi.org/10.1007/s00417-018-3982-0

- Esser, S., Spehr, M., & Müller, F. (2019). *Localization and physiological role of the glutamate transporter EAAT5 in the murine retina* (RWTH-2019-12168) [Dissertation, RWTH Aachen University, 2019]. https://publications.rwth-aachen.de/record/775363/export/hm?ln=en

- Euler, T., & Schubert, T. (2015). Multiple Independent Oscillatory Networks in the Degenerating Retina. *Frontiers in Cellular Neuroscience*, *9*, 444. https://doi.org/10.3389/fncel.2015.00444

- Evenseth, L. S. M., Gabrielsen, M., & Sylte, I. (2020). The GABAB Receptor—Structure, Ligand Binding and Drug Development. *Molecules*, *25*(13), Article 13. https://doi.org/10.3390/molecules25133093

- Famiglietti, E. V. (2025). Mammalian Retinal Bipolar Cells: Morphological Identification and Systematic Classification in Rabbit Retina With a Comparative Perspective. *Journal of Comparative Neurology*, *533*(2), e70015. https://doi.org/10.1002/cne.70015

- Famiglietti, E. V., & Kolb, H. (1975). A bistratified amacrine cell and synaptic cirucitry in the inner plexiform layer of the retina. *Brain Research*, *84*(2), 293–300. https://doi.org/10.1016/0006-8993(75)90983-x

- Feigenspan, A., Janssen-Bienhold, U., Hormuzdi, S., Monyer, H., Degen, J., Söhl, G., Willecke, K., Ammermüller, J., & Weiler, R. (2004). Expression of connexin36 in cone pedicles and OFF-cone bipolar cells of the mouse retina. *The Journal of Neuroscience :*

The Official Journal of the Society for Neuroscience, *24*(13). https://doi.org/10.1523/JNEUROSCI.5598-03.2004

- Ferlauto, L., Airaghi Leccardi, M. J. I., Chenais, N. A. L., Gilliéron, S. C. A., Vagni, P., Bevilacqua, M., Wolfensberger, T. J., Sivula, K., & Ghezzi, D. (2018). Design and validation of a foldable and photovoltaic wide-field epiretinal prosthesis. *Nature Communications*, *9*(1), 992. https://doi.org/10.1038/s41467-018-03386-7

- Fraser, A. D. (1998). Use and abuse of the benzodiazepines. *Therapeutic Drug Monitoring*, *20*(5), 481–489. https://doi.org/10.1097/00007691-199810000-00007

- Fried, S. I., Hsueh, H. A., & Werblin, F. S. (2006). A Method for Generating Precise Temporal Patterns of Retinal Spiking Using Prosthetic Stimulation. *Journal of Neurophysiology*, *95*(2), 970–978. https://doi.org/10.1152/jn.00849.2005

- Fried, S. I., Lasker, A. C. W., Desai, N. J., Eddington, D. K., & Rizzo, J. F. (2009). Axonal Sodium-Channel Bands Shape the Response to Electric Stimulation in Retinal Ganglion Cells. *Journal of Neurophysiology*, *101*(4), 1972–1987. https://doi.org/10.1152/jn.91081.2008

- Fung, A. T., Tran, T., Lim, L. L., Samarawickrama, C., Arnold, J., Gillies, M., Catt, C., Mitchell, L., Symons, A., Buttery, R., Cottee, L., Tumuluri, K., & Beaumont, P. (2020). Local delivery of corticosteroids in clinical ophthalmology: A review. *Clinical & Experimental Ophthalmology*, *48*(3), 366–401. https://doi.org/10.1111/ceo.13702

- Gargini, C., Terzibasi, E., Mazzoni, F., & Strettoi, E. (2007). IRetinal Organization in the retinal degeneration 10 (rd10) Mutant Mouse: A Morphological and ERG Study. *The Journal of Comparative Neurology*, *500*(2), 222–238. https://doi.org/10.1002/cne.21144

- Ge, C., Kasabov, N., Liu, Z., & Yang, J. (2017). A spiking neural network model for obstacle avoidance in simulated prosthetic vision. *Information Sciences*, *399*, 30–42. https://doi.org/10.1016/j.ins.2017.03.006

- Gehlen, J., Esser, S., Schaffrath, K., Johnen, S., Walter, P., & Müller, F. (2020). Blockade of Retinal Oscillations by Benzodiazepines Improves Efficiency of Electrical Stimulation in the Mouse Model of RP, *rd10*. *Investigative Opthalmology & Visual Science*, *61*(13), 37. https://doi.org/10.1167/iovs.61.13.37

- Ghaffari, D. H., Akwaboah, A. D., Mirzakhalili, E., & Weiland, J. D. (2021). Real-Time Optimization of Retinal Ganglion Cell Spatial Activity in Response to Epiretinal Stimulation. *IEEE Transactions on Neural Systems and Rehabilitation Engineering : A Publication of the IEEE Engineering in Medicine and Biology Society*, *29*, 2733–2741. https://doi.org/10.1109/TNSRE.2021.3138297

- Gheorghe, A., Mahdi, L., & Musat, O. (2015). AGE-RELATED MACULAR DEGENERATION. *Romanian Journal of Ophthalmology*, *59*(2), 74–77.

- Ghit, A., Assal, D., Al-Shami, A. S., & Hussein, D. E. E. (2021). GABAA receptors: Structure, function, pharmacology, and related disorders. *Journal of Genetic Engineering and Biotechnology*, *19*(1), 123. https://doi.org/10.1186/s43141-021-00224-0

- Gleason, E. (2012). The influences of metabotropic receptor activation on cellular signaling and synaptic function in amacrine cells. *Visual Neuroscience*, *29*(1), 31–39. https://doi.org/10.1017/S0952523811000204

- Goo, Y. S., Ahn, K. N., Song, Y. J., Ahn, S. H., Han, S. K., Ryu, S. B., & Kim, K. H. (2011). Spontaneous Oscillatory Rhythm in Retinal Activities of Two Retinal Degeneration (rd1 and rd10) Mice. *The Korean Journal of Physiology & Pharmacology : Official Journal of the Korean Physiological Society and the Korean Society of Pharmacology*, *15*(6), 415–422. https://doi.org/10.4196/kjpp.2011.15.6.415

- Goo, Y. S., Park, D. J., Ahn, J. R., & Senok, S. S. (2016). Spontaneous oscillatory rhythms in the degenerating mouse retina modulate retinal ganglion cell responses to electrical stimulation. *Frontiers in Cellular Neuroscience*, *9*. https://doi.org/10.3389/fncel.2015.00512

- Goo, Y. S., Ye, J. H., Lee, S., Nam, Y., Ryu, S. B., & Kim, K. H. (2011). Retinal ganglion cell responses to voltage and current stimulation in wild-type and *rd1* mouse retinas. *Journal of Neural Engineering*, *8*(3), 035003. https://doi.org/10.1088/1741-2560/8/3/035003

- Grant, S. M., & Heel, R. C. (1991). Vigabatrin: A Review of its Pharmacodynamic and Pharmacokinetic Properties, and Therapeutic Potential in Epilepsy and Disorders of Motor Control. *Drugs*, *41*(6), 889–926. https://doi.org/10.2165/00003495-199141060-00007

- Guo, T., Yang, C. Y., Tsai, D., Muralidharan, M., Suaning, G. J., Morley, J. W., Dokos, S., & Lovell, N. H. (2018). Closed-Loop Efficient Searching of Optimal Electrical Stimulation Parameters for Preferential Excitation of Retinal Ganglion Cells. *Frontiers in Neuroscience*, *12*, 168. https://doi.org/10.3389/fnins.2018.00168

- Hadjinicolaou, A. E., Savage, C. O., Apollo, N. V., Garrett, D. J., Cloherty, S. L., Ibbotson, M. R., & O'Brien, B. J. (2015). Optimizing the Electrical Stimulation of Retinal Ganglion Cells. *IEEE Transactions on Neural Systems and Rehabilitation Engineering*, *23*(2), 169–178. IEEE Transactions on Neural Systems and Rehabilitation Engineering. https://doi.org/10.1109/TNSRE.2014.2361900

- Ham, Y., Mehta, H., Kang-Mieler, J., Mieler, W. F., & Chang, A. (2023). Novel Drug Delivery Methods and Approaches for the Treatment of Retinal Diseases. *Asia-Pacific Journal of Ophthalmology*, *12*(4), 402–413. https://doi.org/10.1097/APO.0000000000000623

- Hamel, C. (2006). Retinitis pigmentosa. *Orphanet Journal of Rare Diseases*, *1*, 40. https://doi.org/10.1186/1750-1172-1-40

- Han, Y., & Massey, S. C. (2005). Electrical synapses in retinal ON cone bipolar cells: Subtype-specific expression of connexins. *Proceedings of the National Academy of Sciences of the United States of America*, *102*(37), 13313–13318. https://doi.org/10.1073/pnas.0505067102

- Haq, W., Arango-Gonzalez, B., Zrenner, E., Euler, T., & Schubert, T. (2014). Synaptic remodeling generates synchronous oscillations in the degenerated outer mouse retina. *Frontiers in Neural Circuits*, *8*, 108. https://doi.org/10.3389/fncir.2014.00108

- Hartong, D. T., Berson, E. L., & Dryja, T. P. (2006). Retinitis pigmentosa. *Lancet (London, England)*, *368*(9549), 1795–1809. https://doi.org/10.1016/S0140-6736(06)69740-7

- Haselier, C., Biswas, S., Rösch, S., Thumann, G., Müller, F., & Walter, P. (2017). Correlations between specific patterns of spontaneous activity and stimulation efficiency in degenerated retina. *PLOS ONE*, *12*(12), e0190048. https://doi.org/10.1371/journal.pone.0190048

- Haselier, C., Spehr, M., & Thumann, G. (2016). *In vitro Charakterisierung der elektrophysiologischen Eigenschaften und elektrischen Stimulierbarkeit eines genetischen und eines pharmakologisch induzierten murinen Retinadegenerationsmodells* (RWTH-2016-06926) [Dissertation, RWTH Aachen University, 2016]. https://publications.rwth-aachen.de/record/668661/export/hx?ln=en

- Heckenlively, J. R., Yoser, S. L., Friedman, L. H., & Oversier, J. J. (1988). Clinical Findings and Common Symptoms in Retinitis Pigmentosa. *American Journal of Ophthalmology*, *105*(5), 504–511. https://doi.org/10.1016/0002-9394(88)90242-5

- Hoehn-Saric, R. (1983). Effects of THIP on chronic anxiety. *Psychopharmacology*, *80*(4), 338–341. https://doi.org/10.1007/BF00432116

- Hoon, M., Okawa, H., Santina, L. D., & Wong, R. O. L. (2014). Functional Architecture of the Retina: Development and Disease. *Progress in Retinal and Eye Research*, *42*, 44–84. https://doi.org/10.1016/j.preteyeres.2014.06.003

- Humayun, M. S., Dorn, J. D., Ahuja, A. K., Caspi, A., Filley, E., Dagnelie, G., Salzmann, J., Santos, A., Duncan, J., daCruz, L., Mohand-Said, S., Eliott, D.,

McMahon, M. J., & Greenberg, R. J. (2009). Preliminary 6 month results from the argustm ii epiretinal prosthesis feasibility study. *2009 Annual International Conference of the IEEE Engineering in Medicine and Biology Society*, 4566–4568. https://doi.org/10.1109/IEMBS.2009.5332695

- Humayun, M. S., Weiland, J. D., Fujii, G. Y., Greenberg, R., Williamson, R., Little, J., Mech, B., Cimmarusti, V., Van Boemel, G., Dagnelie, G., & de Juan, E. (2003). Visual perception in a blind subject with a chronic microelectronic retinal prosthesis. *Vision Research*, *43*(24), 2573–2581. https://doi.org/10.1016/S0042-6989(03)00457-7

- Im, M., & Fried, S. I. (2016). Temporal properties of network-mediated responses to repetitive stimuli are dependent upon retinal ganglion cell type. *Journal of Neural Engineering*, *13*(2), 025002. https://doi.org/10.1088/1741-2560/13/2/025002

- Im, M., Werginz, P., & Fried, S. I. (2018). Electric stimulus duration alters network-mediated responses depending on retinal ganglion cell type. *Journal of Neural Engineering*, *15*(3), 036010. https://doi.org/10.1088/1741-2552/aaadc1

- Imai, S., Suzuki, T., Sato, K., & Tokimasa, T. (1999). Effects of quinine on three different types of potassium currents in bullfrog sympathetic neurons. *Neuroscience Letters*, *275*(2), 121–124. https://doi.org/10.1016/S0304-3940(99)00775-2

- Ito, S. (2016). GABA and glycine in the developing brain. *The Journal of Physiological Sciences : JPS*, *66*(5), 375. https://doi.org/10.1007/s12576-016-0442-7

- Jensen, R. J., & Rizzo, J. F. (2008). Activation of retinal ganglion cells in wild-type and rd1 mice through electrical stimulation of the retinal neural network. *Vision Research*, *48*(14), 1562–1568. https://doi.org/10.1016/j.visres.2008.04.016

- Jensen, R. J., & Rizzo, J. F. (2009). Activation of ganglion cells in wild-type and *rd1* mouse retinas with monophasic and biphasic current pulses. *Journal of Neural Engineering*, *6*(3), 035004. https://doi.org/10.1088/1741-2560/6/3/035004

- Jensen, R. J., Rizzo, J. F., Ziv, O. R., Grumet, A., & Wyatt, J. (2003). Thresholds for Activation of Rabbit Retinal Ganglion Cells with an Ultrafine, Extracellular Microelectrode. *Investigative Opthalmology & Visual Science*, *44*(8), 3533. https://doi.org/10.1167/iovs.02-1041

- Jensen, R. J., Ziv, O. R., & Rizzo, J. F. (2005). Responses of rabbit retinal ganglion cells to electrical stimulation with an epiretinal electrode. *Journal of Neural Engineering*, *2*(1), S16. https://doi.org/10.1088/1741-2560/2/1/003

- Johnston, G. a. R., Stephanson, A. L., & Twitchin, B. (1976). Uptake and Release of Nipecotic Acid by Rat Brain Slices. *Journal of Neurochemistry*, *26*(1), 83–87. https://doi.org/10.1111/j.1471-4159.1976.tb04439.x

- Juvenal, G., Higa, G. S. V., Bonfim Marques, L., Tessari Zampieri, T., Costa Viana, F. J., Britto, L. R., Tang, Y., Illes, P., di Virgilio, F., Ulrich, H., & de Pasquale, R. (2025). Regulation of GABAergic neurotransmission by purinergic receptors in brain physiology and disease. *Purinergic Signalling*, *21*(1), 149–177. https://doi.org/10.1007/s11302-024-10034-x

- Kim, H. M., & Woo, S. J. (2021). Ocular Drug Delivery to the Retina: Current Innovations and Future Perspectives. *Pharmaceutics*, *13*(1), 108. https://doi.org/10.3390/pharmaceutics13010108

- Knight, E. M. P., Amin, S., Bahi-Buisson, N., Benke, T. A., Cross, J. H., Demarest, S. T., Olson, H. E., Specchio, N., Fleming, T. R., Aimetti, A. A., Gasior, M., Devinsky, O., Belousova, E., Belyaev, O., Ben-Zeev, B., Brunklaus, A., Ciliberto, M. A., Darra, F., Davis, R., … Zolnowska, M. (2022). Safety and efficacy of ganaxolone in patients with CDKL5 deficiency disorder: Results from the double-blind phase of a randomised, placebo-controlled, phase 3 trial. *The Lancet Neurology*, *21*(5), 417–427. https://doi.org/10.1016/S1474-4422(22)00077-1

- Knop, G. C., Feigenspan, A., Weiler, R., & Dedek, K. (2011). Inputs Underlying the ON–OFF Light Responses of Type 2 Wide-Field Amacrine Cells in TH::GFP Mice. *The Journal of Neuroscience*, *31*(13), 4780–4791. https://doi.org/10.1523/JNEUROSCI.6235-10.2011

- Kolb, H., & Nelson, R. (1983). Rod pathways in the retina of the cat. *Vision Research*, *23*(4), 301–312. https://doi.org/10.1016/0042-6989(83)90078-0

- Kole, M. H. P., & Stuart, G. J. (2012). Signal Processing in the Axon Initial Segment. *Neuron*, *73*(2), 235–247. https://doi.org/10.1016/j.neuron.2012.01.007

- Krogsgaard-Larsen, P. (1980). Inhibitors of the GABA uptake systems. *Molecular and Cellular Biochemistry*, *31*(2). https://doi.org/10.1007/BF00240816

- Kümmerer, M., Wallis, T. S. A., & Bethge, M. (2016). *DeepGaze II: Reading fixations from deep features trained on object recognition* (arXiv:1610.01563). arXiv. https://doi.org/10.48550/arXiv.1610.01563

- Lee, J.-I., & Im, M. (2018). Non-rectangular waveforms are more charge-efficient than rectangular one in eliciting network-mediated responses of ON type retinal ganglion cells. *Journal of Neural Engineering*, *15*(5), 055004. https://doi.org/10.1088/1741-2552/aad416

- Lee, J.-I., Werginz, P., & Fried, S. I. (2023). Variability in Depolarization Sensitivity Underlies Differential Responses to High-frequency Stimulation of ON and OFF RGCs. *2023 11th International IEEE/EMBS Conference on Neural Engineering (NER)*, 1–4. https://doi.org/10.1109/NER52421.2023.10123855

- Lee, J.-I., Werginz, P., Kameneva, T., Im, M., & Fried, S. I. (2024). Membrane depolarization mediates both the inhibition of neural activity and cell-type-differences in response to high-frequency stimulation. *Communications Biology*, *7*, 734. https://doi.org/10.1038/s42003-024-06359-3

- Lin, B., Jakobs, T. C., & Masland, R. H. (2005). Different functional types of bipolar cells use different gap-junctional proteins. *The Journal of Neuroscience: The Official Journal of the Society for Neuroscience*, *25*(28), 6696–6701. https://doi.org/10.1523/JNEUROSCI.1894-05.2005

- Lo, P.-A., Huang, K., Zhou, Q., Humayun, M. S., & Yue, L. (2020). Ultrasonic Retinal Neuromodulation and Acoustic Retinal Prosthesis. *Micromachines*, *11*(10), 929. https://doi.org/10.3390/mi11100929

- Löhler, P., Albert, A., Erbslöh, A., Nruthyathi, Müller, F., & Seidl, K. (2024). A Cell-Type Selective Stimulation and Recording System for Retinal Ganglion Cells. *IEEE Transactions on Biomedical Circuits and Systems*, *18*(3), 498–510. https://doi.org/10.1109/TBCAS.2023.3342465

- Lukasiewicz, P. D., & Shields, C. R. (1998). A diversity of GABA receptors in the retina. *Seminars in Cell & Developmental Biology*, *9*(3), 293–299. https://doi.org/10.1006/scdb.1998.0238

- Margolis, D. J., & Detwiler, P. B. (2011). Cellular Origin of Spontaneous Ganglion Cell Spike Activity in Animal Models of Retinitis Pigmentosa. *Journal of Ophthalmology*, *2011*(1), 507037. https://doi.org/10.1155/2011/507037

- Margolis, D. J., Gartland, A. J., Singer, J. H., & Detwiler, P. B. (2014). Network Oscillations Drive Correlated Spiking of ON and OFF Ganglion Cells in the rd1 Mouse Model of Retinal Degeneration. *PLoS ONE*, *9*(1), e86253. https://doi.org/10.1371/journal.pone.0086253

- Margolis, D. J., Newkirk, G., Euler, T., & Detwiler, P. B. (2008). Functional Stability of Retinal Ganglion Cells after Degeneration-Induced Changes in Synaptic Input. *The Journal of Neuroscience*, *28*(25), 6526–6536. https://doi.org/10.1523/JNEUROSCI.1533-08.2008

- Masland, R. H. (2001). The fundamental plan of the retina. *Nature Neuroscience*, *4*(9), 877–886. https://doi.org/10.1038/nn0901-877

- Masland, R. H. (2012). The Neuronal Organization of the Retina. *Neuron*, *76*(2), 266–280. https://doi.org/10.1016/j.neuron.2012.10.002

- Matsui, K., Hosoi, N., & Tachibana, M. (1998). Excitatory Synaptic Transmission in the Inner Retina: Paired Recordings of Bipolar Cells and Neurons of the Ganglion Cell

Layer. *The Journal of Neuroscience*, *18*(12), 4500–4510. https://doi.org/10.1523/JNEUROSCI.18-12-04500.1998

- McGuire, B., Stevens, J., & Sterling, P. (1984). Microcircuitry of bipolar cells in cat retina. *The Journal of Neuroscience*, *4*(12), 2920–2938. https://doi.org/10.1523/JNEUROSCI.04-12-02920.1984

- Meer, A.-M. van der, Berger, T., Müller, F., Foldenauer, A. C., Johnen, S., & Walter, P. (2020). Establishment and Characterization of a Unilateral UV-Induced Photoreceptor Degeneration Model in the C57Bl/6J Mouse. *Translational Vision Science & Technology*, *9*(9), 21. https://doi.org/10.1167/tvst.9.9.21

- Menzel-Severing, J., Laube, T., Brockmann, C., Bornfeld, N., Mokwa, W., Mazinani, B., Walter, P., & Roessler, G. (2012). Implantation and explantation of an active epiretinal visual prosthesis: 2-year follow-up data from the EPIRET3 prospective clinical trial. *Eye*, *26*(4), 501–509. https://doi.org/10.1038/eye.2012.35

- Menzler, J., Channappa, L., & Zeck, G. (2014). Rhythmic Ganglion Cell Activity in Bleached and Blind Adult Mouse Retinas. *PLOS ONE*, *9*(8), e106047. https://doi.org/10.1371/journal.pone.0106047

- Menzler, J., & Zeck, G. (2011). Network Oscillations in Rod-Degenerated Mouse Retinas. *The Journal of Neuroscience*, *31*(6), 2280–2291. https://doi.org/10.1523/JNEUROSCI.4238-10.2011

- Monaghan, E. P., McAuley, J. W., & Data, J. L. (1999). Ganaxolone: A novel positive allosteric modulator of the GABAA receptor complex for the treatment of epilepsy. *Expert Opinion on Investigational Drugs*, *8*(10), 1663–1671. https://doi.org/10.1517/13543784.8.10.1663

- Morioka, M., Takamura, Y., Nagai, K., Yoshida, S., Mori, J., Takeuchi, M., Sawada, T., Sone, K., Fukuyama, H., Kusuhara, S., Yasukawa, T., Murakami, T., Tabuchi, H., Nagasato, D., Hirano, T., Ueda, T., Jujo, T., Sasajima, H., Mitamura, Y., … Inatani, M. (2020). Incidence of endophthalmitis after intravitreal injection of an anti-VEGF agent with or without topical antibiotics. *Scientific Reports*, *10*(1), 22122. https://doi.org/10.1038/s41598-020-79377-w

- Müller, F., Wässle, H., & Voigt, T. (1988). Pharmacological modulation of the rod pathway in the cat retina. *Journal of Neurophysiology*, *59*(6), 1657–1672. https://doi.org/10.1152/jn.1988.59.6.1657

- Nruthyathi, Jung, M., Wang, J., Montes, V. R., Offenhäusser, A., Willuweit, A., & Müller, F. (2025). Late emergence of pathological oscillatory activity in the retina of the Retinitis pigmentosa model RCS (Royal College of Surgeons) rat. *PLOS One*, *20*(5), e0324345. https://doi.org/10.1371/journal.pone.0324345

- Palanker, D. (2023). Electronic Retinal Prostheses. *Cold Spring Harbor Perspectives in Medicine*, *13*(8), a041525. https://doi.org/10.1101/cshperspect.a041525

- Palanker, D., Le Mer, Y., Mohand-Said, S., Muqit, M., & Sahel, J. A. (2020). Photovoltaic Restoration of Central Vision in Atrophic Age-Related Macular Degeneration. *Ophthalmology*, *127*(8), 1097–1104. https://doi.org/10.1016/j.ophtha.2020.02.024

- Palanker, D., Le Mer, Y., Mohand-Said, S., & Sahel, J. A. (2022). Simultaneous perception of prosthetic and natural vision in AMD patients. *Nature Communications*, *13*(1), 513. https://doi.org/10.1038/s41467-022-28125-x

- Park, D. J., Senok, S. S., & Goo, Y. S. (2015). Degeneration stage-specific response pattern of retinal ganglion cell spikes in rd10 mouse retina. *2015 37th Annual International Conference of the IEEE Engineering in Medicine and Biology Society (EMBC)*, 3351–3354. https://doi.org/10.1109/EMBC.2015.7319110

- Park, J., Goldstein, A. K., Zhuo, Y., Jensen, N., & Palanker, D. (2025). *Simulation of prosthetic vision with PRIMA system and enhancement of face representation* (arXiv:2503.11677). arXiv. https://doi.org/10.48550/arXiv.2503.11677

- Peng, Z., Hauer, B., Mihalek, R. M., Homanics, G. E., Sieghart, W., Olsen, R. W., & Houser, C. R. (2002). GABAA receptor changes in δ subunit-deficient mice: Altered expression of α4 and γ2 subunits in the forebrain. *Journal of Comparative Neurology*, *446*(2), 179–197. https://doi.org/10.1002/cne.10210

- Peretz, A., Degani, N., Nachman, R., Uziyel, Y., Gibor, G., Shabat, D., & Attali, B. (2005). Meclofenamic Acid and Diclofenac, Novel Templates of KCNQ2/Q3 Potassium Channel Openers, Depress Cortical Neuron Activity and Exhibit Anticonvulsant Properties. *Molecular Pharmacology*, *67*(4), 1053–1066. https://doi.org/10.1124/mol.104.007112

- Petoe, M. A., Abbott, C. J., Titchener, S. A., Kolic, M., Kentler, W. G., Nayagam, D. A. X., Baglin, E. K., Kvansakul, J., Barnes, N., Walker, J. G., Karapanos, L., McGuinness, M. B., Ayton, L. N., Luu, C. D., & Allen, P. J. (2024). A Second-Generation (44-Channel) Suprachoroidal Retinal Prosthesis: A Single-Arm Clinical Trial of Feasibility. *Ophthalmology Science*, *5*(1), 100525. https://doi.org/10.1016/j.xops.2024.100525

- Phillips, M. B., Povysheva, N. V., Harnett-Scott, K. A., Aizenman, E., & Johnson, J. W. (2024). *State-specific inhibition of NMDA receptors by memantine depends on intracellular calcium and provides insights into NMDAR channel blocker tolerability* (p. 2024.04.01.587624). bioRxiv. https://doi.org/10.1101/2024.04.01.587624

- Phillips, M. J., Otteson, D. C., & Sherry, D. M. (2010). Progression of neuronal and synaptic remodeling in the rd10 mouse model of retinitis pigmentosa. *Journal of Comparative Neurology*, *518*(11), 2071–2089. https://doi.org/10.1002/cne.22322

- Poboży, K., Poboży, T., Domański, P., Derczyński, M., Konarski, W., & Domańska-Poboża, J. (2025). Evolution of Light-Sensitive Proteins in Optogenetic Approaches for Vision Restoration: A Comprehensive Review. *Biomedicines*, *13*(2), 429. https://doi.org/10.3390/biomedicines13020429

- Poria, D., & Dhingra, N. K. (2015). Spontaneous oscillatory activity in rd1 mouse retina is transferred from ON pathway to OFF pathway via glycinergic synapse. *Journal of Neurophysiology*, *113*(2), 420–425. https://doi.org/10.1152/jn.00702.2014

- Raghuram, V., Datye, A. D., Fried, S. I., & Timko, B. P. (2024). Transparent and conformal microcoil arrays for spatially selective neuronal activation. *Device*, *2*(4). https://doi.org/10.1016/j.device.2024.100290

- Raghuram, V., Werginz, P., Fried, S. I., & Timko, B. P. (2021). Morphological Factors that Underlie Neural Sensitivity to Stimulation in the Retina. *Advanced NanoBiomed Research*, *1*(12), 2100069. https://doi.org/10.1002/anbr.202100069

- Ramerstorfer, J., Furtmüller, R., Sarto-Jackson, I., Varagic, Z., Sieghart, W., & Ernst, M. (2011). The GABAA Receptor α+β− Interface: A Novel Target for Subtype Selective Drugs. *The Journal of Neuroscience*, *31*(3), 870–877. https://doi.org/10.1523/JNEUROSCI.5012-10.2011

- Rincón Montes, V., Gehlen, J., Lück, S., Mokwa, W., Müller, F., Walter, P., & Offenhäusser, A. (2019). Toward a Bidirectional Communication Between Retinal Cells and a Prosthetic Device – A Proof of Concept. *Frontiers in Neuroscience*, *13*, 367. https://doi.org/10.3389/fnins.2019.00367

- Roh, H., Otgondemberel, Y., & Im, M. (2022). Short pulses of epiretinal prostheses evoke network-mediated responses in retinal ganglion cells by stimulating presynaptic neurons. *Journal of Neural Engineering*, *19*(5), 055006. https://doi.org/10.1088/1741-2552/ac8ed7

- Rösch, S., Johnen, S., Müller, F., Pfarrer, C., & Walter, P. (2014). *Correlations between ERG, OCT, and Anatomical Findings in the rd10 Mouse*. https://doi.org/10.1155/2014/874751

- Rowley, N. M., Madsen, K. K., Schousboe, A., & Steve White, H. (2012). Glutamate and GABA synthesis, release, transport and metabolism as targets for seizure control. *Neurochemistry International*, *61*(4), 546–558. https://doi.org/10.1016/j.neuint.2012.02.013

- Ruffolo, R. R., Gellai, M., Hieble, J. P., Willette, R. N., & Nichols, A. J. (1990). The pharmacology of carvedilol. *European Journal of Clinical Pharmacology*, *38*(S2), S82–S88. https://doi.org/10.1007/BF01409471

- Rüland, T., Doerenkamp, K., Graff, P. S., Wetz, S., Jain, A., Nabbefeld, G., Gehlen, J., Gilissen, S. R. J., Arckens, L., Musall, S., Müller, F., & Kampa, B. M. (2025). Lack of cross modal plasticity potentially linked to ongoing activation of visual cortex and superior colliculus in the rd10 mouse model of retinitis pigmentosa. *Cerebral Cortex*, *35*(10), bhaf273. https://doi.org/10.1093/cercor/bhaf273

- Ryu, S. B., Ye, J. H., Lee, J. S., Goo, Y. S., Kim, C. H., & Kim, K. H. (2009). Electrically-evoked Neural Activities of rd1 Mice Retinal Ganglion Cells by Repetitive Pulse Stimulation. *The Korean Journal of Physiology & Pharmacology : Official Journal of the Korean Physiological Society and the Korean Society of Pharmacology*, *13*(6), 443–448. https://doi.org/10.4196/kjpp.2009.13.6.443

- Ryu, S. B., Ye, J. H., Lee, J. S., Goo, Y. S., & Kim, K. H. (2009). Characterization of retinal ganglion cell activities evoked by temporally patterned electrical stimulation for the development of stimulus encoding strategies for retinal implants. *Brain Research*, *1275*, 33–42. https://doi.org/10.1016/j.brainres.2009.03.064

- Sagdullaev, B. T., McCall, M. A., & Lukasiewicz, P. D. (2006). Presynaptic Inhibition Modulates Spillover, Creating Distinct Dynamic Response Ranges of Sensory Output. *Neuron*, *50*(6), 923–935. https://doi.org/10.1016/j.neuron.2006.05.015

- Schilardi, G., Kralik, J., & Kleinlogel, S. (2023). Selective Block of Upregulated Kv1.3 Potassium Channels in ON-Bipolar Cells of the Blind Retina Enhances Optogenetically Restored Signaling. *International Journal of Molecular Sciences*, *24*(18), 14207. https://doi.org/10.3390/ijms241814207

- Scimemi, A. (2014). Structure, function, and plasticity of GABA transporters. *Frontiers in Cellular Neuroscience*, *8*. https://doi.org/10.3389/fncel.2014.00161

- Sekirnjak, C., Hottowy, P., Sher, A., Dabrowski, W., Litke, A. M., & Chichilnisky, E. J. (2006). Electrical Stimulation of Mammalian Retinal Ganglion Cells With Multielectrode Arrays. *Journal of Neurophysiology*, *95*(6), 3311–3327. https://doi.org/10.1152/jn.01168.2005

- Sekirnjak, C., Hulse, C., Jepson, L. H., Hottowy, P., Sher, A., Dabrowski, W., Litke, A. M., & Chichilnisky, E. J. (2009). Loss of Responses to Visual But Not Electrical Stimulation in Ganglion Cells of Rats With Severe Photoreceptor Degeneration. *Journal of Neurophysiology*, *102*(6), 3260–3269. https://doi.org/10.1152/jn.00663.2009

- Sieghart, W., Ramerstorfer, J., Sarto-Jackson, I., Varagic, Z., & Ernst, M. (2012). A novel GABAA receptor pharmacology: Drugs interacting with the α+β− interface. *British Journal of Pharmacology*, *166*(2), 476–485. https://doi.org/10.1111/j.1476-5381.2011.01779.x

- Srinivas, M., Hopperstad, M. G., & Spray, D. C. (2001). Quinine blocks specific gap junction channel subtypes. *Proceedings of the National Academy of Sciences*, *98*(19), 10942–10947. https://doi.org/10.1073/pnas.191206198

- Stanga, P. E., Jr., J. A. S., daCruz, L., Hafezi, F., Merlini, F., Coley, B., Greenberg, R. J., & Group, A. I. S. (2012). Patients blinded by outer retinal dystrophies are able to perceive simultaneous colors using the Argus® II Retinal Prosthesis System. *Investigative Ophthalmology & Visual Science*, *53*(14), 6952.

- Stingl, K., Bartz-Schmidt, K. U., Besch, D., Chee, C. K., Cottriall, C. L., Gekeler, F., Groppe, M., Jackson, T. L., MacLaren, R. E., Koitschev, A., Kusnyerik, A., Neffendorf, J., Nemeth, J., Naeem, M. A. N., Peters, T., Ramsden, J. D., Sachs, H., Simpson, A., Singh, M. S., … Zrenner, E. (2015). Subretinal Visual Implant Alpha IMS – Clinical trial interim report. *Vision Research, Sight Restoration: Prosthetics, Optogenetics and Gene Therapy*, *111*, 149–160. https://doi.org/10.1016/j.visres.2015.03.001

- Stuart, G., Schiller, J., & Sakmann, B. (1997). Action potential initiation and propagation in rat neocortical pyramidal neurons. *The Journal of Physiology*, *505*(Pt 3), 617–632.

- Suzuki, S., Tachibana, M., & Kaneko, A. (1990). Effects of glycine and GABA on isolated bipolar cells of the mouse retina. *The Journal of Physiology*, *421*(1), 645–662. https://doi.org/10.1113/jphysiol.1990.sp017967

- Thomas, C. J., Mirza, R. G., & Gill, M. K. (2021). Age-Related Macular Degeneration. *Medical Clinics of North America, Ophthalmology*, *105*(3), 473–491. https://doi.org/10.1016/j.mcna.2021.01.003

- Tong, W., Meffin, H., Garrett, D. J., & Ibbotson, M. R. (2020). Stimulation Strategies for Improving the Resolution of Retinal Prostheses. *Frontiers in Neuroscience*, *14*, 262. https://doi.org/10.3389/fnins.2020.00262

- Toychiev, A. H., Ivanova, E., Yee, C. W., & Sagdullaev, B. T. (2013). Block of Gap Junctions Eliminates Aberrant Activity and Restores Light Responses during Retinal Degeneration. *Journal of Neuroscience*, *33*(35), 13972–13977. https://doi.org/10.1523/JNEUROSCI.2399-13.2013

- Trenholm, S., & Awatramani, G. B. (1995). Myriad roles for gap junctions in retinal circuits. In H. Kolb, E. Fernandez, B. Jones, & R. Nelson (Eds), *Webvision: The*

Organization of the Retina and Visual System. University of Utah Health Sciences Center. http://www.ncbi.nlm.nih.gov/books/NBK549947/

- Trenholm, S., & Awatramani, G. B. (2015). Origins of spontaneous activity in the degenerating retina. *Frontiers in Cellular Neuroscience*, *9*. https://doi.org/10.3389/fncel.2015.00277

- Trenholm, S., Borowska, J., Zhang, J., Hoggarth, A., Johnson, K., Barnes, S., Lewis, T. J., & Awatramani, G. B. (2012). Intrinsic oscillatory activity arising within the electrically coupled AII amacrine–ON cone bipolar cell network is driven by voltage-gated Na^+ channels. *The Journal of Physiology*, *590*(10), 2501–2517. https://doi.org/10.1113/jphysiol.2011.225060

- Twyford, P., Cai, C., & Fried, S. (2014). Differential responses to high-frequency electrical stimulation in ON and OFF retinal ganglion cells. *Journal of Neural Engineering*, *11*(2), 025001. https://doi.org/10.1088/1741-2560/11/2/025001

- Urbańska, K., Szarpak, J., Biel, N., Woźniak, M., & Kawecka, W. (2023). Endophthalmitis—A rare but dangerous complication of intravitreal anti-VEGF injections. *Ophthalmology Journal*, *8*(0), Article 0. https://doi.org/10.5603/OJ.2023.0010

- Varela, C., Igartua, I., De La Rosa, E. J., & De La Villa, P. (2003). Functional modifications in rod bipolar cells in a mouse model of retinitis pigmentosa. *Vision Research*, *43*(8), 879–885. https://doi.org/10.1016/S0042-6989(02)00493-5

- Veleri, S., Lazar, C. H., Chang, B., Sieving, P. A., Banin, E., & Swaroop, A. (2015). Biology and therapy of inherited retinal degenerative disease: Insights from mouse models. *Disease Models & Mechanisms*, *8*(2), 109–129. https://doi.org/10.1242/dmm.017913

- Venkatachalam, K. L., Herbrandson, J. E., & Asirvatham, S. J. (2011). Signals and Signal Processing for the Electrophysiologist. *Circulation: Arrhythmia and Electrophysiology*, *4*(6), 974–981. https://doi.org/10.1161/CIRCEP.111.964973

- Versaux-Botteri, C., Martin-Martinelli, E., Nguyen-Legros, J., Geffard, M., Vigny, A., & Denoroy, L. (1986). Regional specialization of the rat retina: Catecholamine-containing amacrine cell characterization and distribution. *Journal of Comparative Neurology*, *243*(3), 422–433. https://doi.org/10.1002/cne.902430311

- Wässle, H. (2004). Parallel processing in the mammalian retina. *Nature Reviews Neuroscience*, *5*(10), 747–757. https://doi.org/10.1038/nrn1497

- Wässle, H., Puller, C., Müller, F., & Haverkamp, S. (2009). Cone Contacts, Mosaics, and Territories of Bipolar Cells in the Mouse Retina. *Journal of Neuroscience*, *29*(1), 106–117. https://doi.org/10.1523/JNEUROSCI.4442-08.2009

- Wässle, H., Schafer-Trenkler, I., & Voigt, T. (1986). Analysis of a glycinergic inhibitory pathway in the cat retina. *Journal of Neuroscience*, *6*(2), 594–604. https://doi.org/10.1523/JNEUROSCI.06-02-00594.1986

- Webster, C. M., Tworig, J., Caval-Holme, F., Morgans, C. W., & Feller, M. B. (2020). The Impact of Steroid Activation of TRPM3 on Spontaneous Activity in the Developing Retina. *eNeuro*, *7*(2), ENEURO.0175. https://doi.org/10.1523/ENEURO.0175-19.2020

- Weiland, J. D., & Humayun, M. S. (2014). Retinal Prosthesis. *IEEE Transactions on Bio-Medical Engineering*, *61*(5), 1412–1424. https://doi.org/10.1109/TBME.2014.2314733

- Weitz, A. C., Nanduri, D., Behrend, M. R., Gonzalez-Calle, A., Greenberg, R. J., Humayun, M. S., Chow, R. H., & Weiland, J. D. (2015). Improving the spatial resolution of epiretinal implants by increasing stimulus pulse duration. *Science Translational Medicine*, *7*(318), 318ra203. https://doi.org/10.1126/scitranslmed.aac4877

- Wu, K. Y., Mina, M., Sahyoun, J.-Y., Kalevar, A., & Tran, S. D. (2023). Retinal Prostheses: Engineering and Clinical Perspectives for Vision Restoration. *Sensors (Basel, Switzerland)*, *23*(13), 5782. https://doi.org/10.3390/s23135782

- Wu, Y., Karetić, I., Stegmaier, J., Walter, P., & Merhof, D. (2023). A Deep Learning-based in silico Framework for Optimization on Retinal Prosthetic Stimulation. *2023 45th Annual International Conference of the IEEE Engineering in Medicine & Biology Society (EMBC)*, 1–4. https://doi.org/10.1109/EMBC40787.2023.10340288

- Xiong, W.-H., Brown, R. L., Reed, B., Burke, N. S., Duvoisin, R. M., & Morgans, C. W. (2015). Voriconazole, an Antifungal Triazol That Causes Visual Side Effects, Is an Inhibitor of TRPM1 and TRPM3 Channels. *Investigative Ophthalmology & Visual Science*, *56*(2), 1367–1373. https://doi.org/10.1167/iovs.14-15270

- Yan, W., Laboulaye, M. A., Tran, N. M., Whitney, I. E., Benhar, I., & Sanes, J. R. (2020). Mouse Retinal Cell Atlas: Molecular Identification of over Sixty Amacrine Cell Types. *Journal of Neuroscience*, *40*(27), 5177–5195. https://doi.org/10.1523/JNEUROSCI.0471-20.2020

- Ye, J. H., & Goo, Y. S. (2007). The slow wave component of retinal activity in *rd* / *rd* mice recorded with a multi-electrode array. *Physiological Measurement*, *28*(9), 1079–1088. https://doi.org/10.1088/0967-3334/28/9/009

- Ye, J. H., Kim, K. H., & Goo, Y. S. (2008). Comparison of electrically-evoked ganglion cell responses in normal and degenerate retina. *2008 30th Annual International Conference of the IEEE Engineering in Medicine and Biology Society*, 2465–2468. https://doi.org/10.1109/IEMBS.2008.4649699

- Yee, C. W., Ivanova, E., Toychiev, A. H., Willis, D. E., & Sagdullaev, B. T. (2018). Atypical expression and activation of GluN2A and GluN2B-containing NMDA receptors at ganglion cells during retinal degeneration. *Neuroscience*, *393*, 61–72. https://doi.org/10.1016/j.neuroscience.2018.09.048

- Yee, C. W., Toychiev, A. H., & Sagdullaev, B. T. (2012). Network Deficiency Exacerbates Impairment in a Mouse Model of Retinal Degeneration. *Frontiers in Systems Neuroscience*, *6*. https://doi.org/10.3389/fnsys.2012.00008

- Yoo, Y., Cha, S., & Goo, Y. S. (2024). Comparison of modulation efficiency between normal and degenerated primate retina. *Frontiers in Cell and Developmental Biology*, *12*, 1419007. https://doi.org/10.3389/fcell.2024.1419007

- Yue, L., Castillo, J., Gonzalez, A. C., Neitz, J., & Humayun, M. S. (2021). Restoring Color Perception to the Blind. *Ophthalmology*, *128*(3), 453–462. https://doi.org/10.1016/j.ophtha.2020.08.019

- Zeck, G. (2016). Aberrant Activity in Degenerated Retinas Revealed by Electrical Imaging. *Frontiers in Cellular Neuroscience*, *10*. https://doi.org/10.3389/fncel.2016.00025

- Zrenner, E., Bartz-Schmidt, K. U., Benav, H., Besch, D., Bruckmann, A., Gabel, V.-P., Gekeler, F., Greppmaier, U., Harscher, A., Kibbel, S., Koch, J., Kusnyerik, A., Peters, T., Stingl, K., Sachs, H., Stett, A., Szurman, P., Wilhelm, B., & Wilke, R. (2011). Subretinal electronic chips allow blind patients to read letters and combine them to words. *Proceedings of the Royal Society B: Biological Sciences*, *278*(1711), 1489–1497. https://doi.org/10.1098/rspb.2010.1747

8. Acknowledgement

I would like to express my immense gratitude to my supervisor, Prof. Frank Müller, for his invaluable guidance, patience and unwavering support to materialise a fruitful PhD journey. I have greatly benefited from, and have personally enjoyed, our insightful discussions and experimental troubleshooting sessions throughout my four-year long endeavour at Forschungszentrum Jülich. I also owe my special gratitude to my doctoral committee, Prof. Björn Kampa, Dr. Sandra Johnen and Prof. Marc Spehr for their constructive criticism and helpful guidance which improved the quality of my thesis.

I am deeply thankful to Christoph Aretzweiler von Schwartzenberg for his exceptional technical support and for always being there to rely on when facing difficulties. With his support, I was able to develop skills in mouse-retina preparations and in-vitro recordings. I would also like to thank Dr. Anja Mataruga for sharing her expertise in immunohistochemistry staining and for being a constant source of encouragement throughout my PhD. I would like to thank all the members of IBI-1 for their kind support and words of encouragement when they were needed the most. Especially, Suryapriya and Ahmadreza, who made the working sessions more enjoyable, despite being a late addition to our group. A warm thank you to Victor, Piersilvio, Joel and Cansu for making my time at FZJ truly memorable.

I gratefully acknowledge the support received from the research training group RTG2610 funded by DFG (German Research Foundation). The meetings, discussions and collaborations with the RTG members shaped the direction of my research. I would especially like to thank Philipp Löhler, Marie Jung and Jing Wang for the many enjoyable moments of teamwork as well as the insightful discussions that enriched this research experience. I would also like to thank RTG for the extensive training sessions that have improved my skills as a researcher.

Special thanks to my friend and colleague, Nikhil Mohan, for his help in analysing large datasets and developing new algorithms. I truly enjoyed brainstorming ideas with him. In addition, he has been a constant source of support and friendship throughout my PhD journey.

I am very grateful to my friends for their companionship and understanding throughout this demanding journey. I am especially thankful to "Team Jülich": Ashish, Vidhya, Shilpa, Varun, Nikhil, Honey and Akshay for the time spent planning activities, travelling together, and sharing moments of relaxation, which helped me manage the stresses of doctoral research. I would also like to thank Vishakettan, Sindhu Chechi, baby Shanvik, Godwin, Sourav, Anjana, Amal, Supriya, Kavya, and Mahesh, who organised wonderful get-togethers and shared home-cooked meals, which brought comfort and a sense of home while being away from my family.

Above all, I am profoundly grateful to my amazing family: Mohanakumar achan, Asha amma, Nikhitha and fiancé (Akshay) for standing by me through every high and low of this journey. I am equally thankful to my in-law family: Salini amma, Sasidharan achan and Arathi for their unwavering support, love, and encouragement. Their constant reassurance and belief in my abilities gave me the strength and motivation to persevere and successfully complete this work.